NORSAR

NORSAR Scientific Report No. 1-2013

Semiannual Technical Summary

1 January – 30 June 2013

Tormod Kværna (Ed.)

Kjeller, December 2013

Table of Contents

1   Summary

This report provides summary information on operation and maintenance (O&M) activities at the Norwegian National Data Center (NOR-NDC) for CTBT verification during the period 1 January − 30 June 2013, as well as scientific and technical contributions relevant to verification in a broad sense. The O&M activities, including operation of monitoring stations and transmission links within Norway and to Vienna, Austria are being funded jointly by the CTBTO/PTS and the Norwegian Government, with the understanding that the funding of O&M activities for primary stations in the International Monitoring System (IMS) will gradually be transferred to the CTBTO/PTS. The O&M statistics presented in this report maintain consistency with long-standing reporting practices. Research activities described in this report are mainly funded by the Norwegian Government, with other sponsors acknowledged where appropriate.

A summary of the activities at NOR-NDC relating to field installations, data acquisition, data forwarding and processing during the reporting period is provided in chapters 2 − 4 of this report. Norway is contributing primary station data from two seismic arrays: the Norwegian Seismic Array NOA (IMS code PS27) and the Arctic Regional Seismic Array ARCES (IMS code PS28), one auxiliary seismic array on Spitsbergen (SPITS, IMS code AS72), and one auxiliary three-component station at Jan Mayen (JMIC, IMS code AS73). These data are being provided to the International Data Centre (IDC) in Vienna via the Global Communications Infrastructure (GCI).

This report presents operational statistics for NOA, ARCES, SPITS and JMIC, as well as for additional seismic stations which through cooperative agreements with institutions in the host countries provide continuous data to the NOR-NDC. These additional stations include the Finnish Regional Seismic Array (FINES, IMS code PS17) and the Hagfors array in Sweden (HFS, IMS code AS101). Operational statistics for the reestablished NORES array and two other three-component stations operated by NORSAR are also provided. These two stations are Åknes (AKN) and TROLL in Antarctica.

So far among the Norwegian IMS stations, the NOA and the ARCES arrays (PS27 and PS28, respectively), the radionuclide station at Spitsbergen (RN49) and the auxiliary seismic stations on Spitsbergen (AS72) and Jan Mayen (AS73) have been certified by the CTBTO/PTS. Provided that adequate funding continues to be made available (from the CTBTO/PTS and the Norwegian Ministry of Foreign Affairs), we envisage continuing the provision of data from these and other Norwegian IMS-designated stations in accordance with current procedures. As part of NORSAR's obsolescence management, a recapitalization plan for PS27 and PS28 was submitted to CTBTO/PTS in October 2008, with the purpose of preventing severe degradation of the stations due to lack of spare parts. The recapitalization of PS27 was concluded in 2012. In parallel the recapitalization of P28 has started with development and testing of particular equipment for PS28, like a central timing system and a hybrid sensor for surface vaults.

The IMS infrasound station IS37, originally planned to be located near Karasjok, is being established at another site, since the local authorities did not grant the permissions required. A site at Bardufoss, at 69.10° N, 18.60° E, was approved by the municipal authorities for installation of IS37. The CTBTO Preparatory Commission has approved a corresponding coordinate change for the station, and construction of the station commenced during the spring of 2013.
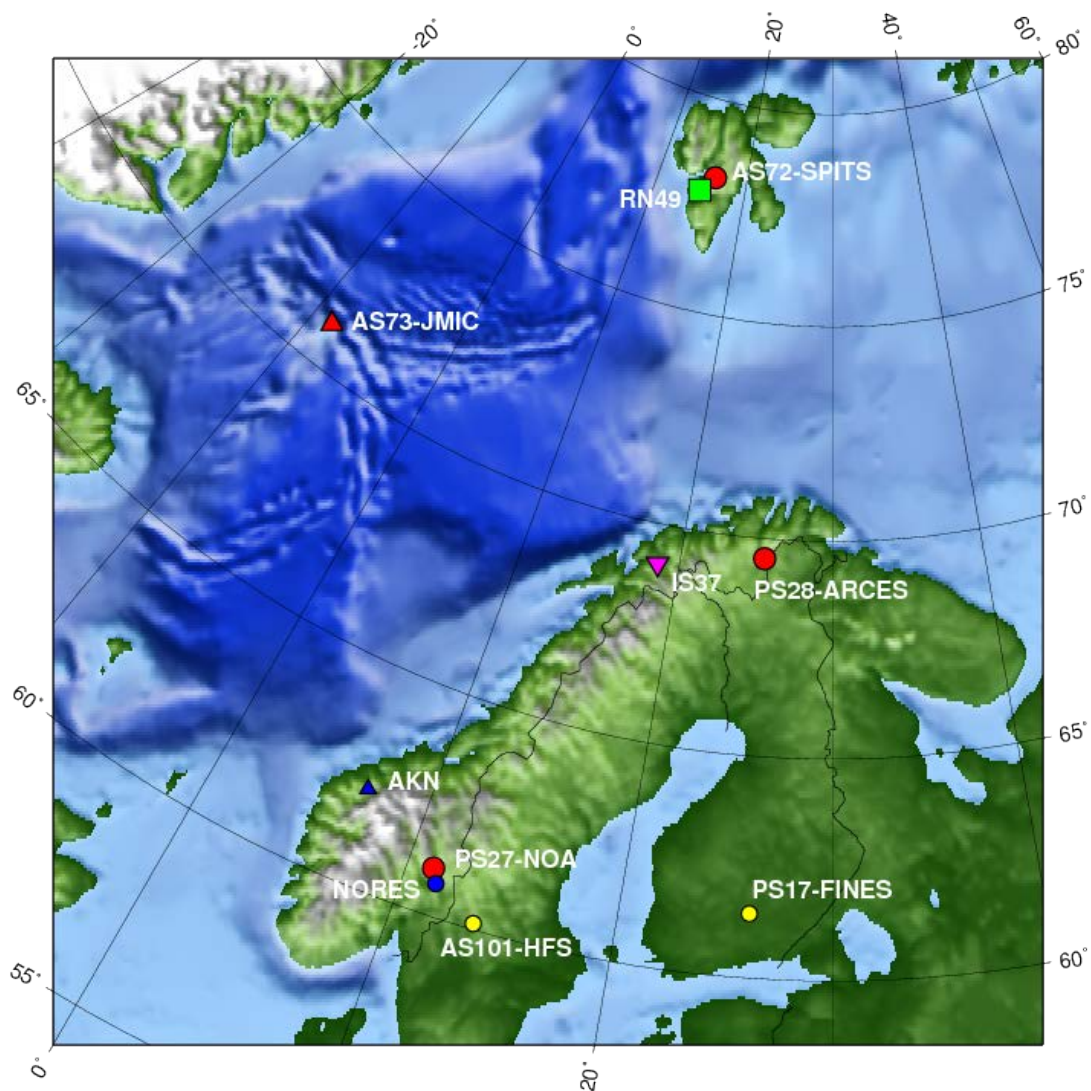
Fig. 1.1   *Locations for stations covered in this report (except TROLL in Antarctica, see Fig. 3.5.1). Norwegian seismic IMS stations are shown in red. Other Norwegian seismic stations are shown by blue symbols. Contributing IMS seismic stations in other countries are yellow. Circles indicate seismic arrays and triangles indicate single 3-component seismic stations. The IMS infrasound station IS37 is shown by a purple inverted triangle, and the IMS radionuclide station RN49 is shown by a green square.*

Five scientific and technical contributions presented in chapter 6 of this report are provided as follows:

Section 6.1 describes an application of coda envelopes for estimation of stable event magnitudes in southern Norway. It has previously been demonstrated that that coda amplitude measurements have significantly less variability than measurements of direct wave amplitudes, and that stable estimates of source moment spectra and event magnitudes can be derived from regional coda envelopes observed at only 1-3 stations. Is this study we have analyzed events from the time period

2009-2013 observed at the three stations NOA, BER and AKN, located in different parts of southern Norway. For events with magnitudes larger than 2.25, Mw(coda) estimates from different stations are in very good agreement, having interstation standard deviations varying between 0.04 and 0.06. For events with magnitudes below 2.25, the interstation standard deviations are higher and vary between 0.08 and 0.13, which we believe is caused by increasingly shorter usable coda window lengths for smaller events. Significant differences in the shape of the source moment spectra between presumed earthquakes and explosions have also been demonstrated.

Section 6.2 entitled "Examination of the Storfjorden Aftershock Sequence Using an Autonomous Event Detection and Grouping Framework: Preliminary Results" presents results from analysis of more than 4 years of SPITS array data using a processing tool ("detection framework") developed in a collaborative effort between the Lawrence Livermore National Laboratory and NORSAR. The autonomous event detection and grouping system produced an event catalog whose completeness is 1.3 magnitude units lower than the NORSAR analyst reviewed bulletin for the area of the Storfjorden aftershock sequence. The cluster lifespan plot highlights the source heterogeneity within the fjord, and the space-time distribution of clusters suggests that the evolution of the sequence follows an epidemic type aftershock model rather than the smooth exponential decay predicted by Omori's law.

In section 6.3 we report on an investigation of local anisotropy and lateral heterogeneity using P-wave polarization and fk analysis of NORSAR array data. More than 600 first-arriving teleseismic P-phases recorded since 1996 were analyzed at seven three-component broadband sites of the array. The estimated azimuthal deviation shows a clear dependence on the event backazimuth. The high velocity directions are consistent at each station of the NORSAR array and are in good agreement with observations made with different approaches in the array area. The anisotropic contribution to azimuthal deviations observed by polarization analysis is significant only at stations NC303 and NC204 and fast directions match the fast directions estimated at those stations with SKS splitting.

Section 6.4 is entitled "Detection Capability of the Seismic Station TROLL in Antarctica". The seismic station at the Norwegian Research Base Troll in Dronning Maud Land, Antarctica, has been operational and sending continuous data to NORSAR since 5 February 2012. During the first year of operation, relatively large diurnal, long-period oscillations were observed at TROLL, presumably caused by temperature variations within the protected dome. In addition, the gain setting of the Q330HR digitizer was observed to be too low for sufficient resolution of the high frequencies. Consequently, the gain setting of the Q330HR digitizer was increased on 4 February 2013 by a factor of 20, and on 9 February 2013, the TROLL station was upgraded with additional thermal insulation.

The detection capability of TROLL has been assessed though a comparative study with the neighboring IMS station at Sanae (SNAA). We show that TROLL has an overall event detection capability which is $0.1 - 0.2$ magnitude units better than SNAA for teleseismic events. As SNAA shows to be among the very best performing three-component stations of the IMS, TROLL is thus considered to be even better for detection of teleseismic events. The $1 - 2$ Hz noise levels at SNAA and TROLL are comparable, but there is a tendency of higher noise levels at TROLL for higher frequencies, caused by e.g., periodically occurring small icequakes in the nearby glaciers. Prior to the upgrade of the station in February 2013 it was demonstrated that the TROLL station could well observe the Earth's normal modes for all frequencies above 0.8 mHz. The installation of additional thermal insulation at the TROLL station in February 2013 led to a significant reduction of the long

period noise levels of the vertical component data, and we expect to further enhance the observational capabilities at long periods.

Section 6.5 presents preliminary results from a cooperative project between NORSAR and seismological institutions in NW Russia (Arkhangelsk and Apatity), which each operate seismic networks. To indicate the potential of combining resources to improve the seismic coverage of the European Arctic, we have carried out a comparison based on the first six months of 2013 between the Reviewed Event Bulletin of the CTBT International Data Centre, the NORSAR reviewed regional seismic bulletin using data from Fennoscandia, Spitsbergen and the Kola Peninsula and the bulletin produced by the Arkhangelsk seismological center using data from their own network in combination with the data used to produce the NORSAR bulletin.

We show that the addition of the Arkhangelsk network leads to a considerable increase in the number of located seismic events, both at local distances from the individual stations and in the High Arctic. The latter increase is particularly pronounced along the Gakkel Ridge to the north of the Svalbard and Franz-Josef Land archipelagos. A closer investigation shows that the additional events in the High Arctic are included due to the contribution from the station ZFI on Franz-Josef Land in combination with the Spitsbergen stations SPITS and KBS. We also note that the vast majority of the events along the Gakkel Ridge have been located slightly to the south of the ridge. We interpret this as an effect of the lack of recording stations closer to and north of the Gakkel Ridge, and the use of a one-dimensional velocity model which is not fully representative for travel-times along observed propagation paths. We conclude that while the characteristics of earthquake activity in the European Arctic is currently poorly known, the knowledge can be expected to be significantly improved by establishing the appropriate cooperative seismic recording infrastructures as discussed in this paper.

Tormod Kværna

2   Operation of International Monitoring System (IMS) Stations in Norway

2.1   PS27 — Primary Seismic Station NOA

The mission-capable data statistics were 99.997%, as compared to 99.993% for the previous reporting period. The net instrument availability was 96.356%

There were no outages of all subarrays at the same time in the reporting period.

Monthly uptimes for the NORSAR on-line data recording task, taking into account all factors (field installations, transmissions line, data center operation) affecting this task were as follows:

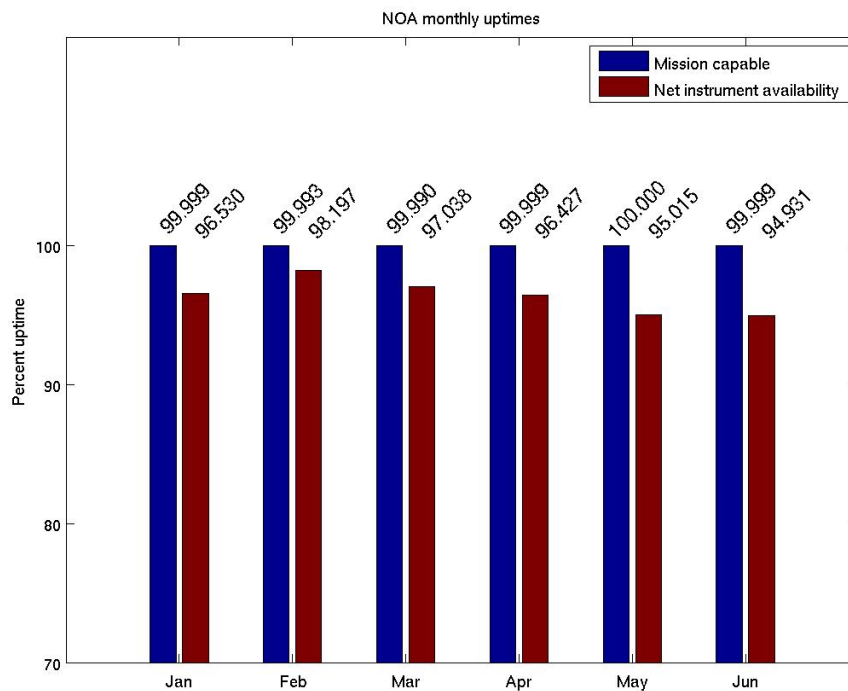|	Mission Capable	Net instrument availability
January 2013:	99.999	96.530
February 2013:	99.993	98.197
March 2013:	99.990	97.038
April 2013:	99.999	96.427
May 2013:	100.000	95.015
June 2013:	99.999	94.931

*Fig. 2.1.1   Monthly uptimes for NOA for the period January – June 2013.*

B. Paulsen

2.1.1 NOA event detection operation

In Table 2.1.1 some monthly statistics of the Detection and Event Processor operation are given. The table lists the total number of detections (DPX) triggered by the on-line detector, the total number of detections processed by the automatic event processor (EPX) and the total number of events accepted after analyst review (teleseismic phases, core phases and total).

	Total DPX	Total EPX	Accepted events P-phases	Core Phases	Sum	Daily average
Jan 13	8361	1280	269	53	322	10.4
Feb	7232	1158	281	178	459	16.4
Mar	7728	1164	242	84	326	10.5
Apr	7409	1321	416	62	478	15.9
May	4438	963	453	60	513	16.5
Jun	4239	841	291	55	346	11.5
	39407	6727	1952	492	2444	13.5

Table 2.1.1. Detection and event processor statistics, 1 January – 30 June 2013.
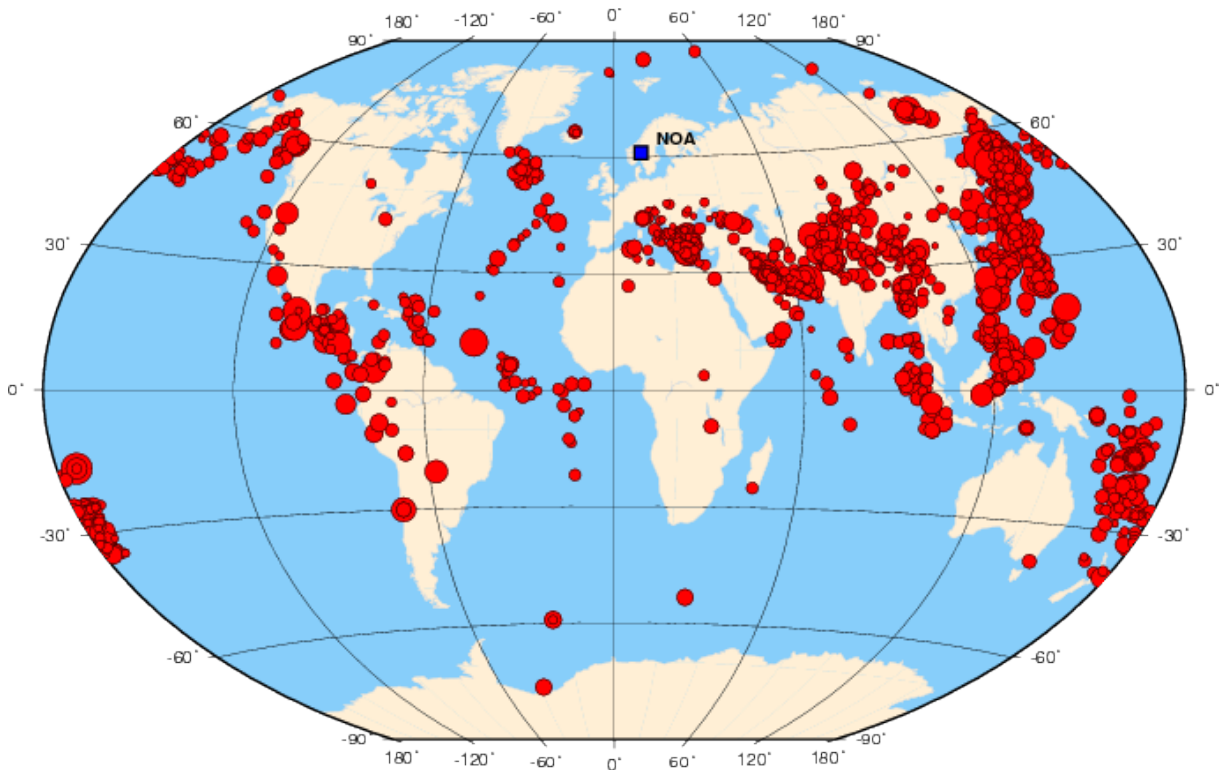
Fig. 2.1.2   Distribution of events in NORSAR's teleseismic reviewed bulletin for the time interval 1 January – 30 June 2013. Event symbols are scaled proportionally to event magnitude. The location of NOA is noted with a blue square. All locations are based on phase interpretation and inversion of slowness and backazimuth into a location, using the NOA array alone.

NOA detections

The number of detections (phases) reported by the NORSAR detector during day 001, 2013, through day 181, 2013, was 39,407, giving an average of 218 detections per processed day (181 days processed).

B. Paulsen
U. Baadshaug

2.2 PS28 — Primary Seismic Station ARCES

The mission-capable data statistics were 99.977%, as compared to 88.048% for the previous reporting period. The net instrument availability was 98.363%.
Monthly uptimes for the ARCES on-line data recording task, taking into account all factors (field installations, transmission lines, data center operation) affecting this task were as follows:

	Mission Capable	Net instrument availability
January 2013:	99.960	99.480
February 2013:	99.982	99.966
March 2013:	99.997	98.872
April 2013:	99.999	99.970
May 2013:	99.925	99.927
June 2013:	100.000	91.963
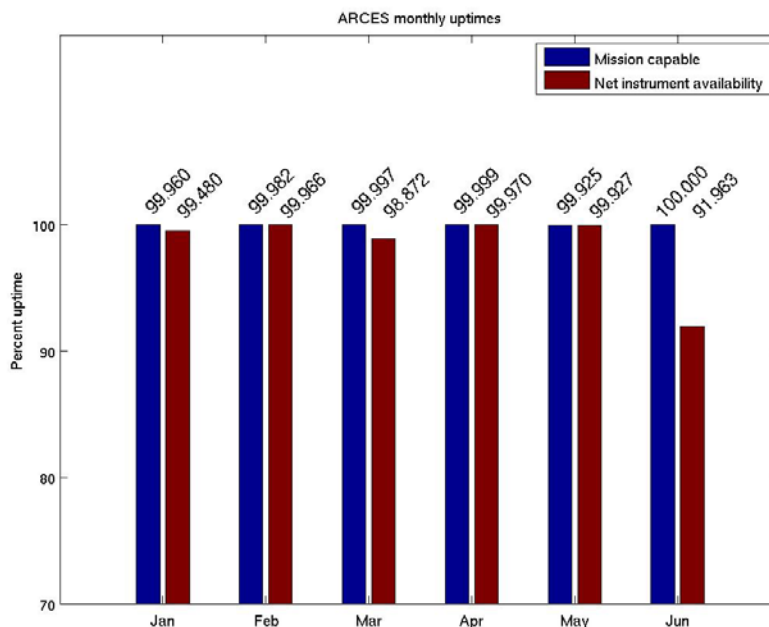
Fig. 2.2.1   Monthly uptimes for ARCES for the period January – June 2013.

B. Paulsen

2.2.1   Event detection operation

ARCES detections

The number of detections (phases) reported during day 001, 2013, through day 181, 2013, was 180,306, giving an average of 996 detections per processed day (181 days processed).

Events automatically located by ARCES

During days 001, 2013, through day 181, 2013, 8,772 local and regional events were located by ARCES, based on automatic association of P- and S-type arrivals. This gives an average of 48.5 events per processed day (181 days processed). 74% of these events are within 300 km, and 93% of these events are within 1000 km.

U. Baadshaug

2.3   AS72 — Auxiliary Seismic Station on Spitsbergen

The mission-capable data for the period were 99.058%, as compared to 99.977% for the previous reporting period. The net instrument availability was 97.157%.

The main outages in the reporting period are presented in Table 2.3.1

Day	Period
Feb 23	17.44-00.00
Feb 24	00.00-21.40
May 13	08.03-08.21

Table 2.3.1. The main interruptions in recording of Spitsbergen data at NOR-NDC,
1 January – 30 June 2013.

Monthly uptimes for the Spitsbergen on-line data recording task, taking into account all factors (field installations, transmissions line, data center operation) affecting this task were as follows:

|	Mission Capable	Net instrument availability
January 2013:	99.992	93.832
February 2013:	94.407	89.431
March 2013:	99.998	99.964
April 2013:	99.998	99.776
May 2013:	99.953	99.942
June 2013:	99.999	99.996
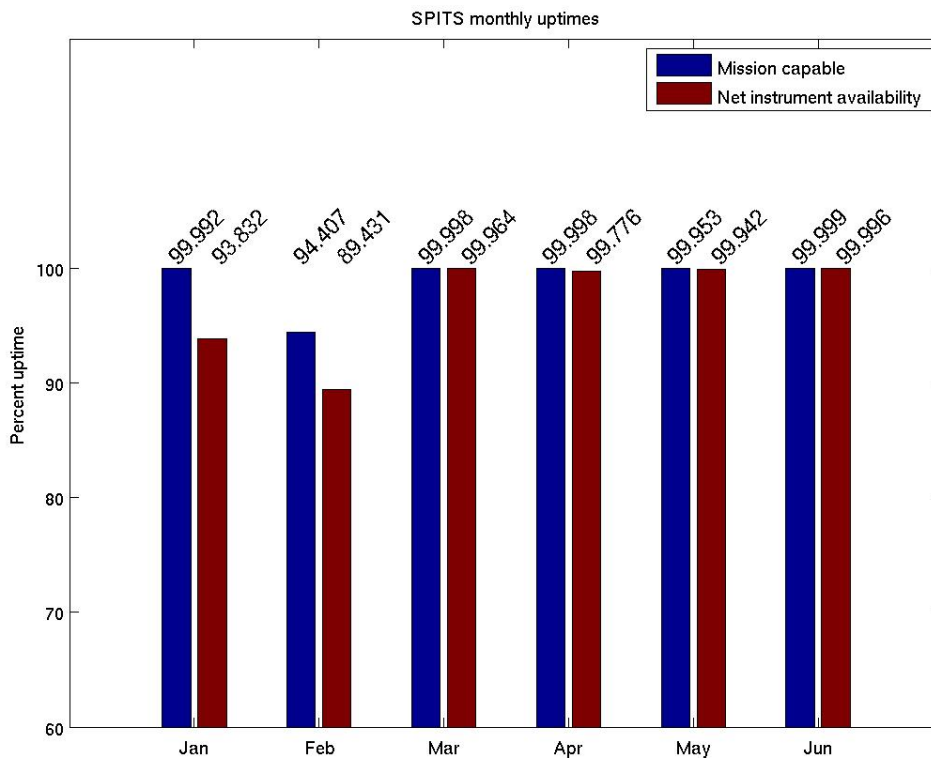
Fig. 2.3.1   Monthly uptimes for SPITS for the period January – June 2013.

B. Paulsen

2.3.1   Event detection operation

Spitsbergen array detections

The number of detections (phases) reported from day 001, 2013, through day 181, 2013, was 321,191, giving an average of 1,775 detections per processed day (181 days processed).

Events automatically located by the Spitsbergen array

During days 001, 2013, through day 181, 2013, 29,555 local and regional events were located by the Spitsbergen array, based on automatic association of P- and S-type arrivals. This gives an average of 163.3 events per processed day (181 days processed). 85% of these events are within 300 km, and 93% of these events are within 1000 km.

U. Baadshaug

2.4   AS73 — Auxiliary Seismic Station at Jan Mayen

The IMS auxiliary seismic network includes a three-component station on the Norwegian island of Jan Mayen. The station location given in the protocol to the Comprehensive Nuclear- Test-Ban Treaty is 70.9°N, 8.7°W.

The University of Bergen has operated a seismic station at this location since 1970. A so-called Parent Network Station Assessment for AS73 was completed in April 2002. A vault at a new location (71.0°N, 8.5°W) was prepared in early 2003, after its location had been approved by the PrepCom. New equipment was installed in this vault in October 2003, as a cooperative effort between NORSAR and the CTBTO/PTS. Continuous data from this station are being transmitted to the NDC at Kjeller via a satellite link installed in April 2000. Data are also made available to the University of Bergen.

The station was certified by the CTBTO/PTS on 12 June 2006.
Monthly uptimes for the Jan Mayen on-line data recording task, taking into account all factors (field installations, transmissions line, data center operation) affecting this task were as follows:

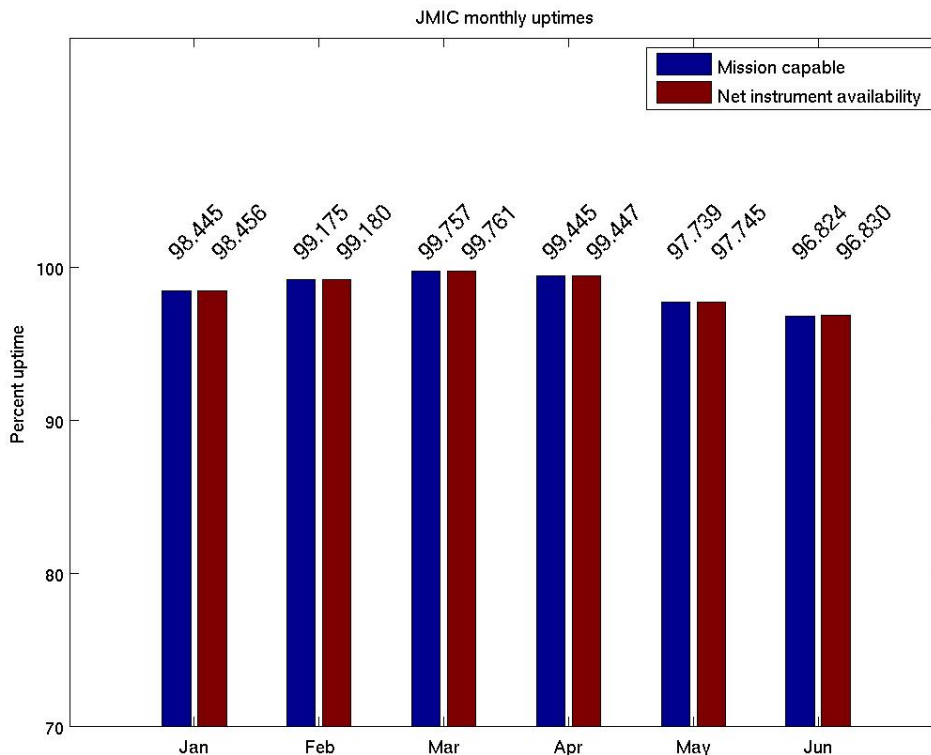|	Mission Capable	Net instrument availability
January 2013:	98.445	98.456
February 2013:	99.175	99.180
March 2013:	99.757	99.761
April 2013:	99.445	99.447
May 2013:	97.739	97.745
June 2013:	96.824	96.830

Fig. 2.4.1   Monthly uptimes for JMIC for the period January – June 2013.

B. Paulsen

2.5 IS37 — Infrasound Station at Bardufoss

The IMS infrasound network should, according to the protocol of the CTBT, include a station at Karasjok in northern Norway. The coordinates given for this station are 69.5°N, 25.5°E. These coordinates coincide with those of the primary seismic station PS28.

It proved, however, impossible to obtain the necessary permits for use of land for an infrasound station at Karasjok. Various alternatives for locating the station at Karasjok were prepared, but all applications to the local authorities to obtain the permissions needed to establish the station were turned down by the local governing council in June 2007.

In 2008, investigations were initiated to identify an alternative site for IS37 outside Karasjok. A site at Bardufoss, at 69.1°N, 18.6°E, was approved in December 2012 by landowners and the municipal authorities for installation of IS37. The CTBTO preparatory Commission has approved the corresponding coordinate change for the station. During the reporting period, IS37 was under installation at the designated Bardufoss location.

J. Fyen

2.6   RN49 — Radionuclide Station on Spitsbergen

The IMS radionuclide network includes a station on the island of Spitsbergen. This station has been selected to be among those IMS radionuclide stations that will monitor for the presence of relevant noble gases upon entry into force of the CTBT.

A site survey for this station was carried out in August of 1999 by NORSAR, in cooperation with the Norwegian Radiation Protection Authority. The site survey report to the PTS contained a recommendation to establish this station at Platåberget, near Longyearbyen. The infrastructure for housing the station equipment was established in early 2001, and a noble gas detection system, based on the Swedish "SAUNA" design, was installed at this site in May 2001, as part of CTBTO PrepCom's noble gas experiment. A particulate station ("ARAME" design) was installed at the same location in September 2001. A certification visit to the particulate station took place in October 2002, and the particulate station was certified on 10 June 2003. Both systems underwent substantial upgrading in May/June 2006. The noble gas system was certified on 21 December 2012. The equipment at RN49 is being maintained and operated under a contract with the CTBTO/PTS.

S. Mykkeltveit

3   Contributing Regional Arrays and Three-Component Stations

3.1   NORES

The NORES array went out of operation on 11 June 2002, when lightning destroyed the station electronics. In December 2011 the array was rebuilt and again became operational in an experimental mode where the 9 inner sites were instrumented with three-component sensors.

Monthly uptimes for the NORES on-line data recording task, taking into account all factors (field installations, transmission lines, data center operation) affecting this task are given in the following table:

	Data availability
January 2013:	100.000
February 2013:	99.993
March 2013:	100.000
April 2013:	99.992
May 2013:	98.238
June 2013:	100.000

B. Paulsen

3.2   Hagfors (IMS Station AS101)

Data from the Hagfors array are made available continuously to NORSAR through a cooperative agreement with Swedish authorities.

The mission-capable data statistics were 99.776%, as compared to 100% for the previous reporting period. The net instrument availability was 99.782%.

Monthly uptimes for the Hagfors on-line data recording task, taking into account all factors (field installations, transmission lines, data center operation) affecting this task were as follows:

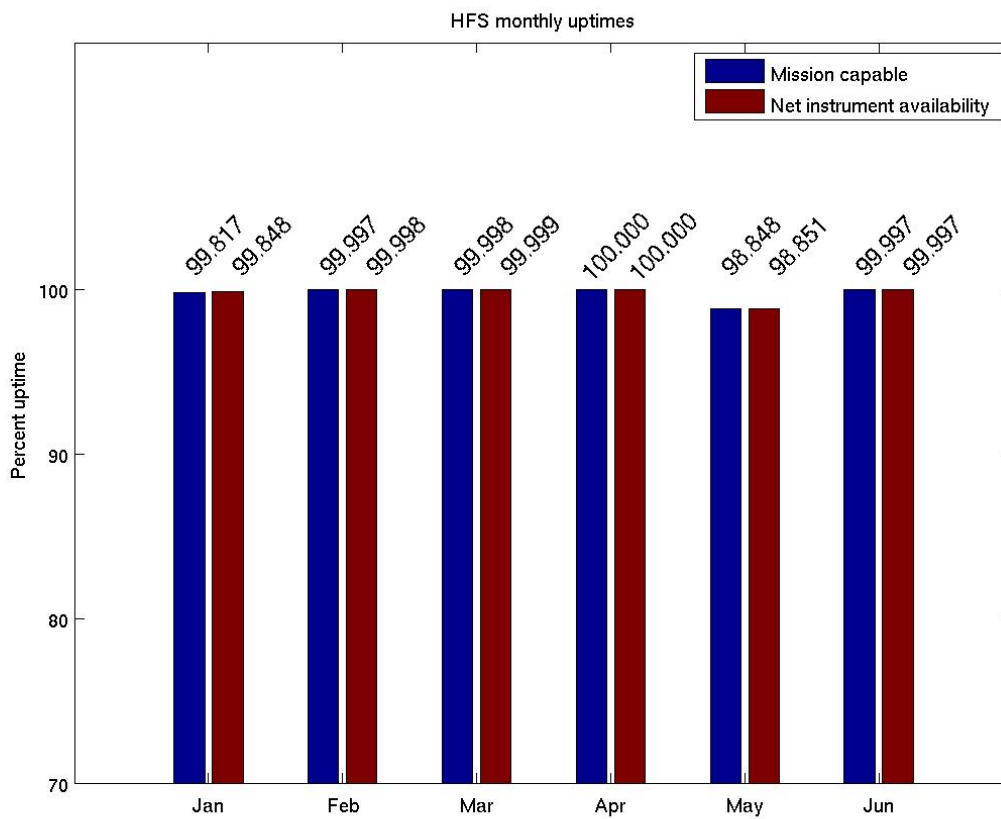|	Mission Capable	Net instrument availability
January 2013:	99.817	99.848
February 2013:	99.997	99.998
March 2013:	99.998	99.999
April 2013:	100.000	100.000
May 2013:	98.848	98.851
June 2013:	99.997	99.997

Fig. 3.2.1   Monthly uptimes for HFS for the period January – June 2013.

B. Paulsen

3.2.1   Hagfors event detection operation

Hagfors array detections

The number of detections (phases) reported from day 001, 2013, through day 181, 2013, was 149,310, giving an average of 825 detections per processed day (181 days processed).

Events automatically located by the Hagfors array

During days 001, 2013, through 181, 2013, 5,034 local and regional events were located by the Hagfors array, based on automatic association of P- and S-type arrivals. This gives an average of 27.8 events per processed day (181 days processed). 78% of these events are within 300 km, and 93% of these events are within 1000 km.

U. Baadshaug

3.3   FINES (IMS Station PS17)

Data from the FINES array are made available continuously to NORSAR through a cooperative agreement with Finnish authorities.

The mission-capable data statistics were 99.833%, as compared to 96.431% for the previous reporting period. The net instrument availability was 99.190%.

Monthly uptimes for the FINES on-line data recording task, taking into account all factors (field installations, transmissions line, data center operation) affecting this task were as follows:

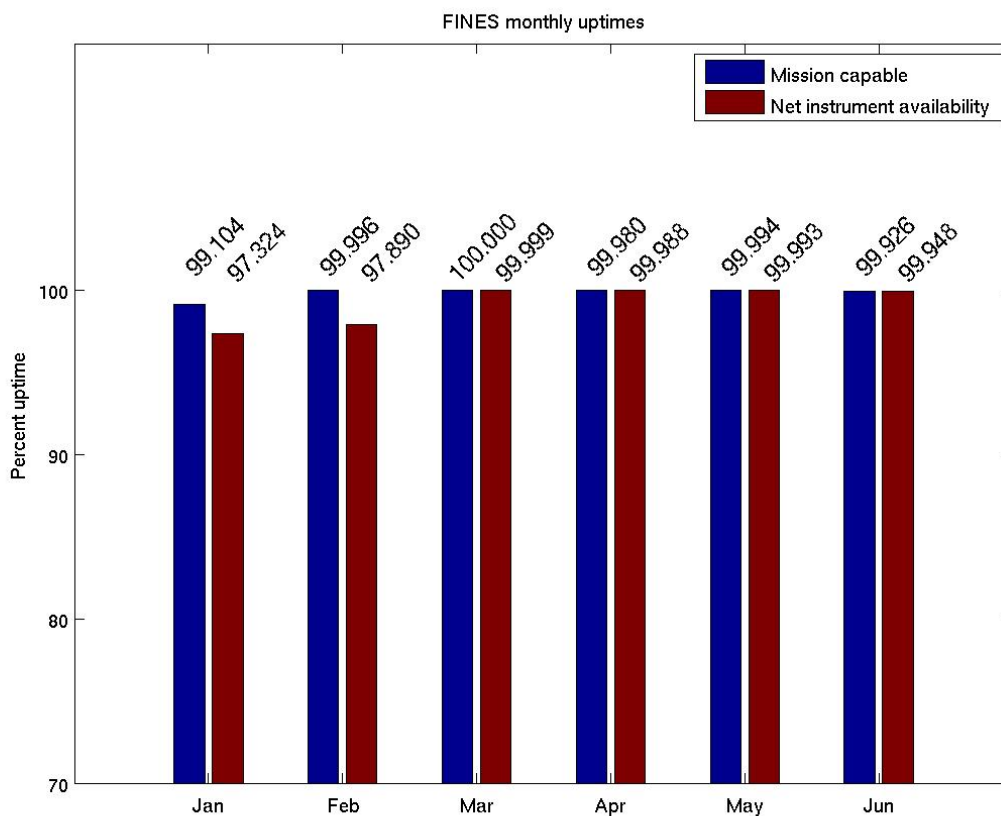|	Mission Capable	Net instrument availability
January 2013:	99.104	97.324
February 2013:	99.996	97.890
March 2013:	100.000	99.999
April 2013:	99.980	99.988
May 2013:	99.994	99.993
June 2013:	99.926	99.948

Fig. 3.3.1   Monthly uptimes for FINES for the period January – June 2013.

B. Paulsen

3.3.1   FINES event detection operation

FINES detections

The number of detections (phases) reported during day 001, 2013, through day 181, 2013, was 49,512, giving an average of 274 detections per processed day (181 days processed).

Events automatically located by FINES

During days 001, 2013, through 181, 2013, 1,950 local and regional events were located by FINES, based on automatic association of P- and S-type arrivals. This gives an average of 10.8 events per processed day (181 days processed). 90% of these events are within 300 km, and 95% of these events are within 1000 km.

U. Baadshaug

3.4   Åknes (AKN)

The seismic broadband station AKN was installed in October 2009 on top of the unstable rock slope site Åknes, Møre og Romsdal. Its primary purpose is the monitoring of local seismic activity related to the movement of the slope, but due to the relatively low ambient noise conditions it also provides excellent data of local, regional and global seismic events. The station has been sending continuous realtime data (200 Hz sampling rate) to NORSAR since 27 October 2009. On 17 January 2013 we added a 40 Hz data tap in order to facilitate data distribution to the seismologic community.
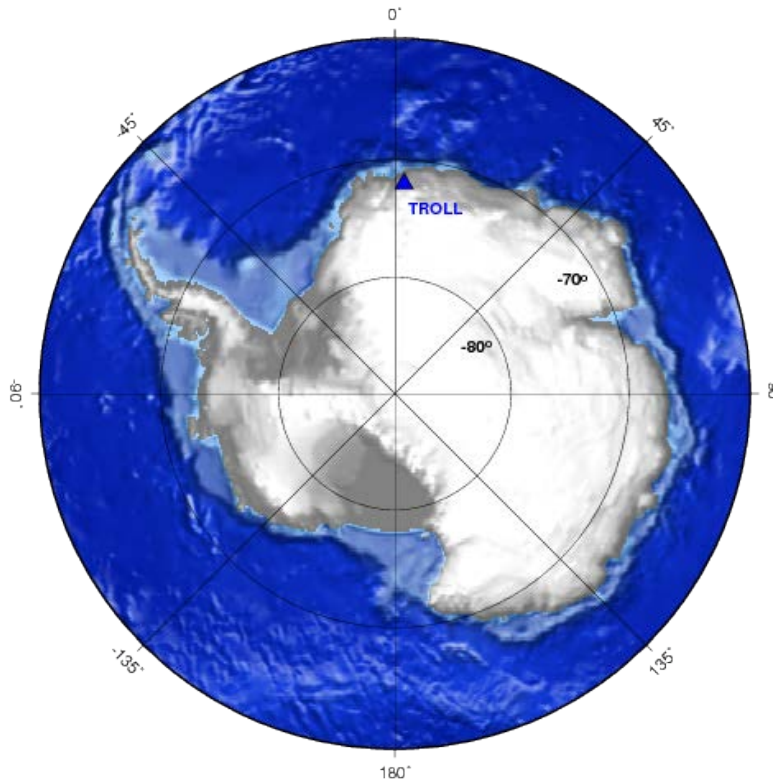
Monthly uptimes for the AKN on-line data recording task, taking into account all factors (field installations, transmission lines, data center operation) affecting this task are given in the following table:

	Data availability
January 2013:	99.886
February 2013:	99.998
March 2013:	100.000
April 2013:	99.996
May 2013:	100.000
June 2013:	100.000

U. Baadshaug

3.5   TROLL, Antarctica

The seismic station at the Norwegian Research Base Troll in Dronning Maud Land, Antarctica, became operational and started sending continuous data to NORSAR on 5 February 2012. On 4 February 2013 the Q330HR digitizer was increased by a factor of 20, and on 9 February 2013, the TROLL station was upgraded with additional thermal insulation. An additional low-gain data stream with a sampling rate of 40 Hz was retained by using the auxiliary 24-bit input and a gain factor of 1.

Fig. 3.5.1
Location of the 3-component seismic station TROLL in Antarctica.

Monthly uptimes for the TROLL on-line data recording task, taking into account all factors (field installations, transmission lines, data center operation) affecting this task are given in the following table:

	Data availability
January 2013:	100.000
February 2013:	99.955
March 2013:	100.000
April 2013:	99.861
May 2013:	100.000
June 2013:	100.000

U. Baadshaug

3.6   Regional Monitoring System Operation and Analysis

The Regional Monitoring System (RMS) was installed at NORSAR in December 1989 and has been operated from 1 January 1990 for automatic processing of data from ARCES and NORES. A second version of RMS that accepts data from an arbitrary number of arrays and single 3-component stations was installed at NORSAR in October 1991, and regular operation of the system comprising analysis of data from the 4 arrays ARCES, NORES, FINES and GERES started on 15 October 1991. As opposed to the first version of RMS, the one in current operation also has the capability of locating events at teleseismic distances.

Data from the Apatity array was included on 14 December 1992, and from the Spitsbergen array on 12 January 1994. Detections from the Hagfors array were available to the analysts and could be added manually during analysis from 6 December 1994. After 2 February 1995, Hagfors detections were also used in the automatic phase association.

Since 24 April 1999, RMS has processed data from all the seven regional arrays ARCES, NORES, FINES, GERES (until January 2000), Apatity, Spitsbergen, and Hagfors. Starting 19 September 1999, waveforms and detections from the NOA array have also been available to the analyst.

3.6.1   Phase and event statistics

Table 3.6.1 gives a summary of phase detections and events declared by RMS. From top to bottom the table gives the total number of detections by the RMS, the number of detections that are associated with events automatically declared by the RMS, the number of detections that are not associated with any events, the number of events automatically declared by the RMS, and finally the total number of events worked on interactively (in accordance with criteria that vary over time; see below) and defined by the analyst.

New criteria for interactive event analysis were introduced from 1 January 1994. Since that date, only regional events in areas of special interest (e.g, Spitsbergen, since it is necessary to acquire new knowledge in this region) or other significant events (e.g, felt earthquakes and large industrial explosions) were thoroughly analyzed. Teleseismic events of special interest are also analyzed.

To further reduce the workload on the analysts and to focus on regional events in preparation for Gamma-data submission during GSETT-3, a new processing scheme was introduced on 2 February 1995. The GBF (Generalized Beamforming) program is used as a pre-processor to RMS, and only phases associated with selected events in northern Europe are considered in the automatic RMS phase association. All detections, however, are still available to the analysts and can be added manually during analysis.

	Jan 13	Feb 13	Mar 13	Apr 13	May 13	Jun 13	Total
Phase detections	154823	120057	140671	111727	119697	119329	766304
- Associated phases	5967	6108	7099	6753	6623	5417	37967
- Unassociated phases	148856	113949	133572	104974	113074	113912	728337
Events automatically declared by RMS	1187	1129	1256	1256	1361	1097	7286
No. of events defined by the analyst	38	46	67	51	44	47	293

Table 3.6.1. RMS phase detections and event summary 1 January - 30 June 2013.

U. Baadshaug

B. Paulsen

4   The Norwegian National Data Center and Field Activities

4.1   NOR-NDC Activities

NORSAR functions as the Norwegian National Data Center (NOR-NDC) for CTBT verification. Six monitoring stations, comprising altogether 87 seismic and infrasound waveform systems plus radionuclide monitoring equipment, will be located on Norwegian territory as part of the future IMS, as described elsewhere in this report. The four seismic IMS stations are all in operation today, and all of them are currently providing data to the CTBTO/PTS on a regular basis. PS27, PS28, AS72, AS73 and RN49 are all certified. Data recorded by the Norwegian stations are being transmitted in real time to the NOR-NDC, and provided to the IDC through the Global Communications Infrastructure (GCI). Norway is connected to the GCI with a MPLS link to Vienna.

Operating the Norwegian IMS stations continues to require significant efforts by personnel both at the NOR-NDC and in the field. Strictly defined procedures as well as increased emphasis on regularity of data recording and timely data transmission to the IDC in Vienna have led to increased reporting activities and implementation of new procedures for the NOR-NDC. The NOR-NDC carries out all the technical tasks required in support of Norway's treaty obligations. NORSAR will also carry out assessments of events of special interest, and advise the Norwegian authorities in technical matters relating to treaty compliance. A challenge for the NOR-NDC is to carry 40 years' experience over to the next generation of personnel.

4.1.1   Verification functions; information received from the IDC

After the CTBT enters into force, the IDC will provide data for a large number of events each day, but will not assess whether any of them are likely to be nuclear explosions. Such assessments will be the task of the States Parties, and it is important to develop the necessary national expertise in the participating countries. An important task for the NOR-NDC will thus be to make independent assessments of events of particular interest to Norway, and to communicate the results of these analyses to the Norwegian Ministry of Foreign Affairs.

4.1.2   Monitoring the Arctic region

Norway will have monitoring stations of key importance for covering the Arctic, including Novaya Zemlya, and Norwegian experts have a unique competence in assessing events in this region. On several occasions in the past, seismic events near Novaya Zemlya have caused political concern, and NORSAR specialists have contributed to clarifying these issues.

4.1.3   International cooperation

After entry into force of the treaty, a number of countries are expected to establish national expertise to contribute to the treaty verification on a global basis. Norwegian experts have been in contact with experts from several countries with the aim of establishing bilateral or multilateral cooperation in this field.

4.1.4   NORSAR event processing

The automatic routine processing of NORSAR events as described in NORSAR Sci. Rep. No. 2-93/94, has been running satisfactorily. The analyst tools for reviewing and updating the solutions have been continually modified to simplify operations and improve results. NORSAR is currently applying teleseismic detection and event processing using the large-aperture NOA array, as well as regional monitoring using the network of small-aperture arrays in Fennoscandia and adjacent areas.

4.1.5   Communication topology

Norway has implemented an independent subnetwork, which connects the IMS stations AS72, AS73, PS28, and RN49 operated by NORSAR to the GCI at the NOR-NDC. A contract has been concluded and VSAT antennas have been installed at each station in the network. Under the same contract, VSAT antennas for 6 of the PS27 subarrays have been installed for intra-array communication. The seventh subarray is connected to the central recording facility via a leased land line. The central recording facility for PS27 is connected directly to the GCI (Basic Topology). All VSAT communication is functioning satisfactorily. As of 10 June 2005, AS72 and RN49 are connected to the NOR-NDC through a VPN link.

Jan Fyen

4.2   Status Report: Provision of Data from Norwegian Seismic IMS Stations to the IDC

4.2.1   Introduction

This contribution is a report for the period January – June 2013 on activities associated with provision of data from Norwegian seismic IMS stations to the International Data Centre (IDC) in Vienna. This report represents an update of contributions that can be found in previous editions of NORSAR's Semiannual Technical Summary. All four Norwegian seismic stations providing data to the IDC have been formally certified.

4.2.2   Norwegian IMS stations and communications arrangements

During the reporting interval, Norway has provided data to the IDC from the four seismic stations shown in Fig. 4.2.1. PS27 — NOA is a 60 km aperture teleseismic array, comprising of 7 subarrays, each containing five vertical broadband sensors and one three-component hybrid broadband instrument. PS28 — ARCES is a 25-element regional array with an aperture of 3 km, whereas AS72 — Spitsbergen array (station code SPITS) has 9 elements within a 1-km aperture. AS73 — JMIC has a single three-component broadband instrument.

The intra-array communication for NOA utilizes a land line for subarray NC6 and VSAT links based on iDirect technology for the other 6 subarrays. The central recording facility for NOA is located at the Norwegian National Data Center (NOR-NDC).

Continuous ARCES data are transmitted from the ARCES site to the NOR-NDC using the same iDirect network as NOA.

Continuous SPITS data are transmitted to NOR-NDC via the central recording facility (CRF) for the SPITS array at the University Centre in Svalbard (UNIS). Data from the array elements to the CRF are transmitted via a 2.4 Ghz radio link (Wilan VIP-110). A 512 Kbps SHDSL link has been established between UNIS and NOR-NDC. Both AS72 and RN49 data are now transmitted to NOR-NDC over this link using VPN technology.

A minimum of 14-day station buffers have been established at the ARCES and SPITS sites and at all NOA subarray sites, as well as at the NOR-NDC for ARCES, SPITS and NOA. In addition, each individual site of the SPITS array has a 14-day buffer.

The NOA and ARCES arrays are primary stations in the IMS network, which implies that data from these stations are transmitted continuously to the receiving International Data Centre. Since October 1999, these data have been transmitted (from NOR-NDC) via the Global Communications Infrastructure (GCI) to the IDC in Vienna. Data from the auxiliary array station SPITS — AS72 have been sent in continuous mode to the IDC during the reporting period. AS73 — JMIC is an auxiliary station in the IMS, and also this station is transmitted in continuous mode to the IDC. In addition, continuous data from all three arrays are transmitted to the US_NDC under a bi-lateral agreement.

NORSAR also provides broadband data from Norwegian IMS stations to ORFEUS and IRIS.

4.2.3   Uptimes and data availability

Figs. 4.2.2 and 4.2.3 show the monthly uptimes for the Norwegian IMS primary stations ARCES and NOA, respectively, for the reporting period given as the red (taller) bars in these figures. These barplots reflect the percentage of the waveform data that is available in the NOR-NDC data archives for these two arrays. The downtimes inferred from these figures thus represent the cumulative effect of field equipment outages, station site to NOR-NDC communication outage, and NOR-NDC data acquisition outages.

Figs. 4.2.2 and 4.2.3 also give the data availability for these two stations as reported by the IDC in the IDC Station Status reports. The main reason for the discrepancies between the NOR-NDC and IDC data availabilities as observed from these figures is the difference in the ways the two data centers report data availability for arrays: Whereas NOR-NDC reports an array station to be up and available if at least one channel produces useful data, the IDC uses weights where the reported availability (capability) is based on the number of actually operating channels.

4.2.4   NOR-NDC automatic processing and data analysis

These tasks have proceeded in accordance with the descriptions given in Sci. Rep. No. 2-95/96 (Mykkeltveit and Baadshaug). For the reporting period NOR-NDC derived information on 293 events and submitted this information to the Finnish NDC as the NOR-NDC contribution to the Bulletin of seismic events in northern Europe. These events are plotted in Fig. 4.2.4.

4.2.5   Current developments and future plans

NOR-NDC is continuing the efforts towards improving and hardening all critical data acquisition and data forwarding hardware and software components, so as to meet the requirements related to operation of IMS stations.

The NOA array was formally certified by the PTS on 28 July 2000, and a contract with the PTS in Vienna currently provides partial funding for operation and maintenance of this station. The ARCES array was formally certified by the PTS on 8 November 2001, and a contract with the PTS is in place which also provides for partial funding of the operation and maintenance of this station. The operation of the two IMS auxiliary seismic stations on Norwegian territory (Spitsbergen and Jan Mayen) is funded by the Norwegian Ministry of Foreign Affairs. Provided that adequate funding continues to be made available (from the PTS and the Norwegian Ministry of Foreign Affairs), we envisage continuing the provision of data from all Norwegian seismic IMS stations without interruption to the IDC in Vienna.

The PS27 - NOA equipment was recapitalized during 2010-2012, and has been revalidated. The PS28 - ARCES equipment was acquired in 1999, and it is no longer possible to get spare digitizers. A recapitalization plan for the array was submitted to the PTS in October 2008, and development and testing of specific equipment for that array are ongoing.

U. Baadshaug
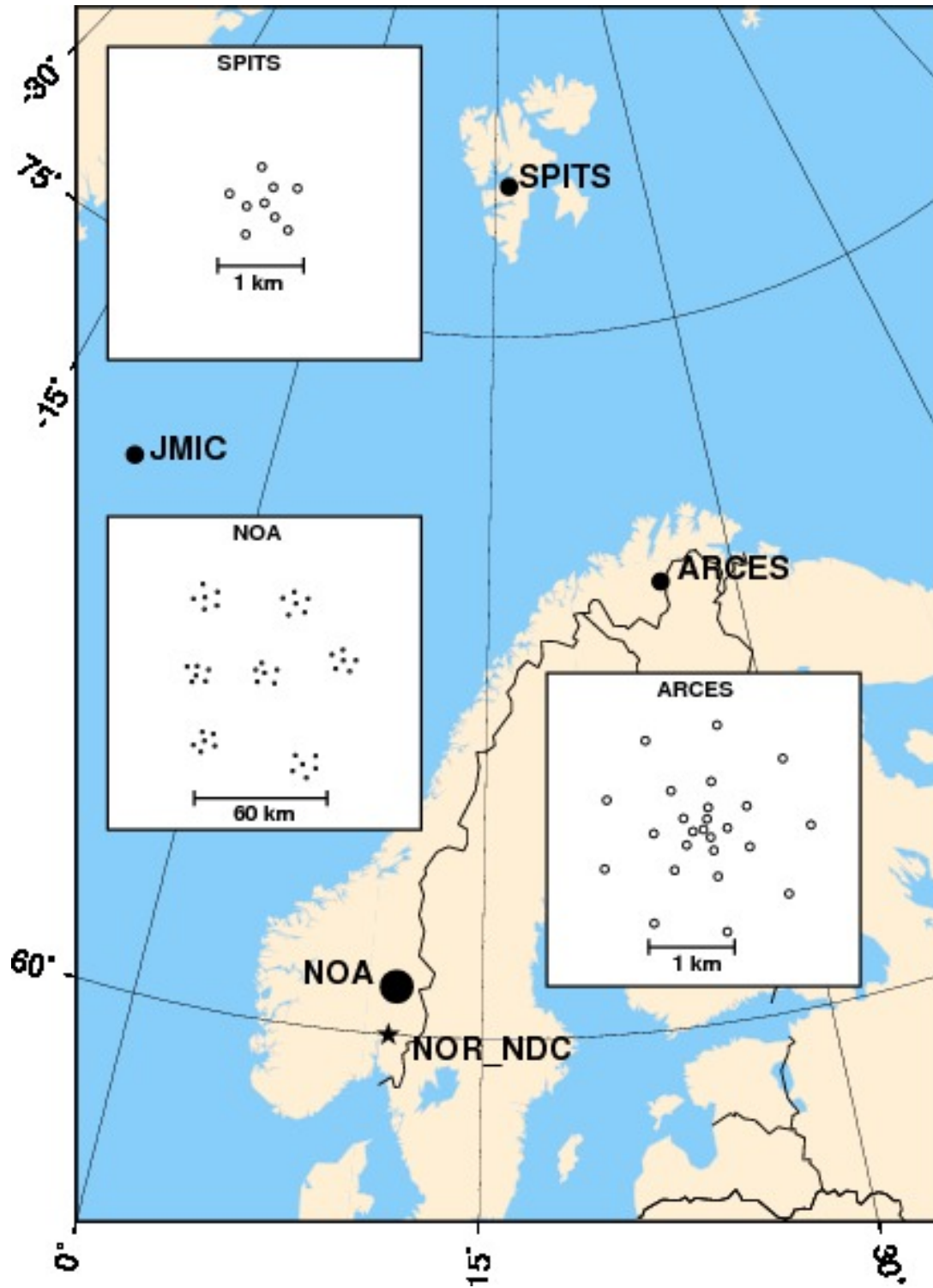**S. Mykkeltveit**
J. Fyen

Fig. 4.2.1. The figure shows the locations and configurations of the three Norwegian seismic IMS array stations that provided data to the IDC during the period January – June 2013. The data from these stations and the JMIC three-component station are transmitted continuously and in real time to the Norwegian NDC (NOR-NDC). The stations NOA and ARCES are primary IMS stations, whereas SPITS and JMIC are auxiliary IMS stations.
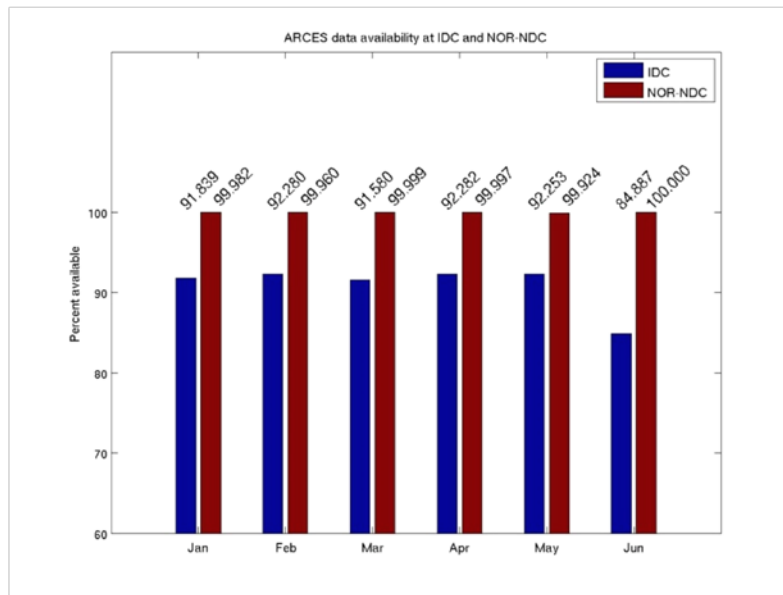
*Fig. 4.2.2   The figure shows the monthly availability of ARCES array data for the period January –
June 2013 at NOR-NDC and the IDC. See the text for explanation of differences in
definition of the term "data availability" between the two centers.*
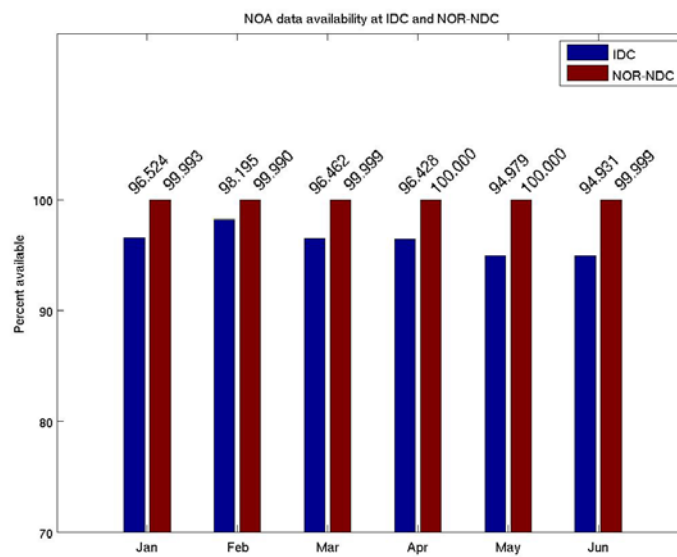
*Fig. 4.2.3   The figure shows the monthly availability of NORSAR array data for the period January –
June 2013 at NOR-NDC and the IDC. See the text for explanation of differences in
definition of the term "data availability" between the two centers.*

Reviewed Supplementary events

Fig. 4.2.4   The map shows the 293 events in and around Norway contributed by NOR-NDC during January – June 2013 to the Bulletin of seismic events in northern Europe compiled by the Finnish NDC. The map also shows the main seismic stations used in the data analysis to define these events.

4.3   Field Activities

The activities at the NORSAR Maintenance Center (NMC) at Hamar currently include work related to operation and maintenance of the following IMS seismic stations: the NOA teleseismic array (PS27), the ARCES array (PS28) and the Spitsbergen array (AS72). Some work has also been carried out in connection with the seismic station on Jan Mayen (AS73), the radionuclide station at Spitsbergen (RN49), and preparations for the infrasound station IS37. NORSAR also acts as a consultant for the operation and maintenance of the Hagfors array in Sweden (AS101).

NORSAR carries out the field activities relating to IMS stations in a manner generally consistent with the requirements specified in the appropriate IMS Operational Manuals, which are currently being developed by Working Group B of the Preparatory Commission. For seismic stations these specifications are contained in the Operational Manual for Seismological Monitoring and the International Exchange of Seismological Data (CTBT/WGB/TL-11/2), currently available in a draft version.

All regular maintenance on the NORSAR field systems is conducted on a one-shift-per-day, five-day-per-week basis. The maintenance tasks include:

- Operating and maintaining the seismic sensors and the associated digitizers, authentication devices and other electronics components.

- Maintaining the power supply to the field sites, as well as backup power supplies.

- Operating and maintaining the VSATs, the data acquisition systems and the intra-array data transmission systems.

- Assisting the NDC in evaluating the data quality and making the necessary changes in gain settings, frequency response and other operating characteristics as required.

- Carrying out preventive, routine and emergency maintenance to ensure that all field systems operate properly.

- Maintaining a computerized record of the utilization, status, and maintenance history of all site equipment.

- Providing appropriate security measures to protect against incidents such as intrusion, theft and vandalism at the field installations.

Details of the daily maintenance activities are kept locally. As part of its contract with CTBTO/PTS, NORSAR submits, when applicable, problem reports, outage notification reports and equipment status reports. The contents of these reports and the circumstances under which they will be submitted are specified in the draft Operational Manual.

P.W. Larsen
K.A. Løken

5   Documentation Developed

Antonovskaya, G., Y. Konechnaya, E.O. Kremenetskaya, V. Asming, T. Kværna, J. Schweitzer, M. Pirli and F.Ringdal (2013). Seismological Research Related to Geophysical Processes in the European Arctic. In: Semiannual Technical Summary, 1 January – 30 June, 2013, NORSAR, Kjeller, Norway.

Bormann, P., D. A. Storchak & J. Schweitzer (2013). IS 2.1: The IASPEI standard nomenclature of seismic phases. http://ebooks.gfz-potsdam.de/pubman/item/escidoc:43265:5; doi: 10.2312/GFZ.NMSOP-2_IS_2.1; 20 pp. In: P. Bormann (ed.) (2012), New Manual of Seismological Observatory Practice (NMSOP-2). 2nd (revised) edition, Potsdam: Deutsches GeoForschungsZentrum GFZ, doi: 10.2312/GFZ.NMSOP-2.

Bormann, P., K. Aki, W.H.K. Lee & J. Schweitzer (2012). Glossary of interest to earthquake and engineering seismologists. http://ebooks.gfz-otsdam.de/pubman/item/escidoc:217068:2; DOI: 10.2312/GFZ.NMSOP-2_Glossary, 196 pp. In: P. Bormann (Ed.), New Manual of Seismological Observatory Practice 2 (NMSOP 2) 2nd (revised) edition, Potsdam: Deutsches GeoForschungsZentrum GFZ, doi: 10.2312/GFZ.NMSOP-2.

Cristiano, L., J. Schweitzer and T. Meier (2013). P-wave Polarization and FK Analysis of NORSAR Array Data to Investigate Local Anisotropy and Lateral Heterogeneity. In: Semiannual Technical Summary, 1 January – 30 June, 2013, NORSAR, Kjeller, Norway.

Junek, W.N., T. Kværna, M. Pirli, D.B. Harris, J. Schweitzer and M.T. Woods (2013). Examination of the Storfjorden Aftershock Sequence Using an Autonomous Event Detection and Grouping Framework: Preliminary Results. In: Semiannual Technical Summary, 1 January – 30 June, 2013, NORSAR, Kjeller, Norway.

Labonne, C., T. Kværna and M. Roth (2013). An Application of Coda Envelopes for Estimation of Stable Event Magnitudes in Southern Norway. In: Semiannual Technical Summary, 1 January – 30 June, 2013, NORSAR, Kjeller, Norway.

Kværna, T., J. Schweitzer, M. Pirli and M. Roth (2013). Detection Capability of the Seismic Station TROLL in Antarctica. In: Semiannual Technical Summary, 1 January – 30 June, 2013, NORSAR, Kjeller, Norway.

Pirli, M., J. Schweitzer & B. Paulsen (2013). The Storfjorden, Svalbard, 2008 – 2012 aftershock sequence: Seismotectonics in a polar environment. Tectonophysics, 601, 192–205, doi:10.1016/j.tecto.2013.05.010.

6   Technical Reports / Papers Published

6.1   An Application of Coda Envelopes for Estimation of Stable Event Magnitudes in Southern Norway

6.1.1   Introduction: motivation and study area

In seismology, applications like the determination of seismic hazard require accurate and reliable magnitude estimates. Previous studies (*e.g.*, Ringdal, 1983; Ringdal and Hokland, 1987; Mayeda and Walter, 1996) have shown that coda amplitude measurements have significantly less variability than measurements of direct wave amplitudes. This property of coda permits an alternative approach in magnitude estimation. It has been demonstrated in several papers (e.g., Mayeda et al., 2003; Eken et al., 2004; Morasca et al., 2005; Morasca et al., 2008) that stable estimates of source moment spectra can be derived from regional coda envelopes observed at only 1-3 stations.

The objective of this study is to test the coda-based method for magnitude estimation at regional distances using broadband and short-period stations located in Norway. Initially, we address the NORSAR array (NOA), which when calibrated, could permit re-estimation of event magnitudes based on coda derived moment source spectra for the large number of events found in its digital archive. Furthermore, two additional stations (BER and AKN) are calibrated in order to evaluate the consistency of our results.

Coda techniques were first developed for local network data using the late coda. This allowed the coda wavefield to homogenize and therefore to be less dependent on a particular travel path and to be less sensitive to source radiation effects. However at regional distances the late coda is measurable only for large events. Mayeda et al., 2003 developed a new technique to analyze coda at regional distance by measuring earlier sections of the coda by introducing corrections for distance dependence effects. Our methodology is mainly based on the "Mayeda" method and consists of the following calibration steps: coda window selection, coda shape calibration, distance normalization, site-response correction using the smaller events as Green's functions, and conversion of the non-dimensional spectra to absolute source spectra using independent moment estimates for the largest events.

In this study, the three stations AKN, BER and NOA are calibrated (see Fig. 6.1.1). Our data set consists mainly of small events with local magnitudes between 1.5 and 3.5 located in the western part of southern Norway (see Appendix for event characteristics). From 2009, seventeen of the largest events had independent seismic moment magnitude estimates reported in the University of Bergen seismic event catalog ($M_W(BER)$).
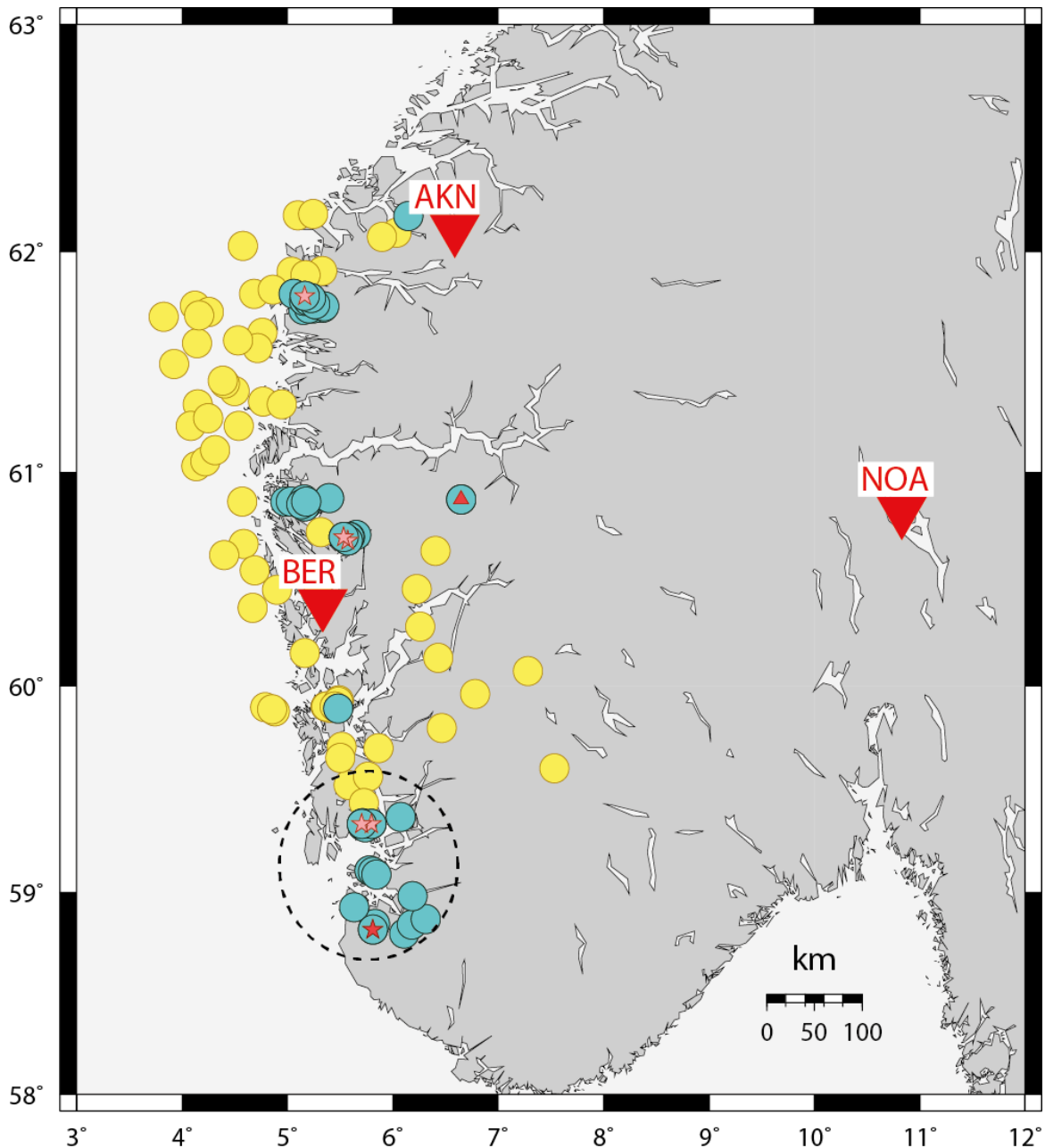
Fig 6.1.1   Stations (red inverted triangles) and events (filled circles) used in this study. BER and AKN are two single broadband stations, and NOA is an array of short period and broadband stations. Yellow circles correspond to events with normal coda derived source spectra and blue circles to events with anomalous coda derived source spectra. See section 6.1.3 for more details. Small symbols inside the filled circles correspond to events which were reported to be landsides (red triangles), or, confirmed (red stars) and probable explosions (pink stars) according to the University of Bergen catalog. The dotted circle in southwestern Norway indicate an area where we had selected a few events for comparison of spectra from explosions and earthquakes (see Fig. 6.1.9).

6.1.2   Methodology

6.1.2.1 **Formation** *of coda envelopes*

The raw data is converted into ground velocity. Then coda envelopes for 12 narrow frequency bands are formed using the equation below:

$$Env(fi, t) = |(x_{fi}(t) + i \times H(x_{fi}(t))| \tag{1}$$

where fi is the center frequency of narrow frequency bands, t the time relative to the origin, x_{fi} the filtered seismogram and H its Hilbert transform.

The envelopes are smoothed with a Hanning window using the envelope parameters given in Table 6.1.1. To provide smoother envelopes, it is possible to stack the envelopes from short-period array stations. That is why we choose in this study to stack the envelopes of the 6 vertical-component sensors of sub-array NB2 to represent the coda of the large-aperture NORSAR (NOA) array. An example of smoothed coda envelopes at NB2 is shown in Fig. 6.1.2.
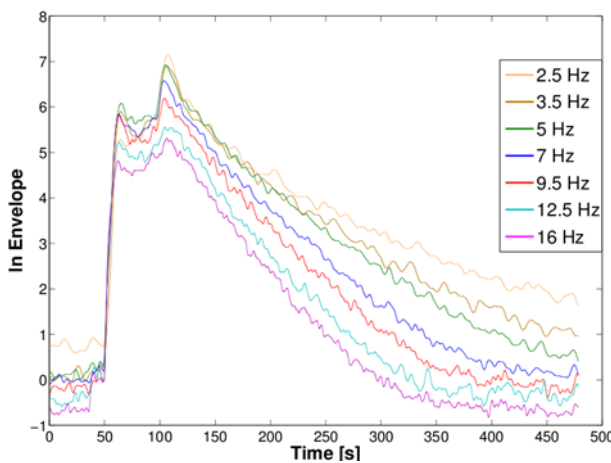
Fig. 6.1.2
Example of selected observed NOA narrowband envelopes of a magnitude 3 earthquake occurring on 22 March 2013, located at a distance of 350 km from the station (see event information in the Appendix). We can see strong frequency dependency in the shape of the coda envelopes. That is why we must define the parameters of the coda shape as a function of frequency.

The analytic expression of the narrowband coda envelopes that we used to fit with the observed ones is defined as follows (Mayeda *et al.*, 2003)**:**

$$A(f_i, t, r) = W(f_i)S(f_i) \overbrace{P(f_i, r) \underbrace{(t - t_S)^{-\gamma} e^{b(f_i)(t - t_S)}}_{\text{Coda Shape function}}}^{\text{Propagation term}} H(t - t_s) \tag{2}$$

where f_i is the center frequency of the narrowband envelope, t the time from origin, r the epicentral distance, t_S the direct S-wave travel time, γ and b the coda shape parameters, H the Heaviside function, $W(f_i)$ the S-wave source amplitude, $S(f_i)$ the site response and $P(f_i, r)$ the distance effect. To obtain the source spectra, we remove all the propagation and site effects over all frequency bands.

Table 6.1.1 Coda calibration parameters

Envelopes parameters				Shape parameters			Normalization	Site response correction parameter			Moment conversion parameter		
					b				ln(S)			M_p	
Fi (Hz)	Width (Hz)	Smoother Width (s)	γ	AKN	BER	NOA	Tnorm (s)	AKN	BER	NOA	AKN	BER	NOA
0.4	0.2	32	0.5	-	-	-	500	-	-	-	20.25	20.97	20.18
0.6	0.2	26	0.5	-	-	-	500	-	-	-	20.25	20.97	20.18
0.85	0.3	22	0.5	-0.0059	-0.0098	-0.0044	500	0	0	0	20.25	20.97	20.18
1.25	0.5	18	0.5	-0.0071	-0.0028	-0.0072	500	-0.282	3.067	-0.610	20.25	20.97	20.18
1.75	0.5	15	0.5	-0.0078	-0.0093	-0.0073	500	-0.537	0.562	-0.623	20.25	20.97	20.18
2.5	1	13	0.5	-0.0098	-0.0065	-0.0091	500	-0.964	2.063	-0.879	20.25	20.97	20.18
3.5	1	11	0.5	-0.0123	-0.0121	-0.0110	500	-1.766	-0.063	-1.607	20.25	20.97	20.18
5	2	9	0.5	-0.0173	-0.0137	-0.0131	500	-2.982	-0.407	-2.176	20.25	20.97	20.18
7	2	8	0.5	-0.0189	-0.0158	-0.0153	500	-3.249	-1.161	-3.176	20.25	20.97	20.18
9.5	3	6	0.5	-0.0202	-0.0150	-0.0169	500	-3.602	-0.603	-3.825	20.25	20.97	20.18
12.5	3	6	0.5	-0.0203	-0.0187	-0.0179	500	-4.347	-2.353	-4.471	20.25	20.97	20.18
16	4	5	0.5	-0.0233	-0.0181	-0.0185	500	-5.708	-2.145	-4.829	20.25	20.97	20.18

6.1.2.2   Coda window selection

The analytic expression of the coda envelope given in equation (2) is defined for times greater than the direct S-wave arrival t_S. In order to automatically align the observed and synthetic envelopes, we define the time of the direct S-wave arrival t_S as the time identified by the envelope's peak amplitude. This definition of the direct S-wave arrival associates the coda with different phases, most often the L_g phase, but also the S_n phase (see Fig. 6.1.3).

As we expect a group velocity for S waves (L_g, S_n) around 3.5 km/s, we look for the envelope's peak amplitude in the time interval where the group velocity is between 2 and 4 km/s. Then, the coda window is selected manually for each frequency. But pre-selected extreme limits are defined for helping the user: the default left limit of the coda window corresponds to the direct S-wave arrival and the default right limit is when the signal to noise ratio is falling below a predefined threshold.
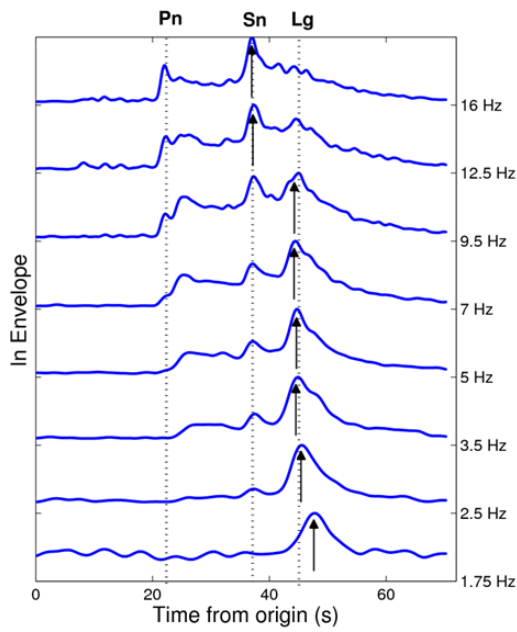
Fig. 6.1.3
Example of selected narrowband envelopes of a magnitude 2 earthquake recorded by NOA. The event occurred on 25 December 2011 at a distance of 380 km from the station (see Appendix). The arrows show the envelope peak amplitude for each frequency. We can note the shift from L_g to S_n coda for the higher frequencies.

6.1.2.3   Create Synthetic envelopes: coda shape calibration, distance normalization

a) Coda shape Parameter

By taking the logarithm of equation (2) we obtain for a fixed frequency f_i:

$$\ln(A(f_i,t,r)(t-t_S)^y) = \underbrace{\ln(W(f_i)\,S(f_i)P(f_i,r))}_{\textbf{Time independent}} + b(t-t_S) \tag{3}$$

Thus, we can obtain b by linear regression by fixing ɣ. Aki and Chouet (1975) showed that the difficulty to exactly define when the coda window starts explains the erratic behavior of the coefficient ɣ when it is estimated from the data. That is why we chose to fix ɣ instead of estimating it from the data by using a grid-search. Aki and Chouet (1975) suggest two extreme models of coda waves: a single scattering model (ɣ = 0.5 or 1 for surface wave or body wave) and a diffusive model (ɣ = 0.75). According to the regional distances in this study (100-400km) we expect more surface waves, so we chose to fix ɣ = 0.5.
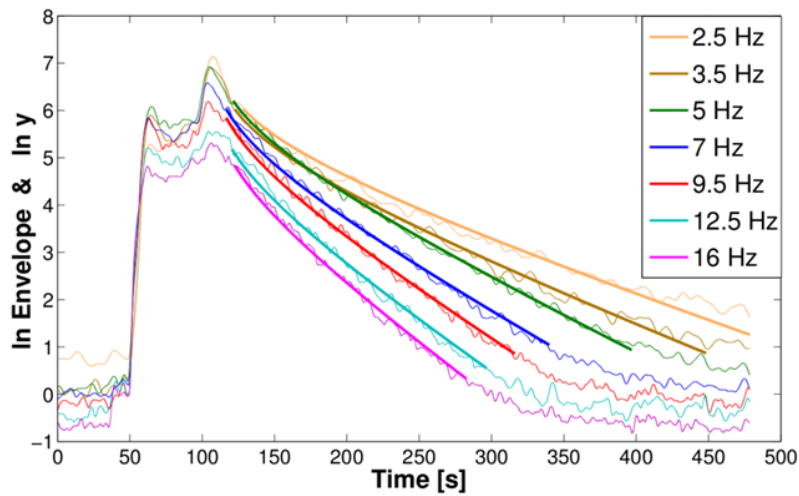
Fig. 6.1.4
Example of selected observed narrowband envelopes (thin lines) of the magnitude 3 earthquake recorded at NOA (see also Fig. 6.1.2). Bold lines show synthetic coda shape fits using equation (3):
$$ln\, y = -ɣ\; ln(t - t_S) + b(t - t_S) + ln(WSP)$$

Fig. 6.1.4 shows an example of coda envelopes of an event used for the calibration with the associated synthetic coda shape estimated by linear regression for ɣ equal to 0.5. We can now determine the coda shape parameters as a function of frequency for the selected region by simply averaging the estimated coda shape parameters from a subset of events. Table 6.1.1 gives the estimated coda shape parameters for the studied area. We chose events which had independent seismic moment magnitude estimates in order to have the same subset for each step of the calibration, and also because these events have a good signal-to-noise ratio.

b) Distance normalization

At this point, we have determined the coda shape function. The near-regional coda energy appears to be homogeneously distributed. Fig 6.1.5.a illustrates this by using three events which have approximately the same magnitude (2.2<M_L<2.3), but being located at different distances from the recording station AKN, i.e., 120 km, 180 km and 250 km, respectively. The observed coda envelopes attain roughly the same level and shape at larger lapse times. However, the coda shape functions shown in Fig. 6.1.5.b show different amplitude levels, revealing a distance-dependence. The two approaches for estimating distances corrections proposed by Mayeda *et al*. (2003), using a source normalization or a simultaneous grid search, are not feasible. This is because we do not have a sufficiently large number of events in our database with a narrow magnitude range spanning a range of distances, or common events observed at two stations that span a range of distances. We therefore decided to use the observation at large lapse times to correct the synthetic envelopes coda for distance dependence. We simply normalize the synthetic envelopes at a fixed large lapse time (500 seconds) in order to overlay the envelopes at large lapse time and mimic the real behavior as proposed by Morasca *et al.* (2005). The distance normalized envelopes are shown in Fig. 6.1.5.c.
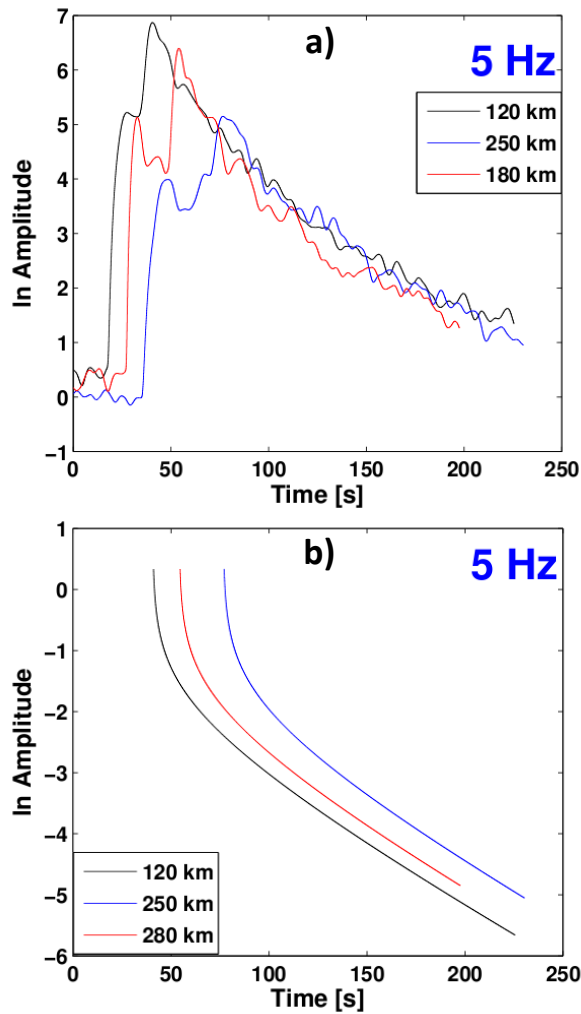
Fig. 6.1.5
(a) Observed envelopes of three events recorded at AKN having approximately the same magnitudes (2.2<M_L<2.3), but being located at different epicentral distances (120km, 180km and 250km). We observe that at large lapse time the coda envelopes converge to the same level. (b) Coda shape function for these three events. We see that they do not have the same amplitude level, revealing a distance-dependence. (c) Synthetic envelopes after distance normalization.

c) Coda amplitude measurement

The distance corrected synthetic envelopes are then used to measure the coda amplitude of the observed envelopes by vertically shifting the synthetics until they fit the observed ones.

6.1.2.4   Site response correction

At this point, we can measure distance-corrected coda amplitude from narrowband envelopes, which includes both the source and site effects. So, we need to correct the amplitude measurement by the site effect to obtain the source term. We used the procedure outlined by Mayeda *et al.* (2003) which assumes that the S-wave source spectrum is flat below the corner frequency (see Fig. 6.1.6). The corner frequency for each event is estimated according to local magnitudes in the Bergen catalog using a model of source spectrum for an input stress drop of 3 MPa.
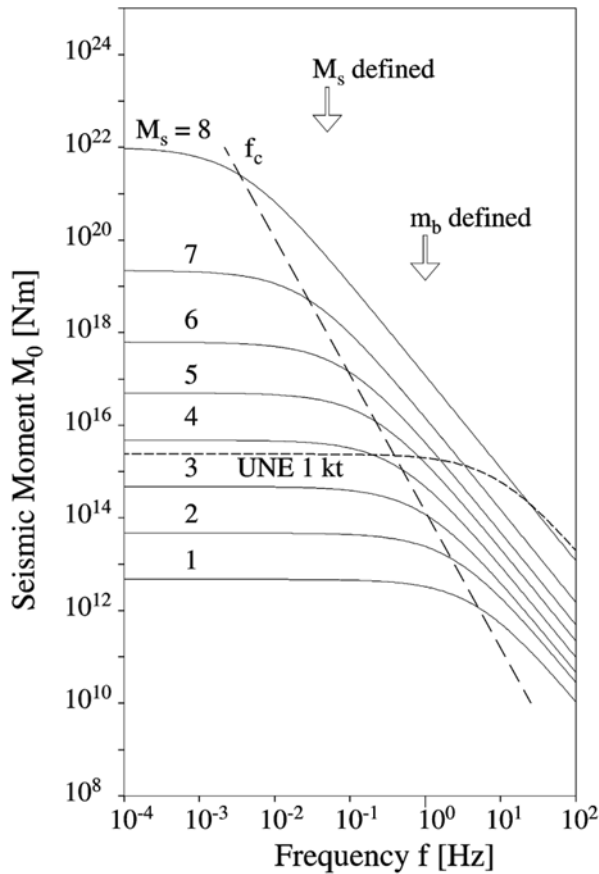
Fig. 6.1.6
Extracted from Bormann (2002). Source spectra of ground displacement for a seismic shear source for different magnitudes. Source spectra are characterized by a plateau of constant displacement spectral amplitudes for frequencies smaller than the corner frequency f_c and a decay of spectral displacement amplitude proportional to f^{-2} for frequencies above the corner frequency. The long-dashed line shows the increase of corner frequency with decreasing seismic moment of the event.

We apply a correction to each frequency band that flattens the portion of the source spectrum for frequencies below the estimated corner. Because of the increase of corner frequency with decreasing magnitude, the smaller events are used as empirical Green's functions to derive corrections for all events for each frequency. The corrections used to flatten the smaller events are also applied to the larger events (Fig. 6.1.7). We obtain after correction dimensionless coda-derived spectra.
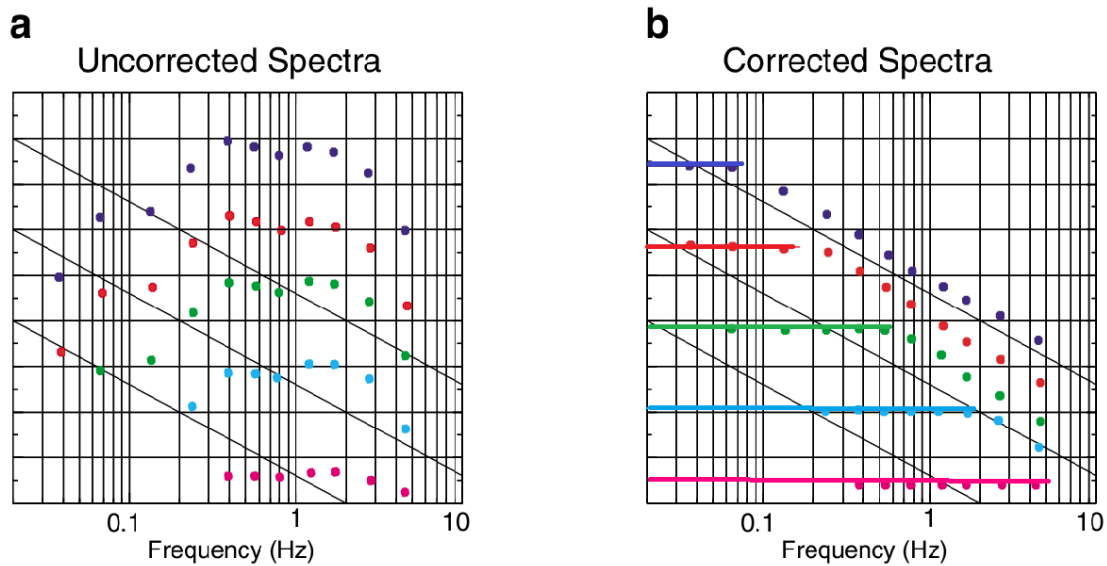
Fig. 6.1.7   Figure illustrating the site response correction (adopted from Mayeda at al., 2003). (a) Distance corrected coda amplitude before correction. (b) Distance corrected coda amplitude after correction. Bold solid lines show that the applied corrections flatten the portion of source spectrum for frequencies below the estimated corner frequency. The diagonal black lines have a slope proportional to f^{-2}. We assume that the coda amplitude decay fits this slope for frequencies above the corner frequency.

6.1.2.5   Tying the source spectra to an absolute scale

In order to tie our dimensionless spectra to an absolute scale, we use a linear relation between our dimensionless coda-derived moment A_0 (which is the mean value of distance-site effect corrected coda amplitude (*CorrAmp*) for frequencies below the estimated corner frequency f_c and the estimated seismic moment M_0 using independent moment magnitudes (M_w) given in the Bergen catalog:

$$\log_{10} A_0 = mean_{f_i < f_c}\left(\log_{10} CorrAmp(f_i)\right) \qquad \text{[Dimensionless units]} \qquad (4)$$

$$\log_{10} M_0 = \frac{3}{2}\left(M_w + 10.75\right) \qquad \text{[$\log_{10}$dyne-cm] [Hanks and Kanamori 1979]}$$

We obtain the moment conversion parameter M_p using our subset of 17 events with independently determined moments by simply matching the dimensionless coda derived moment $log_{10}A_0$ with the estimated seismic moment $log_{10}M_0$. The estimated M_p values are given in Table 6.1.1. Once we have obtained the coda derived source spectra, the seismic moment M_0 *(coda)* is estimated by averaging the measurements of the moment rate spectra for frequencies lower than the estimated corner frequency. And the coda moment magnitude M_w *(coda)* is then computed using the relation given by Hanks and Kanamori (1979):

$$M_w\left(coda\right) = \frac{2}{3}\log_{10} M_0\left(coda\right) - 10.75 \qquad (5)$$

6.1.3   Results

6.1.3.1   Coda wave stability

Fig. 6.1.8 shows direct S and coda waves interstation amplitudes before and after distance corrections. The interstation coda amplitude scatter is reduced after distance correction, which means that our distance normalization is a good approximation to the coda distance attenuation. Secondly, the distance corrected coda interstation standard deviation is usually lower than 0.1 whereas the direct-wave deviation is 3 to 4 times larger. This is consistent with previous studies (Morasca *et al.*, 2005; Mayeda and Walter, 1996).
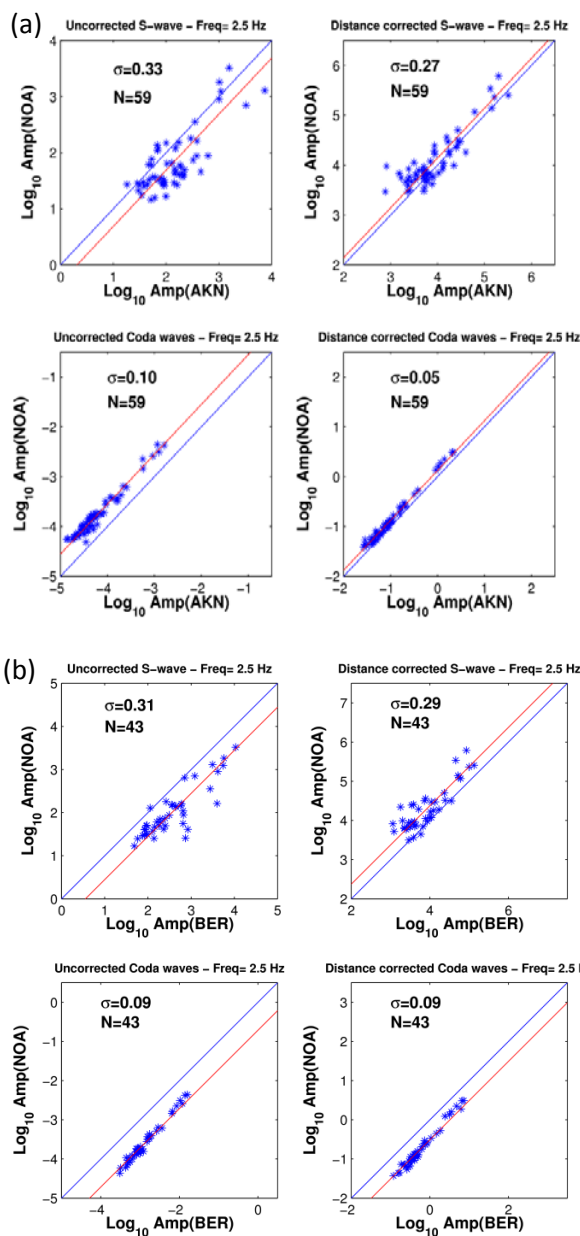

Fig 6.1.8
(a) Plots of amplitudes at station AKN versus amplitudes at NOA for the frequency band at 2.5 Hz. The left panels show the uncorrected distance amplitudes, and the right panels the distance corrected amplitudes. The top panels show the direct S-wave amplitudes and the bottom panels the coda amplitudes. Direct-wave amplitudes are corrected for distance using correction table provided by Båth et al. (1976). (b) Same as (a), but for station BER versus NOA. (c) Same as (a), but for station AKN versus BER. For each panel the associated standard deviation σ is computed using N events and takes into account the shift due to the site effect (shift between the blue and the red lines). Note the large variance reduction when coda measurements are used.

6.1.3.2   *Moment source spectra*

Fig. 6.1.9 shows the S-wave power spectral density of four selected events in our database, all recorded by the same station AKN. Each spectrum has been instrument corrected. These four events are located in the same area in southwestern Norway (see Fig. 6.1.1), so we expect similar attenuation and other path effects for all. The top panels show displacement spectra of a confirmed explosion and a confirmed earthquake and the bottom panels correspond to two events of unknown origin (as reported in the Bergen seismic bulletin). Here, we have a relatively good illustration of the difference of spectral shape between earthquakes and explosions. Note that our power spectral density is not corrected by the attenuation or other path effects. The earthquake source spectrum is clearly characterized by a plateau of constant spectral amplitudes (see Fig 6.1.9.b), whereas the explosion source spectrum (Fig 6.1.9.a) has a deficiency in the high frequency content as compared with the earthquake. According to this observation, one of the unknown events is therefore explosion like (Fig. 6.1.9.c), whereas the other unknown event is more earthquake like (Fig. 6.1.9.d).
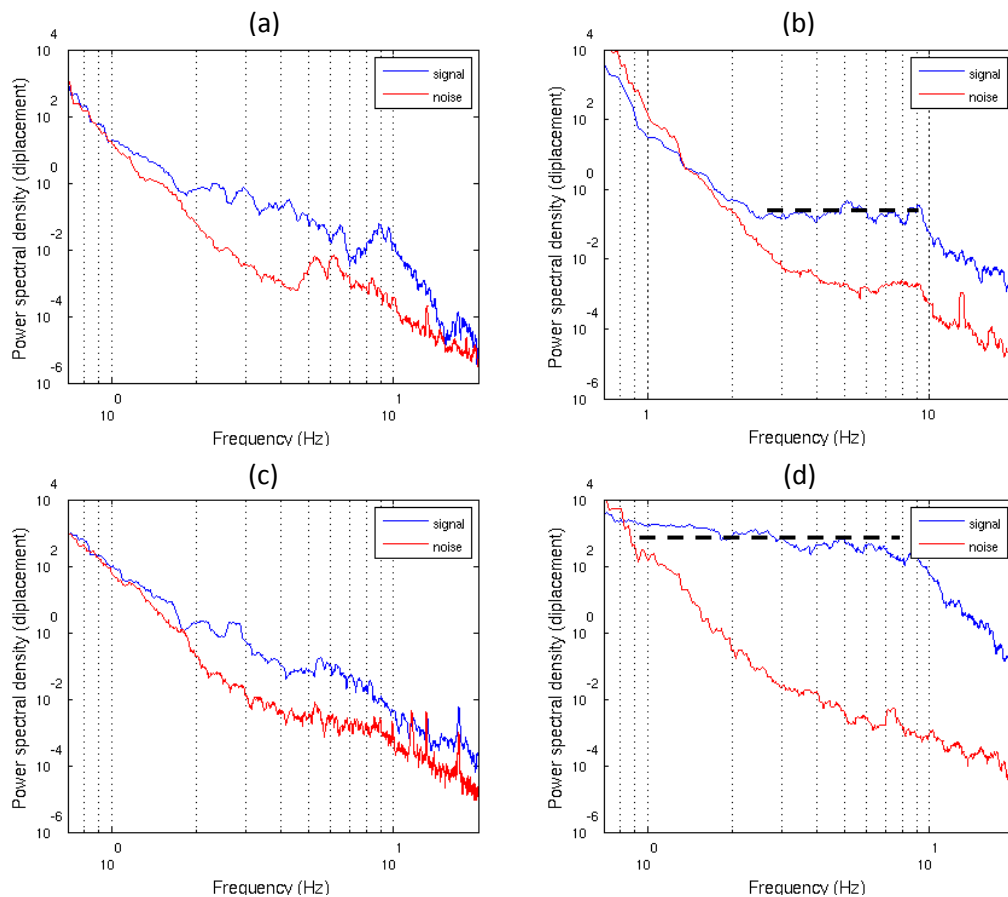

Fig 6.1.9   Power spectral density of S-wave and noise windows for four selected events which are all recorded by AKN and occurred in the same area marked by a dotted circle in Fig. 6.1.1. All spectra have been corrected for instrument response, but not corrected for attenuation or other path effects. (a) Spectrum of a confirmed explosion. (b) Spectrum of a confirmed earthquake. (c) Spectrum of a suspected explosions (occurring during working hours with a source depth less than 5 km). (d) Spectrum of a suspected earthquake (occurring at night with a source depth greater than 10 km and a magnitude larger than 3). The dotted lines indicate a typical spectral plateau for earthquakes.

Fig. 6.1.10 shows the coda derived source moment spectra at the three calibrated stations for all events listed in the Appendix. The site response corrections had been done twice, once using all events, and thereafter using only the events with earthquake-like ("normal") coda derived source moment spectra. The site response corrections are listed in Table 6.1.1.
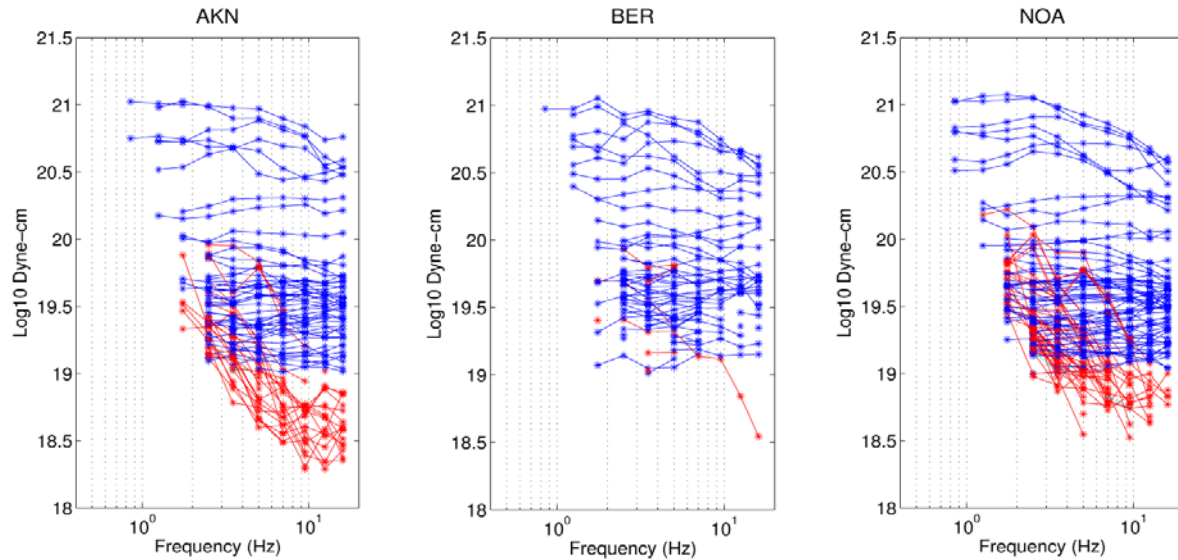

Fig. 6.1.10 Coda derived source moment spectra estimated at the three different stations AKN, BER and NOA. Blue lines correspond to earthquake-like ("normal") spectra and red lines to explosion-like ("anomalous") spectra. The site response corrections are estimated using only selected events with "normal" spectra in order to remove bias introduced by man-made events.

In Fig. 6.1.11, a number of coda-derived source moment spectra from common events are placed on top of each other showing the consistency of the estimates at the three stations.
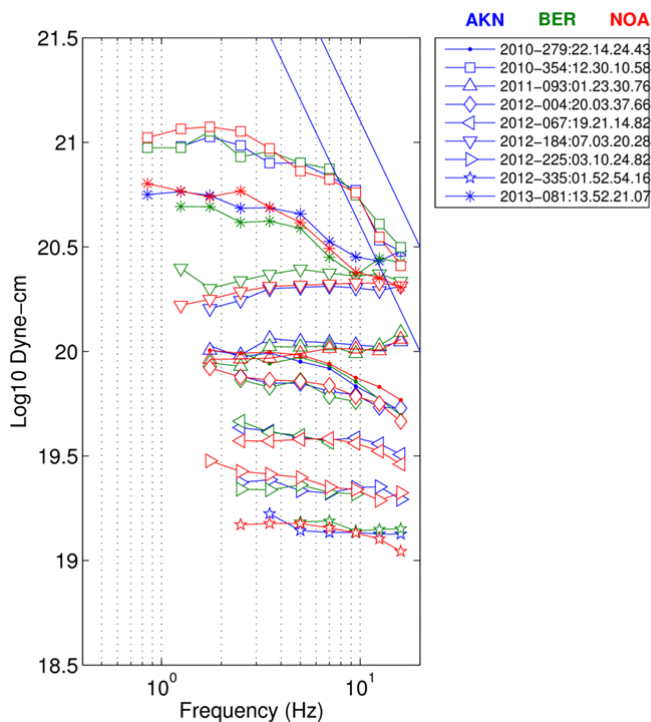

Fig 6.1.11
Example of coda derived source moment spectra for common events at three different stations AKN (blue), BER (green) and NOA (red). Diagonal blue lines have a slope proportional to f^{-2}. Note that the estimates of the source spectrum at each of the three stations are very consistent for each of the events.

6.1.3.3   Coda magnitude

The coda magnitude estimates from the three stations ($M_w(coda\text{-}AKN)$, $M_w(coda\text{-}BER)$ and $M_w(coda\text{-}NOA)$) are listed for each event listed in the Appendix. Notice that for a number of events it was not possible to do the coda analysis because of low signal-to-noise ratio or data quality problems at the recording station. For the station AKN data were not available before November 2009. Fig. 6.1.12 shows that $M_w(coda)$ estimates from different stations are in good agreement with interstation standard deviations below 0.15. This study shows very promising results for events larger than 2.25. We can see a larger scatter for the smaller events due to the fact that the coda length is shorter for these events. Mayeda *et al.* (2003) studied the dependence of coda length window with the amplitude measurement error. They show that the interstation scatter increases when using increasingly shorter window lengths and becomes quickly asymptotic to those of the direct waves as the window length approach the direct arrival. In any case the scatter for the smaller events will not be larger than the scatter we could have using the direct waves.

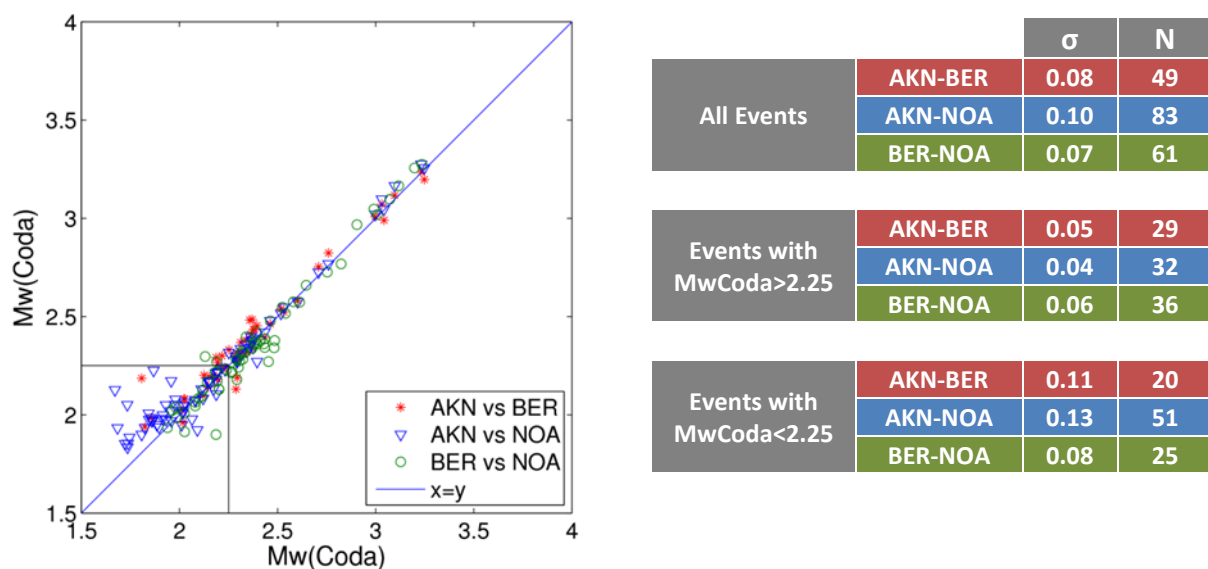|		σ	N
All Events	**AKN-BER**	0.08	49
	AKN-NOA	0.10	83
	BER-NOA	0.07	61
Events with MwCoda>2.25	**AKN-BER**	0.05	29
	AKN-NOA	0.04	32
	BER-NOA	0.06	36
Events with MwCoda<2.25	**AKN-BER**	0.11	20
	AKN-NOA	0.13	51
	BER-NOA	0.08	25

Fig. 6.1.12   Interstation scatter plot between stations AKN, BER and NOA obtained by plotting estimated moment magnitude from our coda-derived source spectra. The associated standard deviation σ is computed using N events.

6.1.3.4   Events with anomalous spectra

The locations of events used in this study (yellow and blue filled circles) as well as the location of all probable and confirmed explosions reported in the Bergen catalog (stars) since 2009 are shown in Fig. 6.1.13. We note that most of events with anomalous coda derived source spectra (blue circles) are located in areas where explosions occur frequently. This is a strong indication that most of these "anomalous events" are man-made.
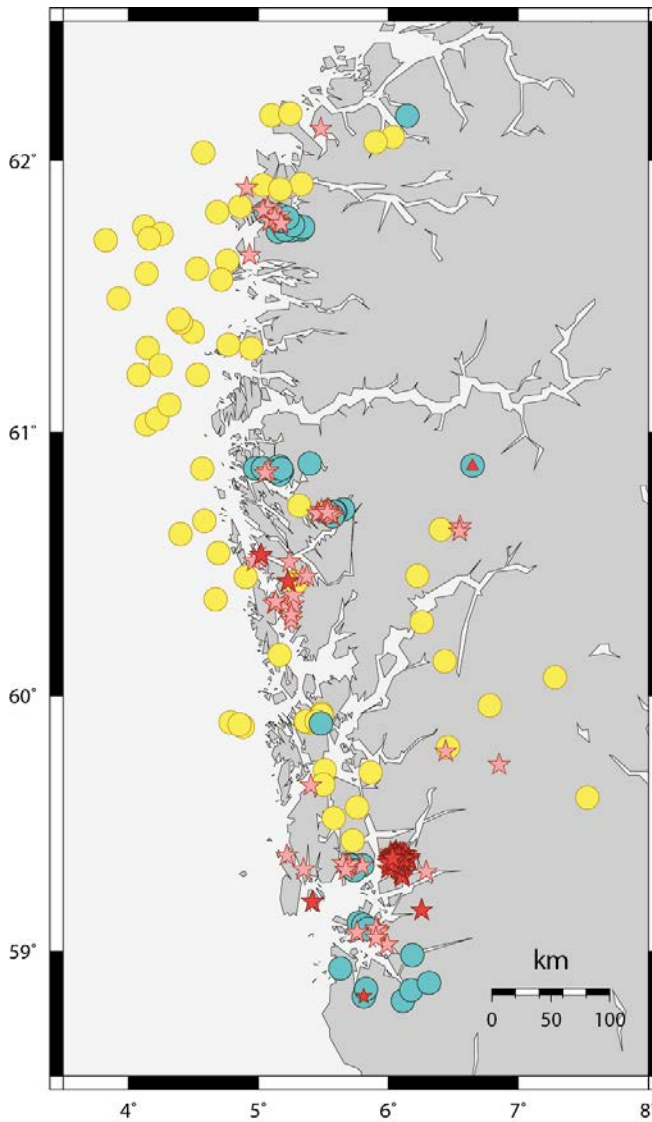
Fig. 6.1.13
Events (filled circles) used in this study. Yellow circles correspond to events with normal coda-derived source spectra and blue circles to events with anomalous coda-derived source spectra. Small red triangles correspond to reported landslides. Pink and red stars, respectively, correspond to all probable and confirmed explosions since 2009 as reported in the Bergen catalog, also including events not used in this study. Notice that the basis for our study was events reported in the NORSAR catalog which is less complete than the Bergen catalog. Also note that most of events with anomalous coda derived source spectra are located in areas where explosions occur frequently.

In order to further investigate the events with anomalous spectra, we have made time-of-day histograms of events used in this study, and of events since 2009 located in the same area as reported in the Bergen catalog (see Fig. 6.1.14). We first notice by separating out the explosions (yellow) an increase in the number of remaining events during the working hours, which means that our dataset as well as the Bergen catalog contain unidentified man-made events. We also notice from Fig. 6.3.14.a that the number of events with normal spectra remains relatively constant during all hours of the day whereas the events with anomalous spectra occur almost only during working hours, meaning that most of the "anomalous events" are likely to be man-made.
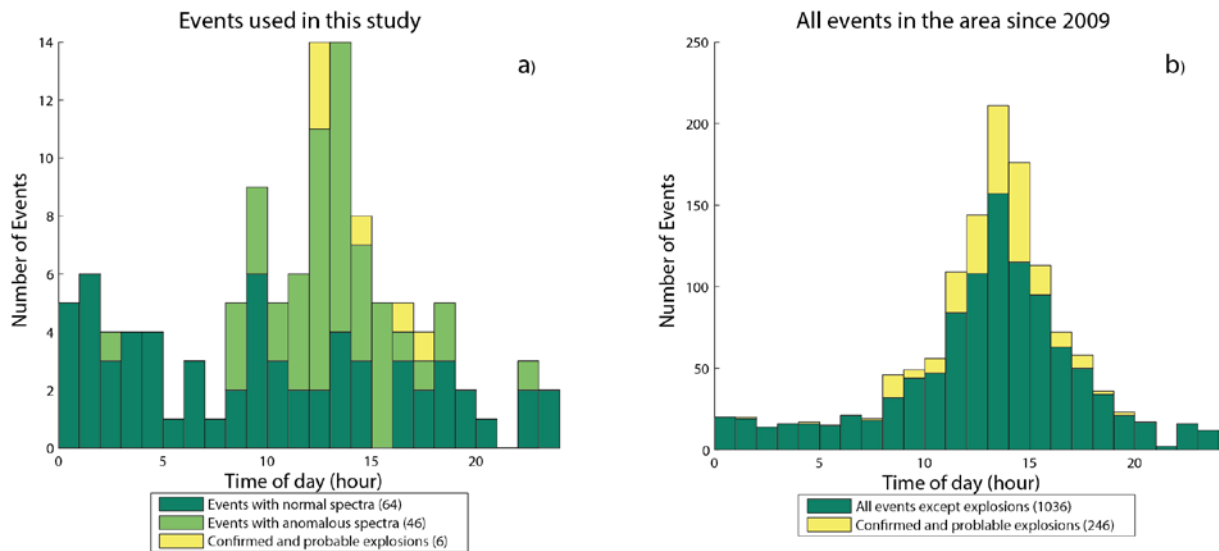
Fig. 6.1.14 Histograms of events over the 24 hours of the day. (a) Histogram of events used in the study. (b) Histogram using all events since 2009 reported in the Bergen catalog.

6.1.4   Summary and suggestions for improvements

As confirmed by this study, coda amplitude measurements are significantly more consistent between stations than amplitude measurements of the direct wave. The use of regional coda envelopes for estimation of source moment spectra and event magnitudes of events in Norway is promising. Indeed, a coda based procedure permits quite accurate estimation of moment magnitudes for events observed at a few stations only. For Norway, where the seismicity is characterized as low-to-intermediate with a large offshore component, this is very advantageous as a large fraction of the events are recorded at relatively few stations. In contrast, classical estimates of moment magnitudes require observation at a relatively large number of stations.

A natural follow-up to this study would be to calibrate other regions and stations and to estimate the magnitude uncertainty as proposed by Mayeda (2003). In connection with the estimation of coda magnitudes for older, and possibly also clipped events, in the NORSAR and Bergen catalogs, it would be interesting to investigate the use of 1-D or 2-D path corrections.

In this study, only the vertical component data has so far been used. We also suggest investigating the additional use of the horizontal components where we in many cases expect more S-wave energy than on the verticals.

The analytic expression of coda envelopes is known to fit long cods poorly. Many investigations found lapse time dependence of the coda decay rate which suggests that the later portion of the coda is dominated by energy that has propagated in zones with different attenuation characteristics than the energy in the early coda (Sato *et al.*, 2009). It would thus be interesting to restrict the length of the coda window to avoid this effect and only use the early coda for fitting of the synthetic envelopes. Another alternative would be to introduce a lapse time dependence of the coda decay, by using a polynomial regression instead of linear regression.

Another improvement would be to better classify and eliminate man-made events from the event population prior to the estimation of the site response corrections. In this study, the site response corrections was done twice, first using all events, and then after discarding events having anomalous coda derived source moment spectra. Phillips *et al.*, (2008) suggest a procedure using only events with magnitudes below 3 that occurred at night, or with reliable source depths below 5 km. Further improvements to the separation of earthquakes from man-made events could *e.g.*, be made by analyzing the time-domain and/or frequency-domain characteristics of the waveforms.

C. Labonne
T. Kværna
M. Roth

References

Aki, K., and B.Chouet (1975). Origin of Coda Waves: Source, Attenuation and Scattering Effects. *J. Geophys. Res*. **80**, 23, 3322-3342.

Bormann, P. (Ed.) (2002). New Manual of Seismological Observatory Practice (NMSOP-1), IASPEI, GFZ German Research Centre for Geosciences, Potsdam.

Båth, M., O. Kulhanek, T. Van Eck and R. Wahlstrøm (1976). Engineering analysis of ground motion in Sweden, *Report No 5-76*, Seismological Institute, Uppsala, Sweden, 59 pp.

Eken, T., K. Mayeda, A. Hofstetter, R. Gök, G. Örgülü and N.i Turkelli (2004). An application of the coda methodology for moment-rate spectra using broadband stations in Turkey. *Geophys. Res. Lett.* **31**.

Hanks, T. C. and H. Kanamori (1979). A moment magnitude scale. *J. Geophys. Res*., **84**, 2348-2350

Mayeda, K. and W. R. Walter (1996). Moment, energy, stress drop, and source spectra of western United States earthquakes from regional coda envelopes. *J. Geophys. Res.* **101**, 11,195-11,208.

Mayeda, K., A. Hofstetter, J. L. O'Boyle and W.R. Walter (2003). Stable and Transportable Regional Magnitudes Based on Coda-Derived Moment-Rate Spectra. *Bull. Seism. Soc. Am,.* **93** , 224-239.

Morasca, P., K. Mayeda, L. Malagnini and W.R. Walter (2005). Coda-derived source spectra, moment magnitudes and energy-moment scaling in the western Alps. *Geophys. Res. Lett*., **32**, no. 22.

Morasca, P., K. Mayeda, R. Gök and L. Malagnini (2008). Source effects from broad area network calibration of regional distance coda waves. *Bull. Seism. Soc. Am*. **98**, 1936-1946.

Phillips, W.S., R.J. Stead, G.E. Randall, H.E. Hartse and K.M. Mayeda (2008). Earth Heterogeneity and Scattering Effects on Seismic Waves. In: *Advances in Geophysics*, vol 50, Chapter 12, Source effects from broad area network calibration of regional distance coda waves.

Ringdal, F. (1983). Magnitudes from P coda and Lg using NORSAR data. In NORSAR Semiannual Technical Summary, 1 October 82-31 March 83, *NORSAR Sci. Rep. No. 2-82/83*, NTNF/NORSAR, Kjeller, Norway.

Ringdal, F. Hokland, B. K. (1987). Magnitudes of large Semipalatinsk explosions using P coda and Lg measurements at NORSAR. In Semiannual Technical Summary, 1 April-30 September 1987, *NORSAR Sci. Rep. 1-87/88*, Kjeller, Norway.

Sato, H., M. C. Fehler and T. Maeda (2009). Seismic wave propagation and scattering in the heterogeneous Earth. Chapter 2.4, Scattering of high-frequency seismic waves. *Springer-Verlag Berlin Heidelberg*. 19-40

Appendix

Origin time, latitude, longitude and depth of events used in this study, with event label as provided in the Bergen bulletin (L for local event, LE for confirmed local explosion, LX for landslide and LQ for confirmed earthquakes), label of the obtained spectrum (A for Anomalous, N for Normal, and U for Unknown), the corresponding local magnitude from NORSAR, local magnitude from Bergen, moment magnitude from Bergen, and the estimated coda magnitudes from AKN, BER and NOA.

T0 YYYY-DOY:HH.MM.SS.S	Lat (°)	Lon (°)	Depth (km)	Event Label	Spectrum Label	M_L NOA	M_L BER	M_W BER	M_{coda} AKN	M_{coda} BER	M_{coda} NOA
2009-008:14.27.26.2	60.71	5.652	0	L	A	1.58	1.4	-	-	-	1.907
2009-040:23.31.09.9	60.157	5.165	15	L	N	-	1.8	-	-	-	1.962
2009-049:12.03.51.9	58.801	6.11	15	L	A	1.93	2.0	-	-	-	2.208
2009-088:02.39.52.7	62.16	6.144	15	L	A	2.53	2.1	-	-	-	2.268
2009-113:09.18.47.7	61.754	5.215	15	L	A	2.07	-	-	-	-	-
2009-132:15.16.57.8	60.436	5.23	0.0F	LE	-	1.64	1.7	-	-	-	-
2009-136:16.41.51.3	59.71	5.513	0.1	L	N	2.28	2.3	-	-	2.385	2.369
2009-139:04.16.36.6	62.162	5.1	13.0F	L	N	-	3.0	3.0	-	2.904	2.968
2009-148:14.08.25.7	60.702	5.592	0	L	U	-	1.3	-	-	-	1.774
2009-154:12.57.30.2	61.748	5.275	15.0F	L	A	2.18	2.2	-	-	-	2.305
2009-156:12.28.06.6	58.842	5.822	0	L	A	1.62	1.7	-	-	-	2.022
2009-158:17.30.56.7	60.132	6.433	3	L	N	1.74	1.9	-	-	2.117	2.127
2009-170:09.45.26.2	58.845	6.177	15.0F	L	A	1.89	1.7	-	-	-	2.014
2009-184:01.12.03.6	62.084	6.033	2.4	L	N	1.87	1.7	-	-	1.980	2.039
2009-211:12.44.44.5	61.748	5.332	15.0F	L	A	1.95	1.8	-	-	-	2.082
2009-223:12.39.54.8	58.872	6.312	3.5	L	A	1.69	1.7	-	-	-	2.022
2009-237:12.26.02.2	61.74	5.152	15.0F	L	A	2.18	2.0	-	-	-	2.302
2009-238:18.19.47.2	61.91	5.037	17.3	L	N	2.17	2.1	2.4	-	2.430	2.361
2009-239:18.27.49.9	60.864	4.976	0.1	L	A	1.54	1.3	-	-	-	1.979
2009-253:09.07.54.9	61.71	3.825	18.1	L	N	2.57	2.7	2.7	-	2.646	2.660
2009-257:00.39.48.4	60.667	4.585	15	L	N	2.34	2.6	2.5	-	2.619	2.573
2009-282:08.11.55.2	61.745	5.244	0	L	A	2.19	2.0	-	-	-	2.282
2009-288:10.13.57.3	59.326	5.735	0	L	A	1.57	1.8	-	-	-	2.007
2009-289:09.37.35.7	61.373	4.495	0	L	N	1.87	-	-	-	-	-
2009-297:16.18.19.6	61.407	4.406	1.6	L	N	1.83	1.8	-	-	2.113	2.093
2009-301:06.09.53.4	59.703	5.861	12.3	L	N	2.54	2.2	2.6	-	2.394	2.359
2009-303:03.42.38.2	61.313	4.147	20.2	L	N	1.85	2.0	-	-	2.263	2.215
2009-308:12.52.28.1	59.328	5.711	2	L	A	1.74	1.9	-	-	-	2.023
2009-310:11.35.46.3	60.701	5.594	0	L	A	2.09	1.6	-	1.978	-	2.079
2009-344:12.49.14.9	60.714	5.622	0	L	U	1.60	1.6	-	1.932	-	1.975
2009-344:13.03.14.1	61.746	5.205	0	L	A	1.80	1.7	-	1.868	-	2.226
2010-031:00.04.28.0	61.588	4.139	12.3	L	N	2.42	2.2	-	2.383	2.435	2.387
2010-036:13.26.17.1	61.812	5.055	0	L	A	2.17	1.9	-	1.930	-	2.050

2010-041:06.04.35.6	59.8	6.46	12.0F	L	N	2.31	2.2	2.5	2.365	2.340	2.397
2010-060:00.41.48.0	62.027	4.576	10.0F	L	N	2.07	2.1	2.5	2.343	2.318	2.323
2010-062:15.54.23.1	58.819	5.809	0.0F	LE	A	1.85	1.9	-	2.063	-	1.978
2010-063:14.36.17.7	59.34	5.708	0	L	A	1.63	1.6	-	2.091	-	1.923
2010-067:13.18.37.8	61.762	5.287	0	L	A	1.64	1.5	-	1.737	-	1.854
2010-084:15.22.20.1	58.848	5.828	0	L	A	1.61	1.7	-	1.896	-	1.937
2010-085:13.05.54.0	61.782	5.158	0	L	A	1.86	1.7	-	1.855	1.983	1.984
2010-096:11.29.11.4	61.779	5.197	5.0F	L	A	1.89	1.8	-	2.079	-	2.076
2010-099:13.02.08.5	60.7	5.584	0	L	A	1.97	1.5	-	1.858	-	1.974
2010-124:09.53.50.4	60.281	6.258	0	L	N	1.72	1.6	-	1.978	-	2.052
2010-127:17.54.06.7	61.812	4.684	13	L	N	2.25	2.3	2.5	2.433	2.394	2.420
2010-155:14.30.40.4	60.683	5.572	0.0F	LP	A	1.66	1.5	-	2.187	-	2.104
2010-166:04.22.04.1	60.874	6.646	0.0F	LX	A	2.11	1.5	-	1.915	-	1.998
2010-167:08.47.22.6	61.757	5.345	4.5	L	A	1.75	1.0	-	1.744	-	1.885
2010-185:17.40.49.6	61.802	5.165	0.0F	LP	A	1.59	1.8	-	1.845	-	1.975
2010-187:12.40.18.7	59.338	5.799	0.0F	LP	A	1.67	1.6	-	-	-	2.005
2010-210:04.32.27.2	61.028	4.137	17.3	L	N	1.98	2.0	-	2.233	2.240	2.229
2010-213:02.59.58.4	62.067	5.899	15.0F	L	N	1.97	2.0	-	2.293	2.189	2.270
2010-220:23.23.28.3	62.168	5.245	1.9	L	N	1.63	1.7	-	2.12	2.096	2.084
2010-259:11.57.36.4	59.338	5.705	0.0F	LP	A	1.50	1.6	-	2.011	-	1.949
2010-264:10.13.21.5	61.049	4.221	8.8	L	N	2.26	1.8	-	1.956	-	2.019
2010-273:12.51.33.3	60.368	4.67	12.5	L	N	2.10	2.3	-	2.370	2.485	2.378
2010-279:22.14.24.6	61.42	4.385	10.0F	L	N	2.73	2.3	-	2.533	2.524	2.547
2010-281:04.08.32.7	59.604	7.531	15.0F	L	N	1.79	1.5	-	2.112	-	2.13
2010-286:13.18.40.2	60.855	5.16	6.9	L	A	1.72	1.3	-	1.734	-	2.050
2010-316:15.16.01.1	60.853	5.132	0	L	A	1.96	1.4	-	1.86	-	1.968
2010-344:15.14.55.6	58.931	5.632	0	L	A	1.69	1.8	-	1.915	-	1.98
2010-349:12.34.28.9	59.319	5.74	0	L	A	1.77	1.8	-	1.842	-	2.007
2010-354:00.43.23.2	59.901	5.359	8.0F	L	N	3.13	3.0	3.0	3.031	3.072	3.097
2010-354:00.51.18.8	59.899	5.447	8.0F	L	N	2.07	2.2	2.3	2.340	2.379	2.357
2010-354:00.59.31.5	59.93	5.486	12.0F	L	N	1.58	1.8	1.9	2.027	2.080	2.063
2010-354:01.39.20.1	59.896	5.401	15	L	N	2.29	2.2	2.3	2.312	2.368	2.336
2010-354:12.30.12.7	59.9	5.366	17.0F	L	N	3.36	3.3	3.3	3.232	3.235	3.275
2010-354:12.37.38.3	59.924	5.483	10.0F	L	N	1.73	2.0	2.1	2.195	2.267	2.220
2010-354:12.53.39.4	59.9	5.446	15	LQ	N	1.61	1.7	-	1.959	-	1.969
2010-361:08.57.22.6	61.495	3.926	13.1	L	N	2.13	2.2	-	2.294	2.307	2.274
2011-016:22.43.04.3	59.892	5.482	12.0F	L	A	-	1.7	-	-	2.026	1.914
2011-037:08.02.29.2	61.832	4.858	15	L	N	1.83	1.7	-	2.174	2.200	2.131
2011-037:18.41.39.8	60.723	5.312	29	L	N	1.87	1.8	-	2.217	2.300	2.241
2011-082:14.45.53.6	59.369	6.072	0.0F	L	A	2.12	2.2	-	2.376	2.434	2.3430
2011-088:11.30.38.0	59.111	5.774	0	L	A	2.27	2.1	-	2.395	2.453	2.271
2011-090:13.00.26.9	59.104	5.808	0	L	A	2.44	2.3	-	2.358	2.483	2.341
2011-093:01.23.30.9	61.101	4.315	16.2	L	N	2.45	2.4	-	2.602	2.580	2.575
2011-095:12.30.02.0	59.088	5.84	0	L	A	2.23	2.2	-	-	2.411	2.375
2011-118:22.24.07.4	59.96	6.78	12.0F	L	N	2.01	2.0	-	2.193	2.184	2.217
2011-186:01.22.44.8	60.863	4.568	17.4	L*	N	2.12	2.4	-	2.365	2.411	2.375

2011-273:12.47.26.3	60.699	5.533	0.0F	LP	A	1.90	1.6	-	-	-	2.245
2011-317:02.39.16.5	60.435	5.29	11.1	L	N	1.93	2.0	2.0	2.187	2.292	2.179
2011-359:14.49.23.6	61.214	4.08	22.9	L	N	2.04	1.9	-	2.191	2.182	2.215
2011-365:00.16.17.3	61.635	4.762	1	L	N	2.40	2.1	-	2.314	2.313	2.309
2012-004:20.03.37.8	61.758	4.12	15	L	N	2.42	2.4	-	2.462	2.463	2.478
2012-067:19.21.17.4	61.915	5.331	15	L	N	1.94	2.0	-	2.304	2.324	2.284
2012-074:09.15.55.7	61.895	5.17	15	L	N	2.07	2.1	-	2.364	-	2.357
2012-074:19.22.27.9	59.524	5.578	13.7	L	N	3.07	3.2	-	3.097	3.117	3.166
2012-075:04.10.14.1	59.566	5.761	0	L	N	1.87	2.2	-	2.297	2.289	2.281
2012-084:06.05.18.2	60.616	4.399	15.0F	L	N	2.64	2.9	-	2.708	2.753	2.726
2012-084:11.06.30.5	60.634	6.401	15.3	L	N	3.16	3.0	-	2.997	3.009	3.020
2012-117:05.18.28.8	60.07	7.282	0	L	N	1.93	1.9	-	2.184	-	2.212
2012-146:14.02.27.3	61.732	4.256	2.5	L	N	1.94	2.0	-	2.289	2.293	2.281
2012-166:13.35.17.4	58.827	6.231	0.0F	LE	-	1.82	-	-	-	-	-
2012-169:09.08.59.2	58.983	6.184	0	L	A	2.27	2.1	-	2.288	2.131	2.297
2012-184:07.03.21.3	60.458	6.223	0	L	N	2.70	2.9	-	2.759	2.823	2.768
2012-216:02.55.51.2	60.544	4.69	2.1	L	N	1.66	1.8	-	2.022	2.080	2.045
2012-225:03.10.23.9	61.249	4.247	4	L	N	2.03	1.8	-	2.146	2.141	2.168
2012-227:07.21.30.8	60.442	6.023	15	L	-	1.59	-	-	-	-	-
2012-258:08.03.09.1	60.853	5.133	0	L	A	1.64	1.5	-	-	-	1.965
2012-264:17.32.25.7	60.853	5.182	0.1	L	A	1.67	1.5	-	1.822	-	-
2012-286:13.01.43.9	60.857	5.161	0	L	A	1.67	1.5	-	1.722	-	1.853
2012-298:13.47.48.7	61.325	4.768	15	L	N	1.60	1.6	-	2.082	-	2.074
2012-314:10.07.14.3	61.765	5.265	0.1	L	A	1.72	1.8	-	1.885	-	1.949
2012-335:01.52.53.4	61.31	4.944	0	L	N	1.76	1.7	-	2.015	2.025	2.008
2012-345:13.06.53.2	59.654	5.498	0	L	N	2.05	1.8	-	2.149	2.193	2.173
2012-360:11.06.09.2	61.716	4.162	0.3	L	N	1.57	1.7	-	2.017	1.961	2.020
2013-023:17.42.32.3	61.213	4.535	23.6	L	N	2.03	2.1	-	2.252	2.331	2.317
2013-057:09.21.49.4	60.454	4.901	18.7	L	N	1.98	-	-	-	-	-
2013-066:16.07.29.4	60.865	5.033	0	L	A	1.86	-	-	-	-	-
2013-079:15.00.35.4	60.873	5.158	0.1	L	A	1.62	1.4	-	1.807	2.186	1.899
2013-081:10.32.44.5	61.566	4.714	15	L	N	3.36	3.0	3.3	3.248	3.198	3.257
2013-081:13.52.21.9	61.603	4.528	0	L	N	3.18	2.7	3.1	3.042	2.991	3.048
2013-092:15.02.57.8	60.848	5.163	0	L	A	1.69	1.4	-	1.735	-	1.834
2013-098:02.17.35.3	59.897	4.788	10.0F	L	N	1.77	1.9	-	2.125	2.201	2.129
2013-101:16.10.06.3	61.792	5.222	0	L	A	1.77	1.8	-	1.958	-	2.172
2013-114:14.02.43.0	60.882	5.396	0	L	A	1.60	1.3	-	1.692	-	-
2013-144:12.07.08.4	60.842	5.163	0	L	A	1.65	1.3	-	1.671	-	2.126
2013-150:14.04.41.8	60.851	5.131	0.1	L	A	1.66	1.3	-	1.823	1.938	1.934
2013-154:16.37.27.9	59.436	5.726	5.8	L	N	2.54	2.5	-	2.517	2.540	2.516
2013-157:08.15.47.7	59.879	4.88	0	L	N	1.61	1.6	-	2.015	-	2.012
2013-158:09.15.21.9	59.888	4.853	0	L	N	1.90	1.8	-	2.159	-	2.165
2013-162:18.03.31.0	60.863	5.175	0	L	A	1.71	1.5	-	1.684	-	1.933

6.2 Examination of the Storfjorden Aftershock Sequence Using an Autonomous Event Detection and Grouping Framework: Preliminary Results

6.2.1 Introduction

The Storfjorden aftershock sequence was triggered by a M_w 6.2 earthquake that occurred off the Svalbard archipelago's southeastern coast on February 21, 2008. Over the last five years, it has generated thousands of aftershocks; several have exceeded M_w 4.0. Fig. 6.2.1 shows the locations (in green) of sequence events published in NORSAR's analyst reviewed regional bulletin. Pirli *et al.* (2013) and Junek *et al.* (2014) conducted an investigation of the regional seismotectonics and concluded the source of the sequence was not related to the nearby Billefjorden fault zone. Instead, its source is most likely tied to the Tertiary shear zone shown in red in Fig. 6.2.1. This conclusion is supported by the orientation of the relative relocation catalog, shown in blue in Fig. 6.2.1, and the orientations of focal mechanisms for numerous sequence events (Pirli *et al.*, 2013; Junek *et. al.*, 2014).
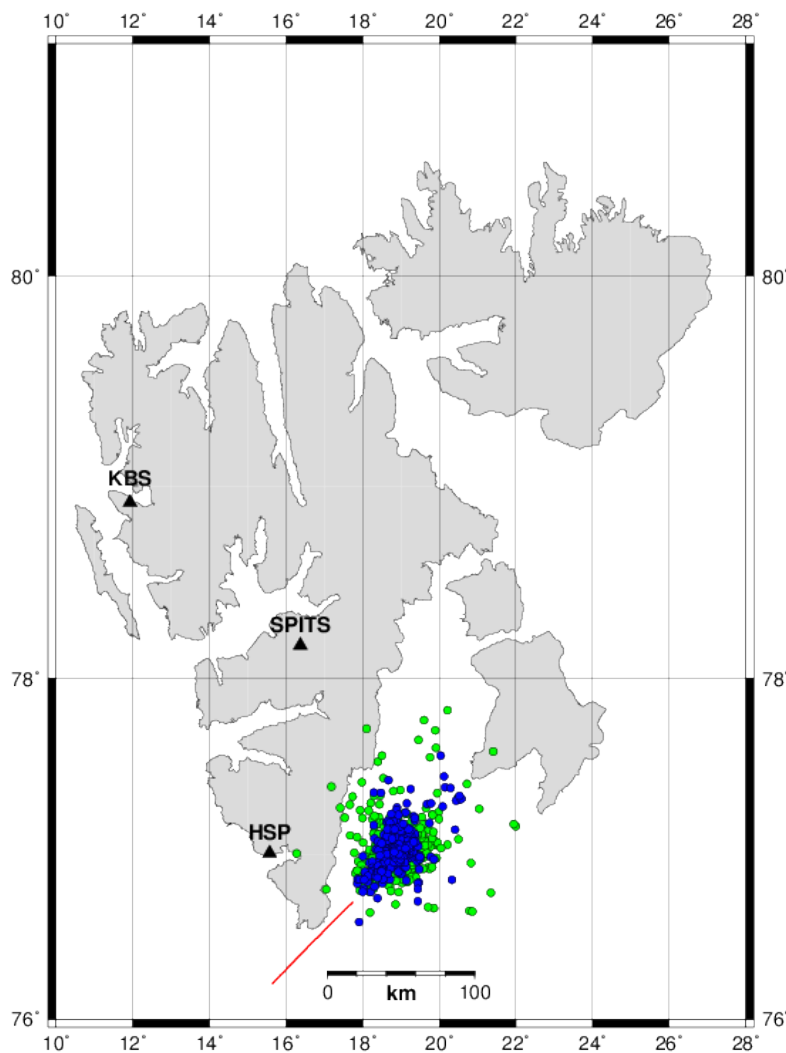
Fig. 6.2.1
The Storfjorden aftershock sequence occurred off Spitsbergen's southeast coast. Events shown in green represent the NORSAR analyst reviewed catalog between 21 February 2008 and 20 April 2012. Blue events represent the relative relocation catalog (Pirli et. al., 2013). The red line shows the location of the shear zone suggested by Bergh and Grogan (2003), believed to be related with the Storfjorden sequence (Pirli et. al., 2013). Black triangles show the locations of some of the permanent seismic stations on Spitsbergen.

The results shown in previous studies (Pirli et. *al.*, 2013; Junek et. *al.*, 2014) were largely based on the analysis of manually reviewed events. However, the number of events in the NORSAR analyst reviewed bulletin represents a small fraction of the total number of events produced by the sequence. Here, an autonomous event detection and clustering framework is used to expand the available dataset. The expanded dataset will be used in future studies to infer additional information about the tectonic structure within the fjord and to examine the sequence's spatiotemporal properties.

The detection framework is a Java based application that was developed as a collaborative effort between Lawrence Livermore National Laboratory and NORSAR. A block diagram of the framework's core functionality is shown in Fig. 6.2.2 and a complete description of an early version of the system is provided in Harris and Dodge (2011). The framework uses power (STA/LTA) detectors operating on array beams to detect events with new waveform patterns, and automatically spawns correlation detectors to search for additional occurrences of events with those patterns. The framework maintains a pool of such empirically-derived correlation detectors, which may be updated upon the detection of new signals approximately matching the patterns. It groups signal detections based on waveform similarity and stores event affiliation information in a relational database. All framework detections are tagged with an identification number (detector ID) that represents new or previously observed signal types. The database can be mined to study the various aspects of the sequence. For example, detector IDs can be grouped and associated detections counted to identify event clusters.
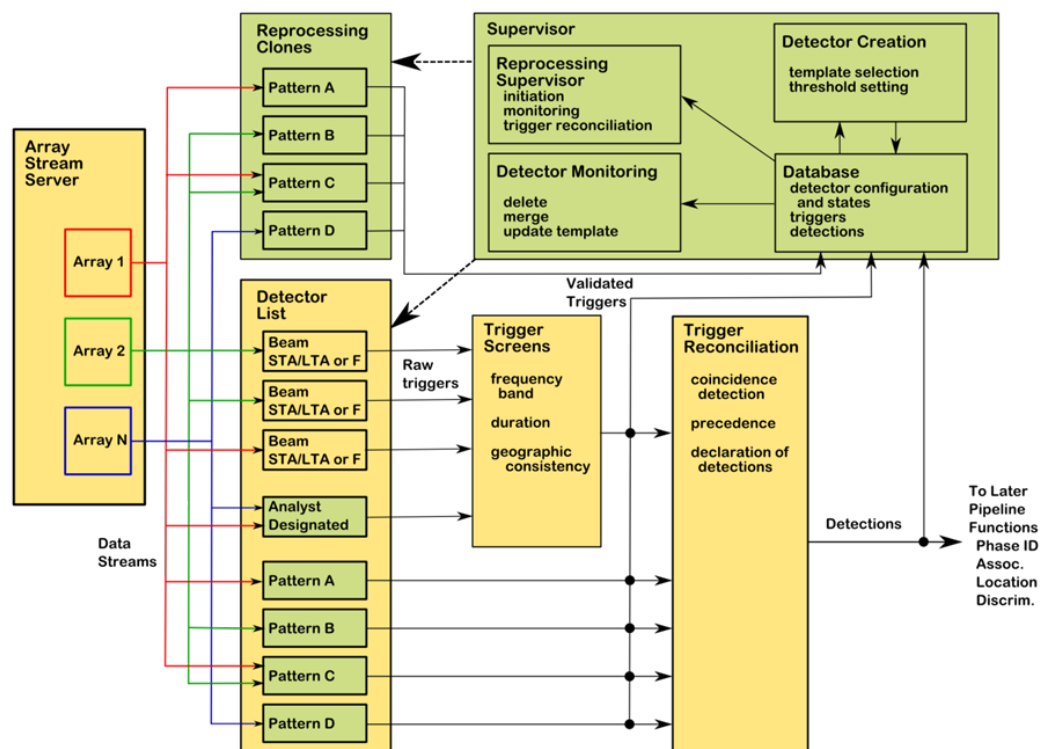
Fig. 6.2.2   Autonomous seismic event detection and grouping framework block diagram.

6.2.2   Completeness Magnitude Estimation

In this study event size is estimated using a relative magnitude (mb_{rel}) relationship that scales newly detected events against a user defined master event. The relative scaling relationship used in this study is defined as

$$mb_{rel} = mb_r + \log_{10}(A_n / A_r) \tag{1}$$

where mb_r is the reference event bodywave magnitude, A_r is the peak amplitude of the reference event seismogram, and A_n is the peak amplitude of the new event seismogram. This relation allows the reference magnitude to be adjusted as a function of the log amplitude ratio. Since all of the events under consideration originate in a small area, no distance correction is needed. The relative magnitude scale allows bodywave magnitudes to be calculated for all SPITS empirical signal detector (ESD) detections. Relative magnitude estimates are used to produce a cumulative frequency magnitude distribution (FMD) that quantifies the detection threshold for SPITS relative to the Storfjorden region.

Determination of the catalog completeness magnitude (M_c) is performed using the method outlined in Wiemer and Wyss (2000). Their method compares the linear sections of the observed and model FMD between the maximum magnitude and an assumed M_c. The goodness-of-fit (GOF) between the modeled and observed FMDs is assessed using

$$R(a,b,M_i) = 100 - \frac{\sum_{M_i}^{M_{max}} |B_i - S|}{\sum_i B_i} 100 \tag{2}$$

where R is the GOF, a and b are the Gutenberg-Richter relationship parameters, M_i is the completeness magnitude being tested, and B and S are the observed and predicted portions of the distribution for each magnitude bin. The Gutenberg-Richter coefficients are determined via least-squares regression before the initiation of the M_c estimation routine. This is an iterative process that tests the validity of many M_c values. Here, the M_c value with the largest GOF measurement is chosen as the catalog completeness magnitude.

6.2.3   Results

The detection framework was used to process waveform data from 7 vertical, broadband, elements of the SPITS array between 21 February 2008 and 20 April 2012. Processing parameter values and descriptions for the four year processing run are listed in Table 6.2.1. The array power detector threshold was set high so only high-quality signals were used as ESD templates. Since our ESDs have a large time bandwidth product and use multiple channels of the array, the correlation detector threshold, T_{ESD}, was set to 0.2. Frequency-Wavenumber (FK) screening was used to remove detections originating outside of Storfjorden. Signal duration was used as an additional screening metric. Valid detections had durations that fell between TL_{min} and TL_{max}.

Table 6.2.1. Processing parameters employed by detection framework for Storfjorden sequence for SPITS array.

Parameter	Value	Description
Filter Type	Bandpass	3 Pole, Butterworth
F_{lo}	2.0 Hz	Filter Low Frequency Coner
F_{hi}	8.0 Hz	Filter High Frequency Corner
TL_{min}	20.0 sec	Minimum Template Length
TL_{max}	33.0 sec	Maximum Template Length
Azimuth	150.0 deg	Detection Beam Azimuth
Velocity	6.2 km/sec	Detection Beam Velocity
Az_{tol}	+/- 20.0 deg	Azimuth Tolerance
Vel_{tol}	+/- 1.0 km/sec	Velocity Tolerance
T_{AP}	20.0	Array Power Detection Threshold
T_{EDS}	0.2	ESD Threshold
FK_{pow}	0.3	Minimum FK Power

Table 6.2.2. Detection framework results, where Y denotes the application of FK screening and N its absence.

Parameter	FK Screening	Results
Detections	Y	15911
	N	76688

The total number of detections and event clusters produced by the detection framework are listed in Table 6.2.2. FK screening was invoked during post processing via an application that runs outside the detection framework. As a result, all array power detections were used to spawn new correlation detectors regardless of their slowness vector. Since the SPITS array observes seismicity from numerous local, regional, and teleseismic sources, a large number of detectors were formed from sources outside of Storfjorden.

Figs. 6.2.3 and 6.2.4 show FK measurements for all detections made over the four-year processing interval. Black dots indicate events that fell within the azimuth, velocity, and FK power constraints listed in Table 6.2.1 and red dots indicate those events which did not. The time series plot shows detections were typically made along the 60, 150, 220, and 330 degree azimuths. The polar plot shows numerous sources of repeating seismicity near the station. Repeating sources include, mining activity, ice quakes, local earthquakes, Mid-Atlantic Ridge earthquakes, and Storfjorden events (shown in black). The large number of off-target detections highlights the need for post detection azimuth and slowness screening for the automatically generated ESDs. Approximately 80% of the detections were rejected after the screening metrics were applied.

Figs. 6.2.5 and 6.2.6 show the magnitude distributions and M_c estimates for the framework and NORSAR catalogs. FMDs have similar b-values and highlight detection threshold differences between the two catalogs. M_c estimates for the framework and NORSAR catalogs with the largest GOF values are 0.8 and 2.1. The difference in M_c estimates shows the framework is providing a 1.3 magnitude unit improvement in detection capability for Storfjorden events observed by SPITS.
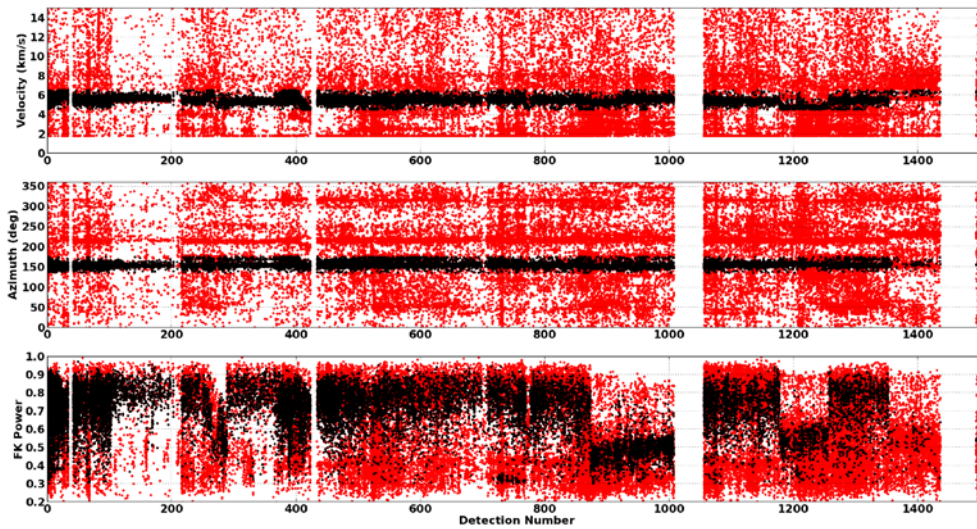
Fig. 6.2.3   *FK measurements for framework detections, where the top plot is velocity, center is back azimuth, bottom is FK power, red dots represent all detections, and black dots denotes detections that passed the screening criteria. The numbers on the x-axis denote the number of days after the start of the sequence (21 February 2008). Gaps in data availability are observed near days 5, 410, 1010, and 1450.*
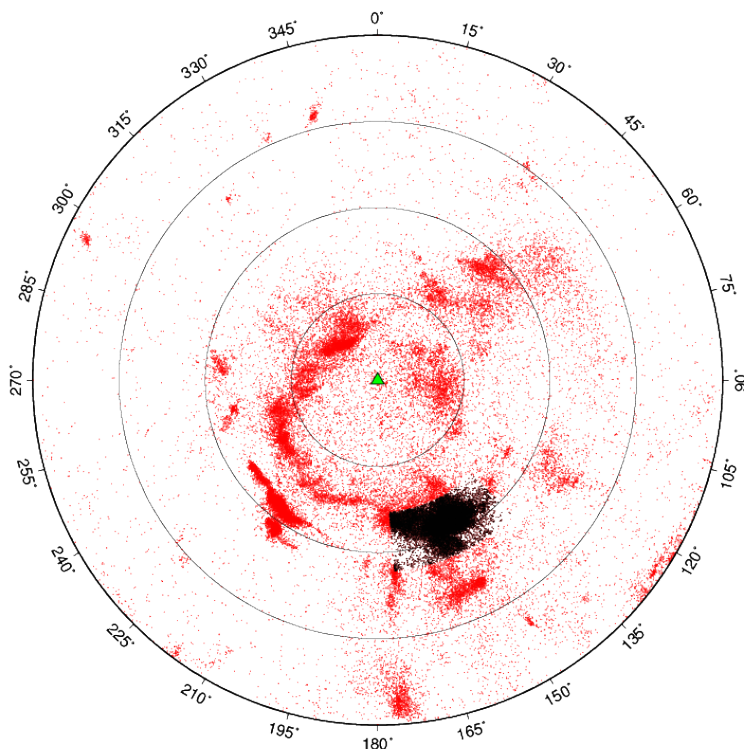
Fig. 6.2.4
Azimuth (angle axis) and slowness measurements (radius axis), where the distance between concentric circles is 0.1 sec/km. The green triangle denotes the SPITS array.
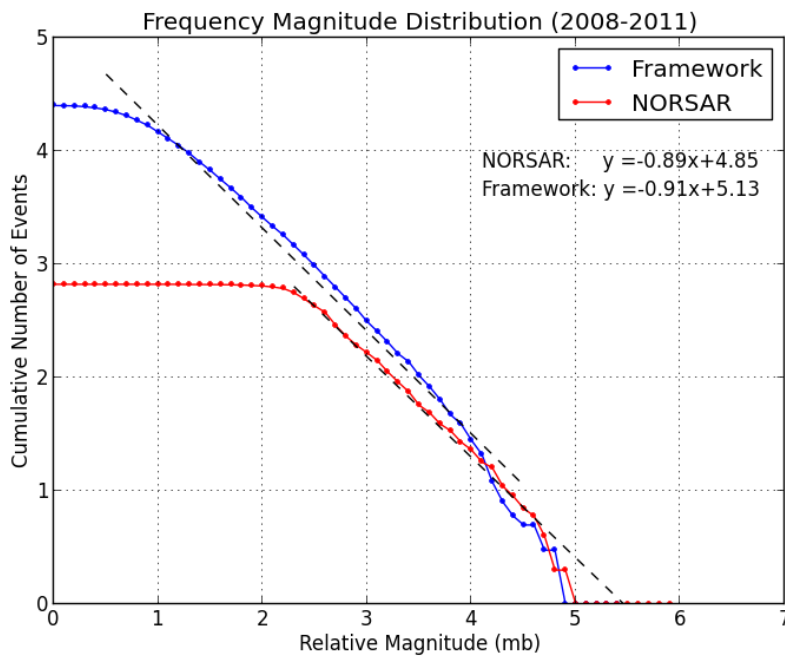
Fig.6.2.5 Cumulative FMD for framework (blue) and NORSAR (red) catalogs.
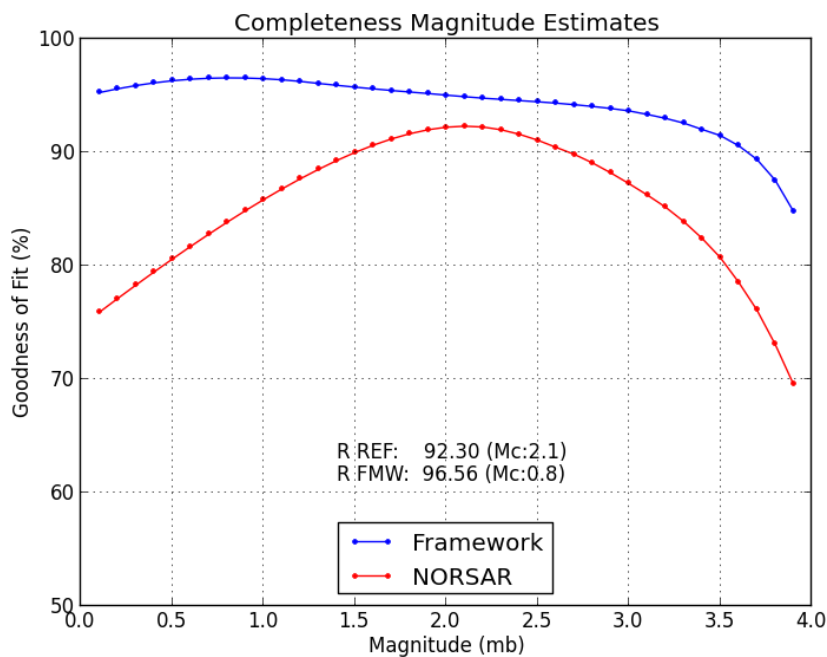
Fig. 6.2.6 GOF measurements for the linear portion of the modeled and observed frequency magnitude distributions for the framework (blue) and NORSAR (red) catalogs.

The initiation day, lifespan, and number of events in each cluster are shown in Fig. 6.2.7. Lifespan bars show the onset and duration of each cluster. The cluster generation rate is greatest at the beginning of the sequence and remains relatively constant until day 100. At this point, the rate decreases and spikes on days where reactivation episodes occur. The lifespan of the clusters vary dramatically, where some last hours and others live for the entire length of the sequence. The

number of events constituting each cluster also varies significantly. Some groups have a single member, while others have between 10 and 85 members.
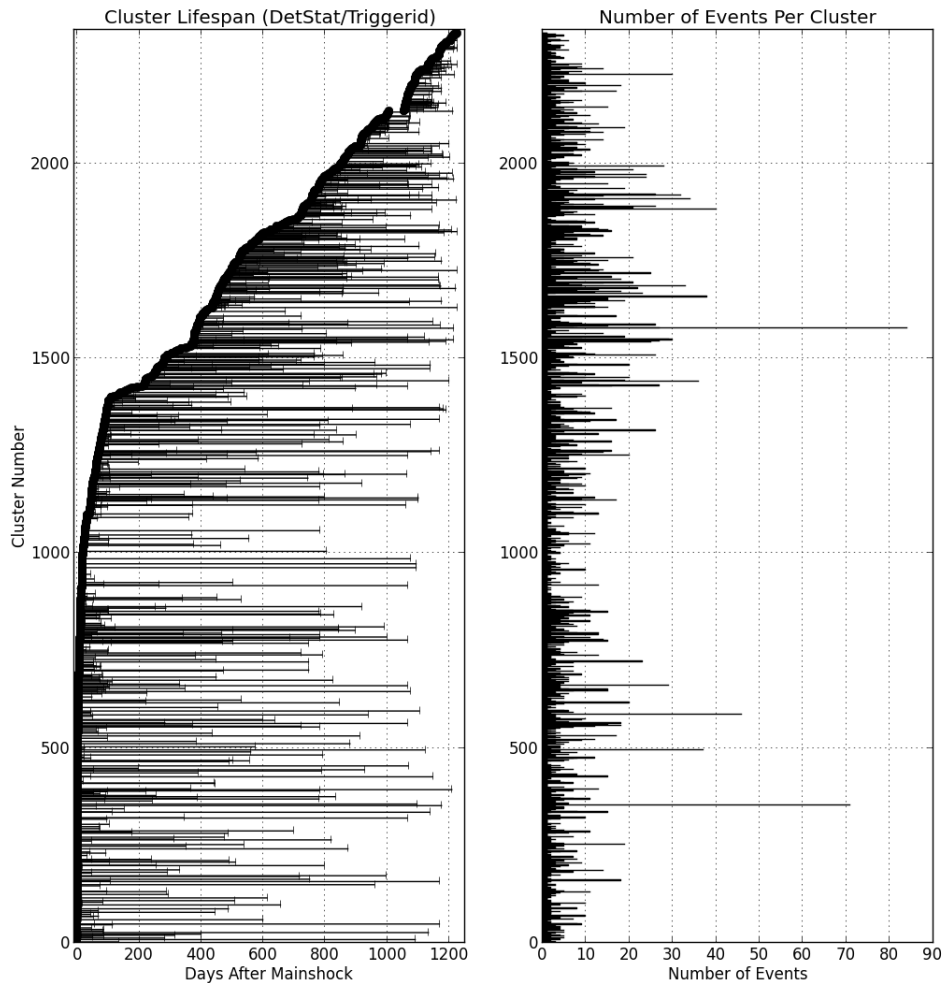
Fig. 6.2.7   Cluster lifespan (left panel) and number of events per cluster (right panel), where each point on the lifespan bars represents the initiation time of the cluster.

6.2.4   Summary

We have demonstrated the use of an autonomous event detection and grouping system for studying the 2008 Storfjorden aftershock sequence. The system exploited data from the SPITS array and produced an event catalog whose completeness is 1.3 magnitude units lower than the NORSAR analyst reviewed bulletin for Storfjorden. The cluster lifespan plot highlights the source heterogeneity within the fjord. The space-time distribution of clusters suggests the evolution of the sequence follows an epidemic type aftershock model Ogata (1988), rather than the smooth exponential decay predicted by Omori's law.

Future work will focus on the further application of the framework to 2008 Storfjorden sequence for inferring tectonic structure within the fjord. In addition, the spatiotemporal distribution of the events will be studied and their adherence to epidemic type aftershock sequence models will be examined.

W. N. Junek   (Air Force Technical Applications Center)
T. Kværna   (NORSAR)
M. Pirli   (NORSAR)
D. B. Harris   (Deschutes Signal Processing)
J. Schweitzer   (NORSAR)
M. T. Woods   (Air Force Technical Applications Center)

References

Bergh, S.G. and P. Grogan (2003). Tertiary structure of the Sørkapp-Hornsund region, South Spitsbergen, and implications for the offshore southern extension of the fold-thurst belt, *Norw. J. Geol.*, **83**, 43-60.

Harris, D. B. and D. A. Dodge (2011). An Autonomous System for Grouping Events in a Developing Aftershock Sequence, *Bull. Seismol. Soc. Am.*, **101**, No. 2, 763-774.

Junek, W. N. Roman-Nieves, J. A., and M.T. Woods (2014). Tectonic Implications of Earthquake Mechanisms in Svalbard, *Geophys. J. Int.* (Accepted for publication)

Ogata, Y. (1988). Statistical Models of Earthquake Occurrences and Residual Analysis of Point Processes, *Journal of the American Statistical Association*, **83** (401), 9-27.

Pirli, M., Schweitzer, J. and B. Paulsen (2013). The Storfjorden, Svalbard, 2008-2012 Aftershock Sequence: Seismotectonics in a Polar Environment, *Tectonophysics*, **601**, 192-205.

Wiemer, S. and M. Wyss (2000). Minimum Magnitude of Completeness in Earthquake Catalogs: Examples from Alaska, The Western United States, and Japan, *Bull. Seismol. Soc. Am.*, **90**, No. 4, 859-869.

6.3   P-wave Polarization and FK Analysis of NORSAR Array Data to Investigate Local Anisotropy and Lateral Heterogeneity

6.3.1   Introduction

Three-component broad-band data from the NORSAR array are ideally suited to apply polarization (*e.g.*, Jurkevics, 1988; Schulte-Pelkum *et al.*, 2001) and fk-analysis (*e.g.*, Davies *et al.* 1971; Capon, 1973; Posmentier and Herrmann, 1971) to estimate anomalies of wave polarization and propagation vectors induced by local wave speed anisotropy and lateral heterogeneities. Long recording time and high quality data guarantee in fact a good azimuthal distribution of events with high signal-to-noise ratio (SNR).

Array techniques as fk-analysis are commonly applied for event location and to enhance the SNR by delaying and stacking of the traces (beamforming). Fk-analysis estimates together with the signal slowness and backazimuth provide also a measure of the coherence of the seismic wave crossing the array. Polarization analysis is mainly used as a single station method to investigate the characteristics of the particle motions.

6.3.2   Data and analysis

Fk- and polarization analysis have been applied to almost 20 years of NORSAR array data to investigate anisotropy of seismic velocities and lateral heterogeneities beneath the array.

We expect that polarization and propagation direction of P waves are both affected by seismic anisotropy, as well as by lateral heterogeneities, but with different sensitivities. Polarization parameters are finite frequency observables mostly related to structures up to about one wavelength from the receiver area. The propagation vector direction is also sensitive to distant heterogeneities and distant anisotropy. By polarization analysis we can estimate the deviation of the P-wave polarization vector and by fk-analysis the deviation of slowness and backazimuth. The dependence of those deviations on event backazimuth, epicentral distance and frequency is studied.

In this study, we used data from all seven three-component sites (NAO01, NBO00, NB201, NC204, NC303, NC405, and NC602) of the NORSAR array, which have recorded broadband data since 1996. The locations of these stations maintain the circular shape and aperture of the whole array. Altogether about 600 first arriving teleseismic P waves were analyzed. Events with high SNR have been selected and a good distribution in backazimuth and distance could be obtained (Fig. 6.3.1).
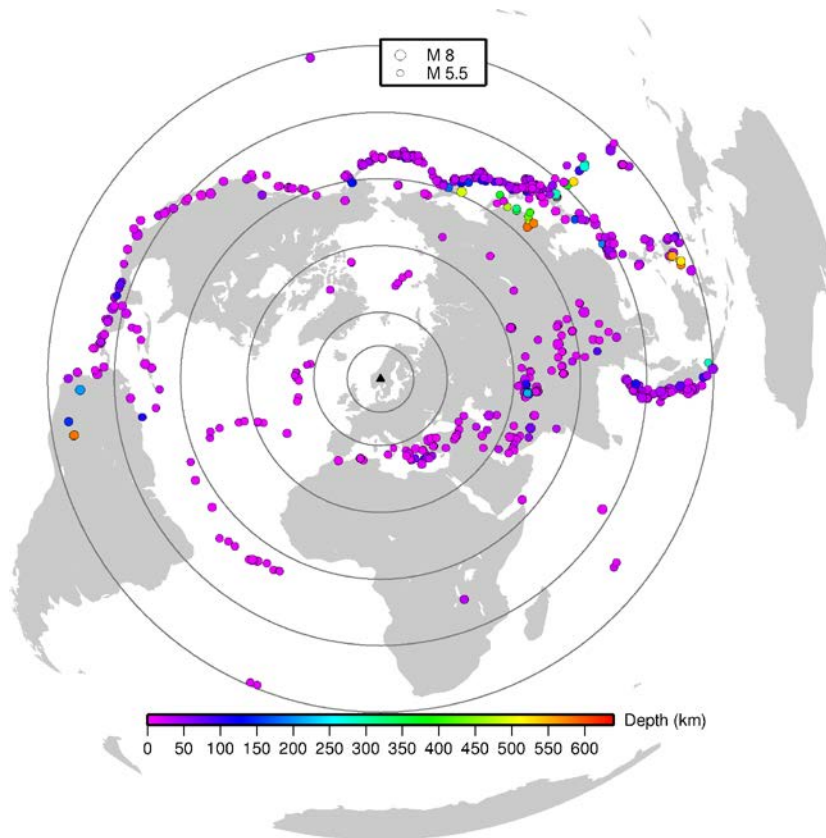
Fig 6.3.1
Epicenter map (circles) of
the seismic events used
in this study. *The map is*
centered at the location
of the NORSAR array.

6.3.3   Fk-analysis

A sliding window fk-analysis algorithm has been applied to estimate backazimuth and slowness of the first arriving P waves of the selected events in the following frequency bands (0.03 – 0.1 Hz, 0.1 – 0.5 Hz, 0.5 – 1 Hz, 1 – 4 Hz).

The effect of filtering (number of poles and values of corner frequencies) and length of time window have been investigated as well. The slowness and backazimuth estimates didn't show any dependence on the filtering nor on window length, whose maximum and minimum were limited by the array aperture and central frequency. Only measurements characterized by high coherence have been considered to study the deviation of P-wave propagation direction from the great circle path direction as a function of backazimuth, distance and frequency.

Fig. 6.3.2 shows the backazimuth anomalies (top) and slowness anomalies (bottom) as function of backazimuth for lower and higher frequencies. By fk-analysis changes in the horizontal slowness vector due to local and distant lateral heterogeneity and due to distant anisotropy may be detected. In case of local lateral homogeneous azimuthal anisotropy, we expect that by fk-analysis changes in the slowness but not in the backazimuth, are observed, as the slowness may change, but the wavefront is not deformed.
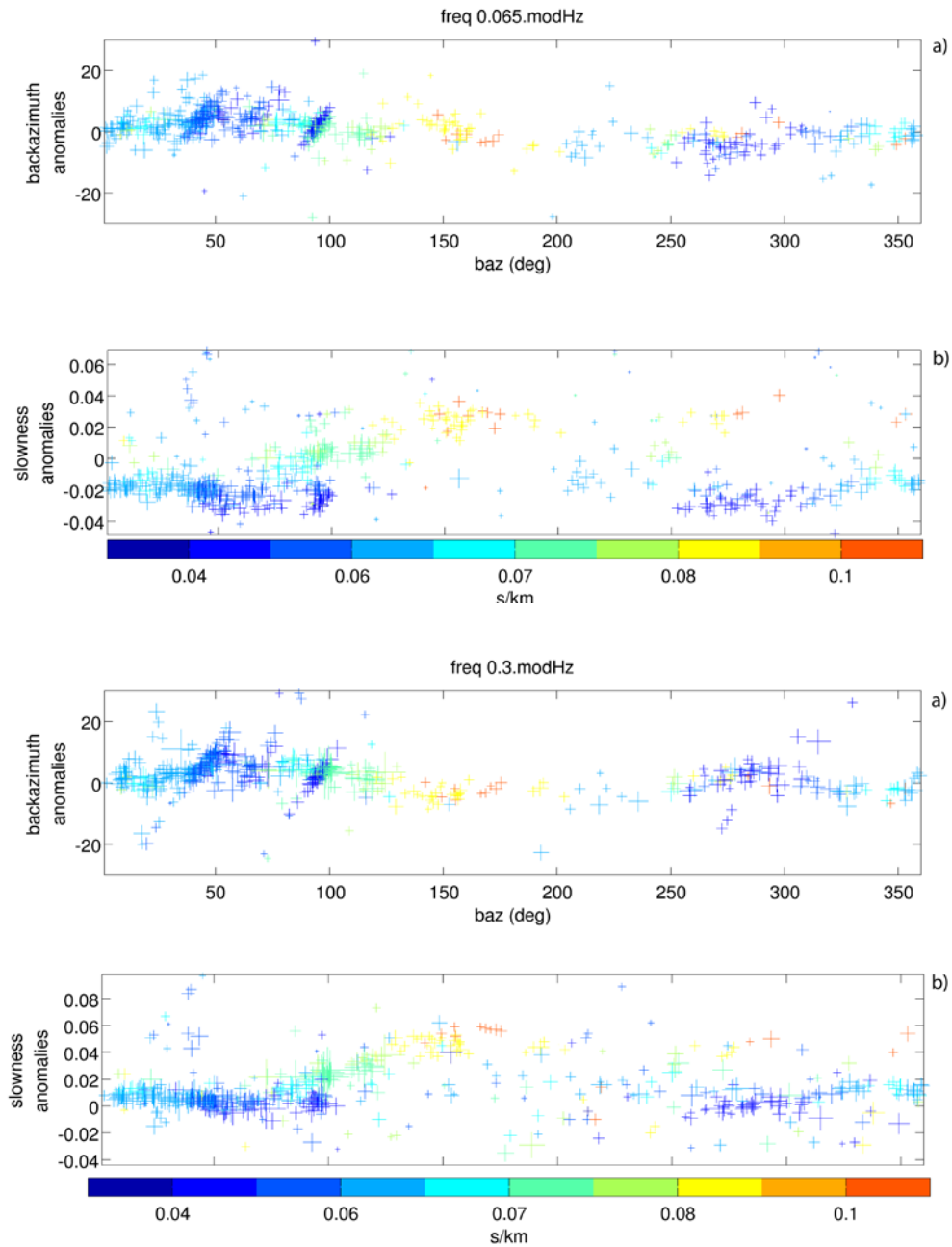
Fig. 6.3.2   Backazimuth (a) and slowness (b) anomalies from fk-analysis plotted as function of the theoretical backazimuth, for low frequencies (up), high frequencies (down). Colors are used here to distinguish between events characterized by different theoretical slowness vectors (from IASPEI tables). We observe slightly negative slowness anomalies for events with small theoretical slowness and positive anomalies for events with large slowness for the backazimuth between 80 and 250°. Sign and amplitude of the deviations seem to have a weak dependence on frequency and a clear dependence on backazimuth. Different slownesses sense differently the structure characteristics. The observed deviations can be interpreted in terms of distant and local heterogeneities.

6.3.4   Harmonic analysis of backazimuth anomalies

As can be seen in Fig. 6.3.2 (a) the azimuthal deviations are mainly a function of backazimuth and frequency. To investigate the characteristics of this dependence, we apply a harmonic analysis. We assume that the azimuthal deviations can be expressed as the sum of cosine functions of backazimuth with different periodicities. For each component it is possible to estimate amplitude (A_k) and phase (phi_k). The dominant periodicity estimated by fk-analysis for the observed azimuthal anomalies at NORSAR is clearly 360°.

This periodicity in the backazimuth anomalies can be generated by a velocity gradient *e.g.*, caused by a dipping interface (see *e.g.*, Niazi, 1966). From the phase of the 360° term it is possible to determine the strike of the structure showing the velocity gradient and the direction to the low velocities. The 180° periodicity term can be explained in terms of azimuthal anisotropy with a horizontal symmetry axis. From the phase of this harmonic it is possible to estimate the direction of the fast axis of anisotropy.

6.3.5   Polarization analysis

P-wave polarization parameters, namely azimuthal deviation and incidence angle, have been estimated by solving the eigenvalue problem of the 3-component signal covariance matrix in a moving window, following the algorithm proposed by Jurkevics (1988). The parameters have been calculated for each 3C-station of the NORSAR array in 3 frequency bands (0.03 – 0.1 Hz, 0.1 – 0.5 Hz and 0.5 – 1 Hz). The procedure has been automatized and an automated picking algorithm has been used to estimate the polarization parameters of the first P-wave onset including a measure for the quality of the estimate (Cristiano *et al.*, in preparation). Fig. 6.3.3 shows as example the results of the polarization analysis for the array sites NB201 and NC204. Also the azimuthal deviation of the P-wave polarization is mainly dependent on the backazimuth and the frequency. Therefore, we do not separate measurements related to events with different epicentral distances. This works as an averaging of deviations over epicentral distances and different source locations and characteristics, and results in a down weighting of the ray path contribution and source area effects.
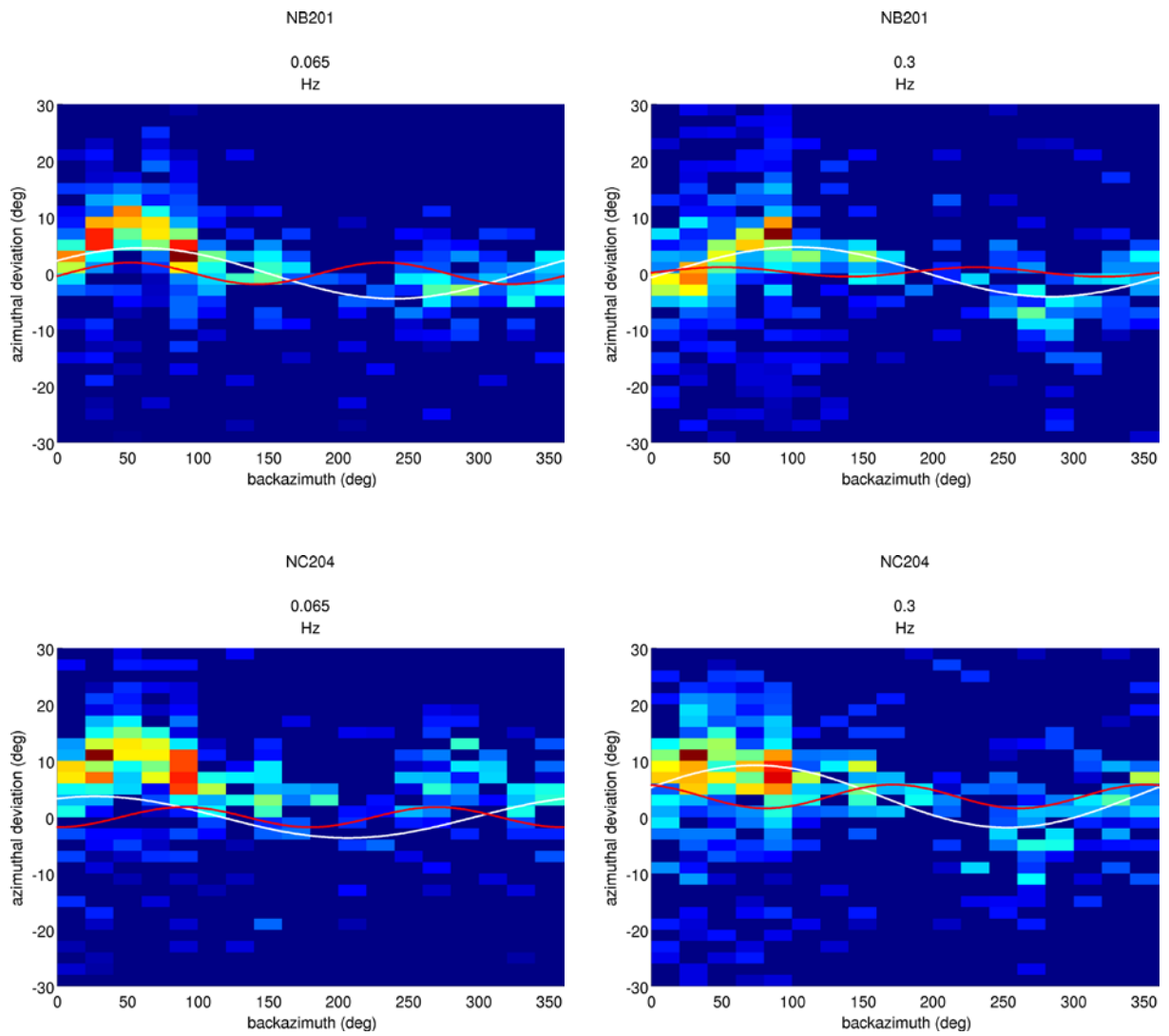
Fig. 6.3.3   2D histogram of the azimuthal deviations estimated by polarization analysis at the NORSAR sites NB201 and NC204 in two frequency bands (0.03 − 0.1Hz, 0.1 − 0.5 Hz). The measurements are distributed in bins of azimuthal deviation and backazimuth ranges. Colors are used to show which bins have the higher number of high quality measurements. Plotted as overlay are the cosine functions with 360° and 180° periodicity from the applied harmonic analysis. Minimum and maximum of the color scale is in dark blue and red, respectively.

6.3.6   Discussion of the results

Harmonic analysis has been applied on the azimuthal deviations estimated by polarization analysis. The dominant periodicities are 360° and 180° for each station of the NORSAR array, but the 180° term is only significant at sites NC204 (see Fig. 6.3.3) and NC303.

The directions to high velocity anomalies estimated by analysis of azimuthal deviations of the first arriving P-wave polarization are consistent on the whole NORSAR array and with the fk-analysis estimate. High velocity directions at low and high frequency point south-southeast (160±8°).

The high velocity directions show a dependence on frequency. High frequency measurements are more sensitive to the shallow structure beneath the array, while low frequency P-waves measurements are related to a deeper structure.

We observe a good agreement between the high velocity directions estimated by polarization analysis at high frequencies and the P-wave velocity anomalies estimated by Stratford (2011) in the upper crust along a profile crossing the Oslo Graben.

There is consistency between the high velocity directions at low frequencies and the Moho topography estimate by receiver functions of Svenningsen *et al.* (2007). So we suggest that the high velocity anomaly estimated by polarization and fk-analysis can be related to this Moho topography. The high frequency observables are related to the upper crust (wavelength of about 20 km).

The directions of fast axis of anisotropy, estimated by polarization analysis, are significant only at NC204 and NC303 and only for low frequency observations. The fast directions are 110° with an uncertainty of few degrees and fully consistent with fast directions estimated by Roy and Ritter (2013) applying the SKS/SKKS splitting method.

6.3.7   Summary

Fk-analysis and polarization analysis of the first-arriving P wave are used for the investigation of lateral heterogeneity and azimuthal anisotropy close to the NORSAR array. Due to the different sensitivities of these methods to local and distant structures, the results of the two methods complement each other.

The estimated azimuthal deviations by polarization analysis and fk-analysis show a clear dependence on the event backazimuth. The high velocity directions are consistent at each station of the NORSAR array and are in good agreement with observations made with different approaches in the array area. The anisotropic contribution to azimuthal deviations observed by polarization analysis is significant only at stations NC303 and NC204 and fast directions match the fast directions estimated at those stations with SKS splitting.

Polarization analysis has been applied for the investigation of anisotropy and lateral heterogeneity beneath the NORSAR array. The estimated deviations are robust for polarization analysis and fk-analysis. The polarization analysis has the advantage to be a single station approach and sensitive also to local anisotropy.

Acknowledgements

L. Cristiano, CAU
J. Schweitzer, NORSAR
T. Meier, CAU

References

Capon, J. (1973). Signal processing and frequency-wavenumber spectrum analysis for a large aperture seismic array. *Methods Comput. Phy.*, **13**, 1-59.

Cristiano *et al.*, Automated P-wave polarization analysis of three-component Graefenberg Array data, *in preparation*.

Davies, D., E.J. Kelly and J.R. Filson (1971). Vespa process for analysis of seismic signals. *Nature Phys. Sci.*, **232**, 8-13.

Jurkevics, A. (1988). Polarization analysis of three-component array data. *Bull. Seism. Soc. Am*., **78**, (5), 1725-1743.

Niazi, M. (1966). Corrections to apparent azimuths and travel-time residualsfor a dipping Mohorovicic discontinuity. *Bull. Seism. Soc. Am*., **56**, 491-509.

Posmentier, E.S. and R.W. Herrmann (1971). Cophase: An ad hoc array processor. *J. Geophys*. Res., **76**, 2194-2201.

Rost, S. and C. Thomas (2002). Array seismology: methods and applications. *Rev. Geophys.*, **40**, (3), 1008, doi: 10.1029/2000RG000100.

Schulte-Pelkum, V., G. Masters and P. Shearer (2001). Upper mantle anisotropy from long period P wave polarization. *J. Geophys. Res.*, **106**, (B10), 21917-21934.

Stratford, W. and H. Thybo (2011). Crustal structure and composition of the Oslo Graben, Norway. *Earth Plan. Sci. Lett.*, **304**, 431-442.

Svenningsen L., N. Balling, B.H. Jacobsen, R. Kind, K. Wylegalla and J. Schweitzer (2007). Crustal root beneath the highlands of southern Norway resolved by teleseismic receiver functions. *Geophys. J. Int*., **170**, 1129-1138.

Wessel, P. and W.H.F Smith (1998). New, improved version of Generic Mapping Tools released. *EOS, Trans. Amer. Geophys. Union*, **79**, 579.

6.4 Detection Capability of the Seismic Station TROLL in Antarctica

6.4.1 Introduction

The seismic station at the Norwegian Research Base Troll in Dronning Maud Land, Antarctica, has been operational and sending continuous data to NORSAR since 5 February 2012. The TROLL station (Fig. 6.4.1) is placed on a bedrock prominence on top of a hill, and is equipped with a Streckeisen STS-2.5 broadband seismometer, which can measure ground movements in the frequency range from below 1 mHz up to about 50 Hz. The digitizer is a Quanterra Q330HR, which converts the analog seismometer signals with an over 150db dynamic range (26 bit AD converter) and samples the data streams with rates of 100 Hz, 40 Hz, 1 Hz, 10 s and 100 s (Schweitzer *et al.*, 2012). During the first year of operation, high-quality recordings of both regional and teleseismic signals were made (Pirli, 2012), indicating that the TROLL station would make a significant contribution to seismicity monitoring on both global, regional and local scales.
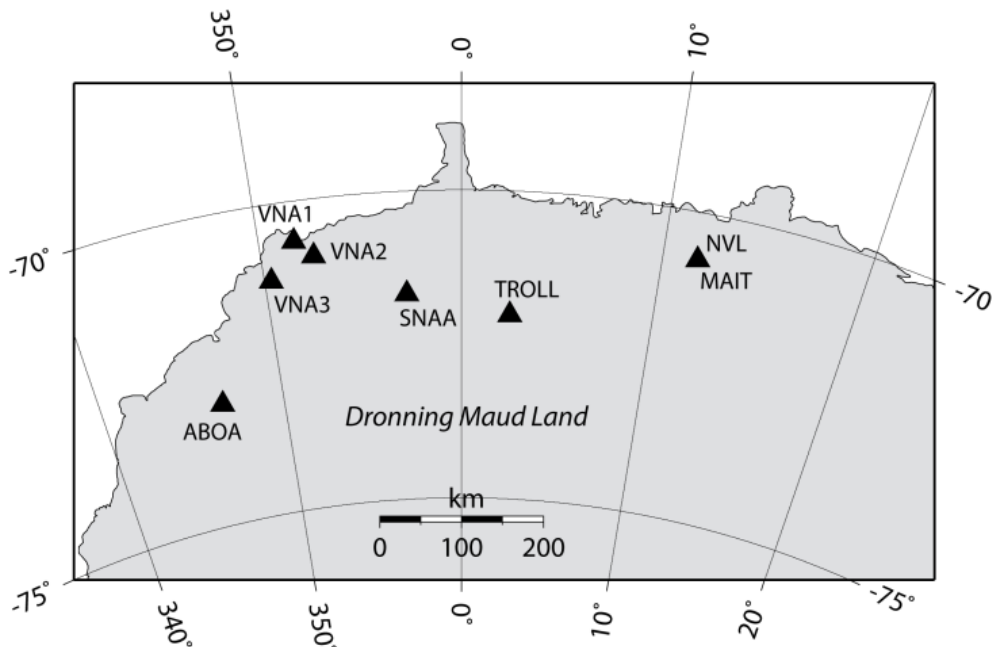
Fig. 6.4.1   Locations of seismic stations in Dronning Maud Land, Antarctica. Seismic data from TROLL, VNA(1-3) and SNAA are accessible in real time.

Figs. 6.4.2 and 6.4.3 show an example of waveforms and corresponding spectra of a PKP-phase recorded at TROLL from a deep earthquake (626 km) located in the Sea of Okhotsk, occurring on 14 August 2012. The event had a magnitude of 7.7 and is located at a distance of 152° from TROLL. Somewhat surprisingly, clear signal energy can be observed well above 10 Hz even at such a large epicentral distance. We also notice from Fig. 6.4.3 that the noise levels at TROLL station stay very close to the Peterson low noise model (Peterson, 1993) for relatively high frequencies, and thus facilitate the observation of small-amplitude high-frequency signals.
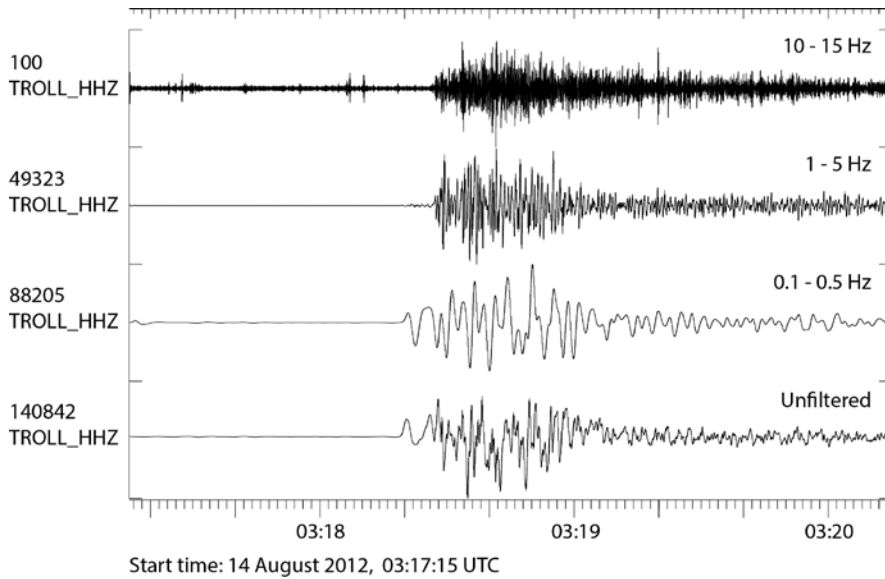
Fig. 6.4.2
PKP-phase from a large deep event in the Sea of Okhotsk recorded at the TROLL station. The event, occurring on 14 August 2012, had a magnitude of 7.7 and was located at a depth of 626 km.
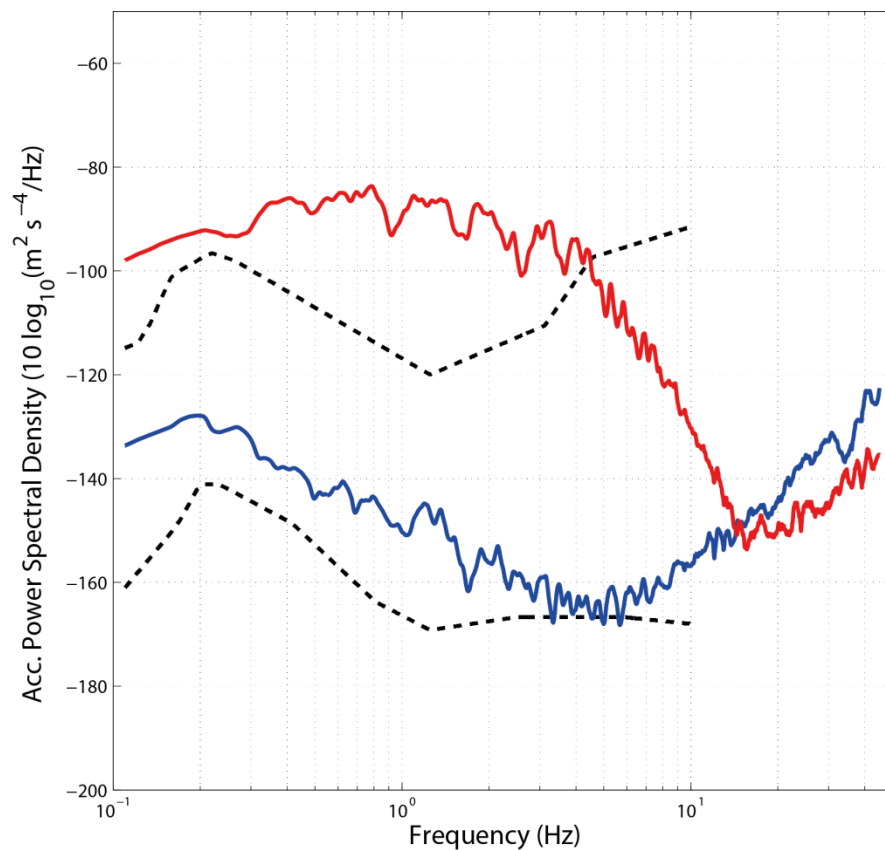
Fig. 6.4.3
TROLL HHZ channel signal acceleration spectrum (red) of the PKP-phase from the Sea of Okhotsk event (see Fig. 6.4.2. A 60 second time segment was used for estimation. The blue curve shows the noise spectrum of a 60 second time window preceding the PKP-phase. The Peterson low- and high-noise models are shown as black dashed lines.

6.4.2   Estimation of detection capability

In the study of Kværna and Ringdal (2013), it was shown that the station SNAA in Antarctica was among the best performing three-component stations of the International Monitoring System (IMS) for monitoring compliance with the Comprehensive Nuclear-Test-Ban Treaty (CTBT).

In order to evaluate the performance of the TROLL station, we have made a comparative study with SNAA using IDC Reviewed Bulletin Data (REB) for the time period 5 February 2012 to 13 March 2013. For a noise window preceding the detected REB P-phases, we measured at TROLL and SNNA the long-term average (LTA) amplitude levels in two different frequency bands, 1 – 2 Hz and 2 – 4 Hz. The results are shown in Fig. 6.4.4 and indicate similar noise levels at these two stations. Also notice the annual variation with lower noise levels during the austral winter.
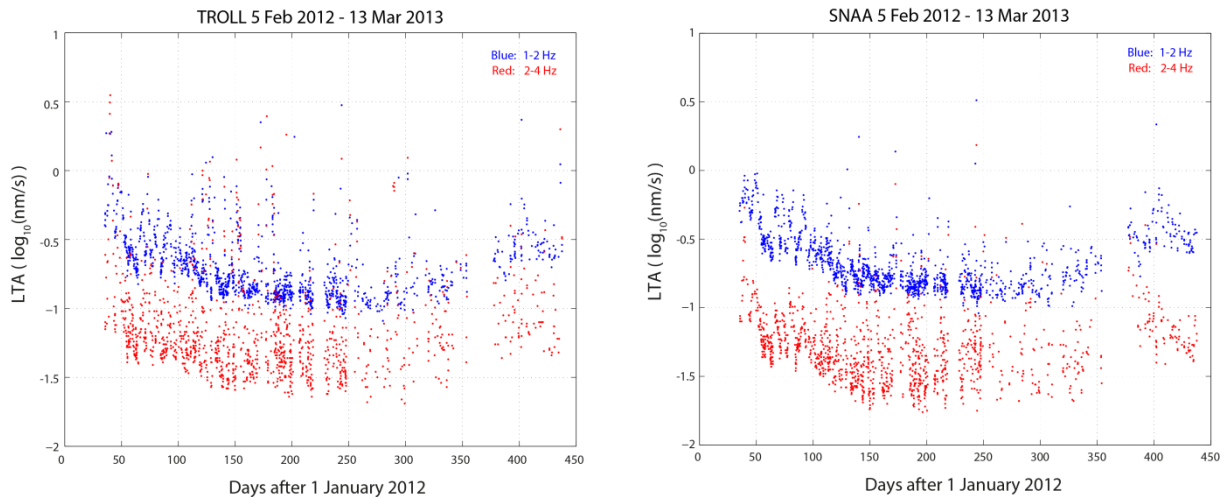
Fig. 6.4.4   *Long-term average (LTA) noise levels at TROLL (left) and SNAA (right) during the time period 5 February 2012 to 13 March 2013. The LTAs are calculated in two frequency bands, 1 – 2 Hz and 2 – 4 Hz, for time intervals preceding the P-phases.*

For a subset of the REB events, covering the 6-month time period 5 February 2012 to 7 August 2012, we have manually screened the TROLL and SNAA detection lists for REB events having P-detections at both stations. This resulted in a list of 1455 events, shown in Fig. 6.4.5. For both TROLL and SNAA, the P-phases from these events were analyzed in the same manner.
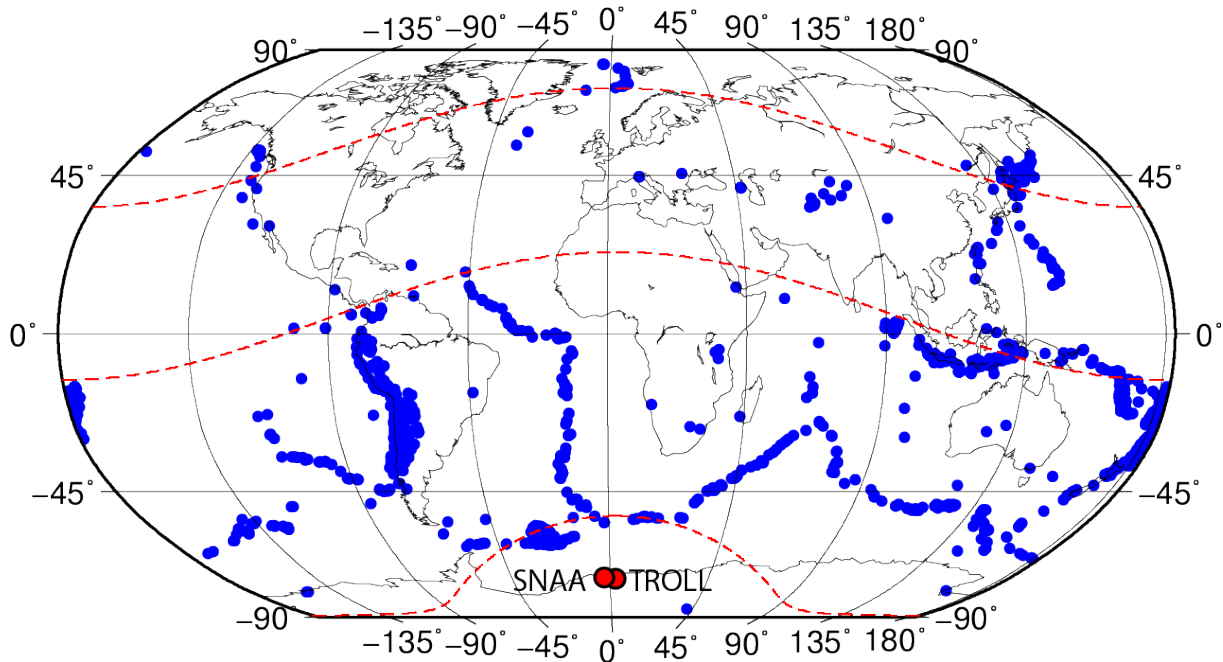
Fig. 6.4.5   Blue symbols show locations 1455 IDC REB events used to estimate the detection capability at the SNAA and TROLL stations. The red dashed curves denote distances of 20, 95 and 144° from TROLL.

To estimate the station detection thresholds, we used a procedure similar to that of Kværna and Ringdal (2013). For each of the events shown in Fig. 6.4.5, we estimated for P-phases at both TROLL and SNAA the instantaneous station detection threshold

$$a_i = m_i - \log(SNR_i) + 0.5$$

where m_i is the reference magnitude (m_{b1}) according to the REB for the i-th event, SNR_i is the signal-to-noise ratio for the i-th event, and the term 0.5 is introduced to take into account the signal-to-noise ratio required for signal detection (0.5 magnitude units correspond to an SNR of ≈ 3). We then fitted the m_{b1} detection capability curve to the instantaneous station detection thresholds, using an average correction (offset) for each of the three distance ranges $0 - 20°$, $20 - 90°$ and $115 - 180°$. The results from this analysis are shown in Fig. 6.4.6. The offset is indicative of the overall station performance, and the lower the offset, the better is the overall performance.

From Fig. 6.4.6 we read that for teleseismic distances $20 - 90°$ and $115 - 180°$ the offset for TROLL is $0.1 - 0.2$ magnitude units lower than for SNAA. Thus, for events in this distance range, TROLL has an overall detection capability which is $0.1 - 0.2$ magnitude units better than SNAA. From Fig. 6.4.5, we also see that the sampling of regional events in the distance range $0 - 20°$ from the two stations is very sparse. The events are limited to very specific areas on the neighboring plate boundaries, like the South Sandwich Islands, and the estimated detection capability from these events may therefore not be very representative for the overall performance within regional distances. However, for the events analyzed, SNAA has a significantly better overall detection capability of 0.5 magnitude units. This may be explained by high frequency noise often observed at TROLL caused by wind and local icequakes (Pirli, 2012). But it is also possible that the propagation path from the geographically clustered regional events to SNAA is particularly favorable in providing strong amplitude signals as

compared with the propagation path to TROLL. Also notice that SNAA is located closer to the regional event cluster than TROLL.
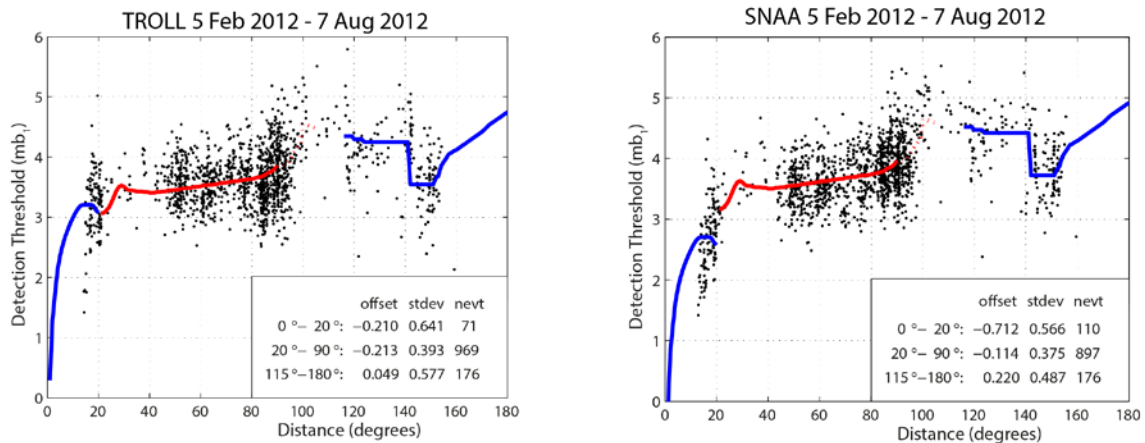

Fig. 6.4.6   *The black dots correspond to the estimated instantaneous detection thresholds of the events shown in Fig. 6.4.5., plotted versus the epicentral distance from the stations TROLL (left) and SNAA (right). The standard m_{b1} amplitude-distance curve for zero-depth events is fitted to the data in three different distance intervals. Information about the m_{b1} curve offset, the standard deviation, and the number of events for the different distance ranges is given in the lower right boxes.*

6.4.3   Improvements to the TROLL station, February 2013

During the first year of operation, relatively large diurnal, long-period oscillations were observed at TROLL (Schweitzer *et al.*, 2012), presumably caused by temperature variations within the protected dome. In addition, the gain setting of the Q330HR digitizer was observed to be too low for sufficient resolution of the high-frequencies. Consequently, the gain setting of the Q330HR digitizer was increased on 4 February 2013 by a factor of 20, and on 9 February 2013, the TROLL station was upgraded with additional thermal insulation. An additional low-gain data stream with a sampling rate of 40 Hz was retained by using the auxiliary 24-bit input and a gain factor of 1. Fig. 6.4.7 illustrates different steps of the thermal insulation procedures.
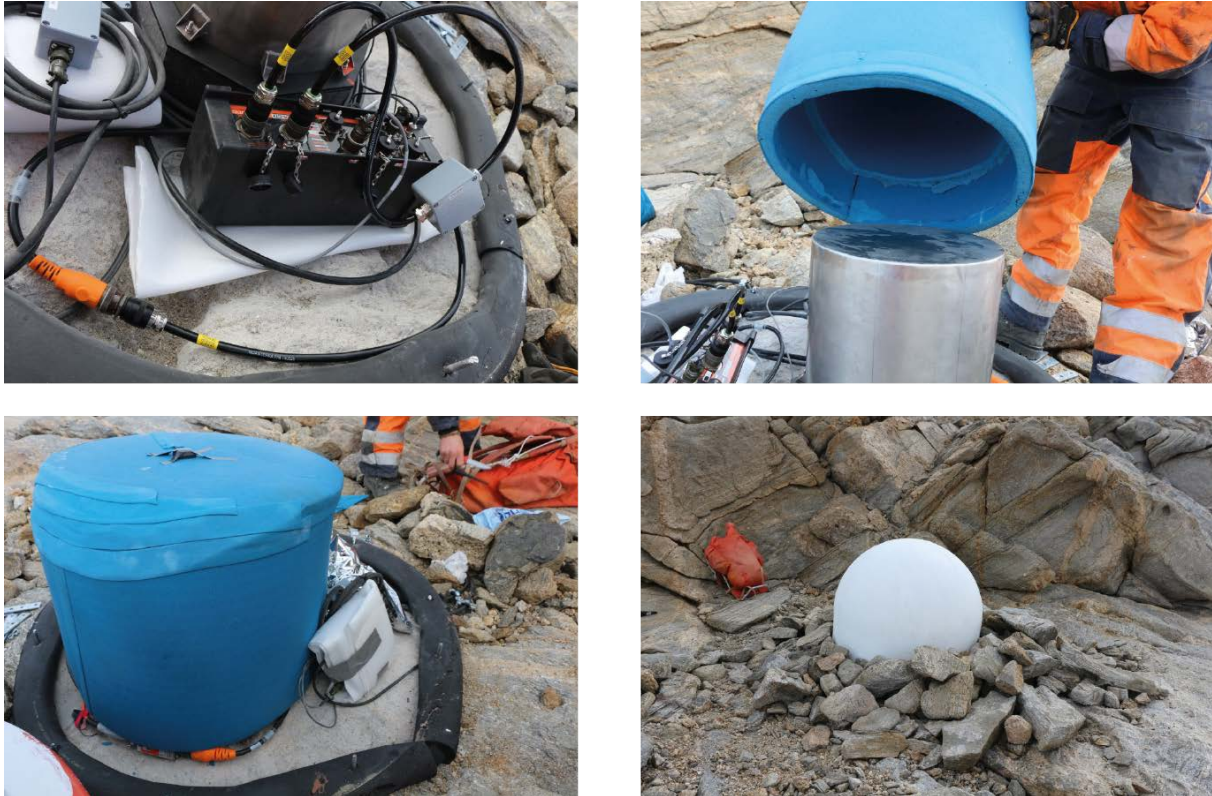
Fig. 6.4.7   Photos taken during the installation of additional thermal insulation at the TROLL station in February 2013.
Upper left: Q330HR digitizer and cables inside the station after the removal of the covering plastic dome.
Upper right: The thermal insulation to be placed around the steel casing covering the seismometer.
*Lower left: The thermal insulation put in place.*
Lower right: Job finished. To avoid heating from the sunlight, the plastic dome covering the station was painted white (it was previously orange) and the surrounding area was again covered with stones.

Fig. 6.4.8 shows 9 days of raw, long-period vertical-component data from two similar time periods of the year in 2012 and 2013. It can be clearly observed that the amplitude of the daily signal is significantly reduced during the entire time period in 2013, after the installation of additional thermal insulation. In order to rule out the potential influence of differences in the weather conditions, we show in Fig. 6.4.9 the corresponding temperature profiles at the TROLL station during these two time periods in 2012 and 2013. The temperature profiles are quite similar. We therefore conclude that the reduction in the daily amplitudes after the installation of additional thermal insulation, shown in Fig. 6.4.8, is not caused by smaller temperature variations in 2013 as compared with 2012.
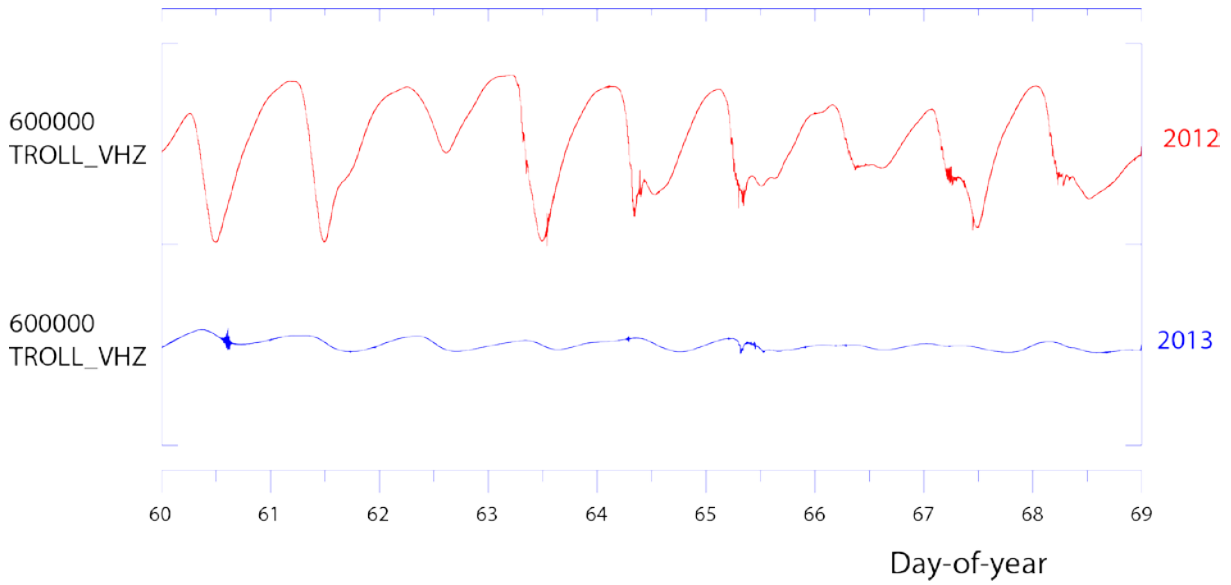
Fig. 6.4.8   Both traces show vertical-component seismograms for the TROLL VHZ channels. TROLL VHZ has a sampling rate of 0.1 Hz.
Upper, red trace: 9 days of data starting on day-of-year 60 in 2012.
Lower, blue trace: 9 days of data starting on day-of-year 60 in 2013, after the installation of additional thermal insulation.
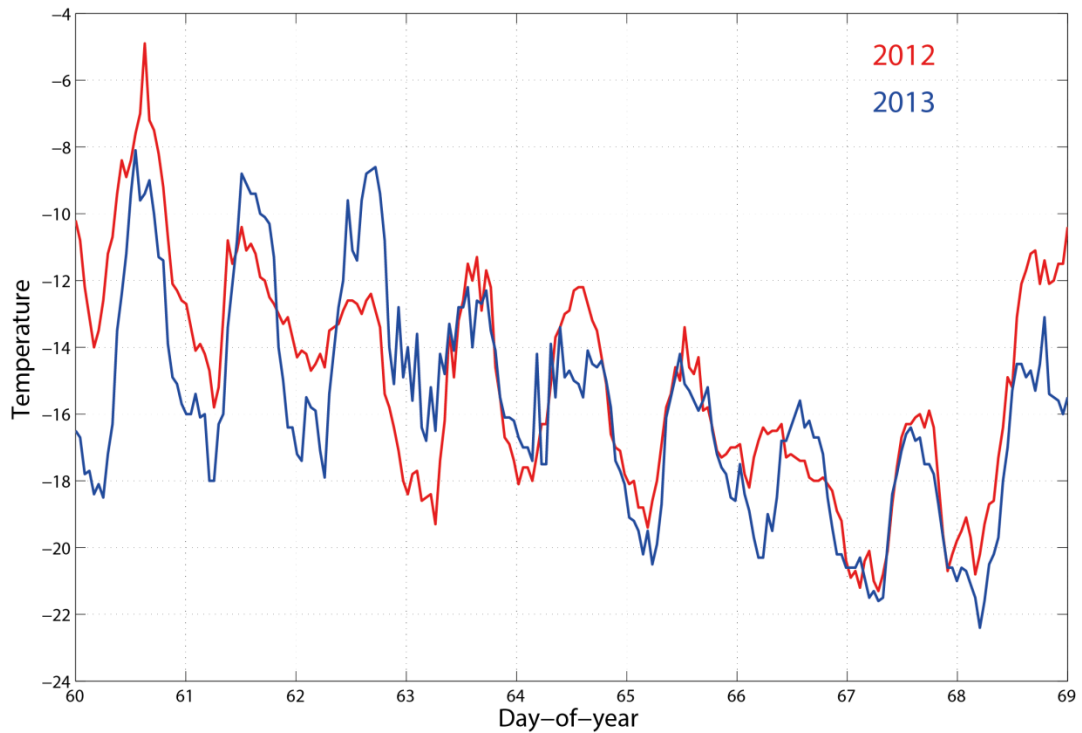

Fig. 6.4.9   Temperature profiles at TROLL for the two 9-day periods in 2012 and 2013. See Fig. 6.4.8 for details.

Fig. 6.4.10 shows the corresponding acceleration spectra for both the vertical and the horizontal components of the TROLL station. For the vertical component we observe in 2013 about 20 dB reduction for the diurnal period (86400 s). A similar improvement is also observed for periods between 100 and 3000 s. For 100 s period we observe in 2013 noise levels approaching the Peterson low-noise model on the vertical component. For the horizontal components, and in particular for the North-South component, the improvement is much smaller. It should also be noted that the long-period noise levels on the horizontal components are generally higher than on the vertical component (Peterson, 1993). We currently have the hypothesis that the thermal insulation may have been installed in such a way that it is slightly squeezed between the steel casing covering the seismometer and the covering plastic dome. This may explain the very small improvement in the north-south component noise levels, and we plan to investigate and, if necessary, correct this during the next summer season in January-February 2014.
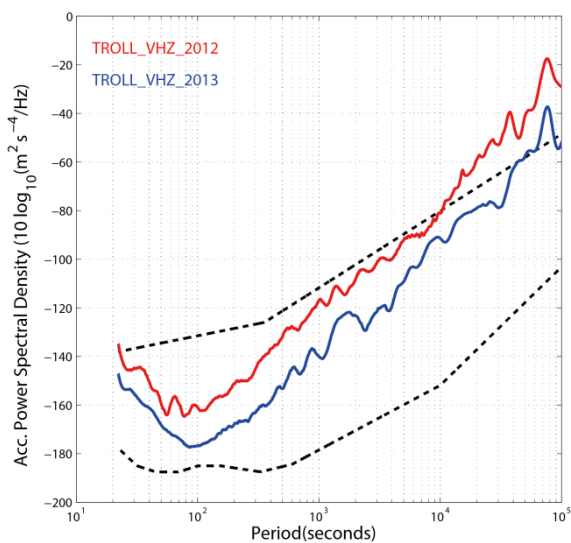
Fig. 6.4.10
TROLL acceleration spectra for the two 9-day time periods in March 2012 (red) and March 2013 (blue).
Left: Vertical component
Lower left: North-South component
Lower right: East-West component
The Peterson low- and high-noise models are shown as black dashed lines. Notice that the Peterson noise models are derived from long-period vertical component data, and may thus not be generally representative for the horizontal components.
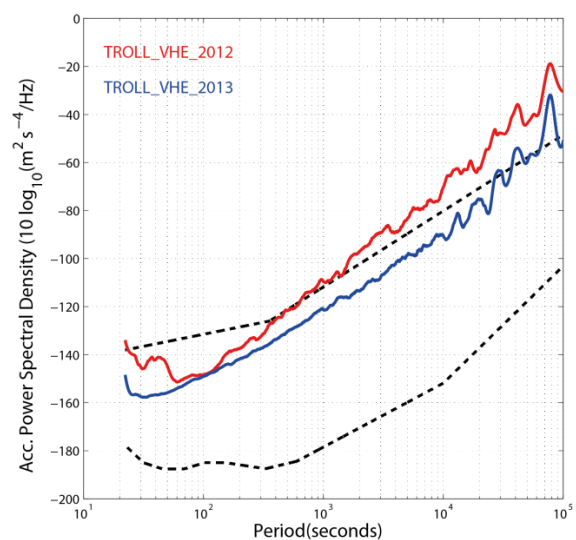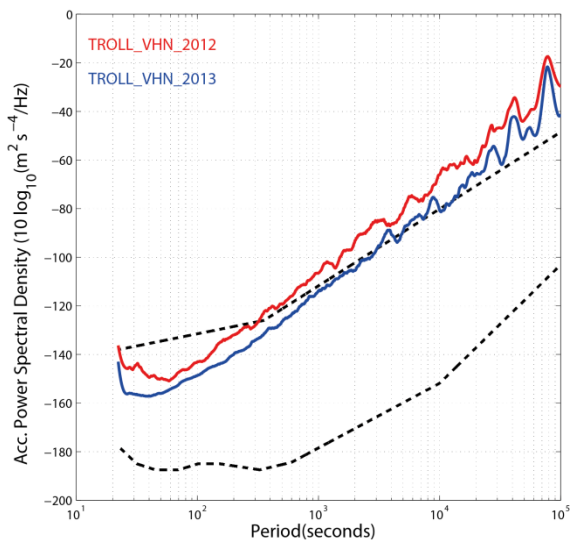
6.4.4 Observation of the Earth's normal modes with TROLL

Each strong seismic event (*i.e.*, with surface magnitudes above ~ 7) generates normal modes of the whole Earth. The largest Earth's normal mode period is 3233 s and many modes have periods between 500 and 1000 s. The generation of the different modes depends on the magnitude and double couple orientation of the event.

TROLL can record seismic energy with frequencies below 1 mHz (or periods above 1000 s), therefore it is of interest to investigate how well normal modes of the Earth can be observed at this new station. Since the installation of the station in February 2013, several earthquakes occurred, which were large enough to generate normal modes. In Fig. 6.4.11 we show spectra between 0.25 and 2.5 mHz of the vertical component after two such strong events. Unfortunately, none such strong events (here we used a threshold of MS >= 7.3) occurred after improving the thermal insulation of the STS-2.5 in February 2013. Therefore, the effect of the lower, long period noise level (see Figs. 6.4.8 and 6.4.10) cannot be tested yet.
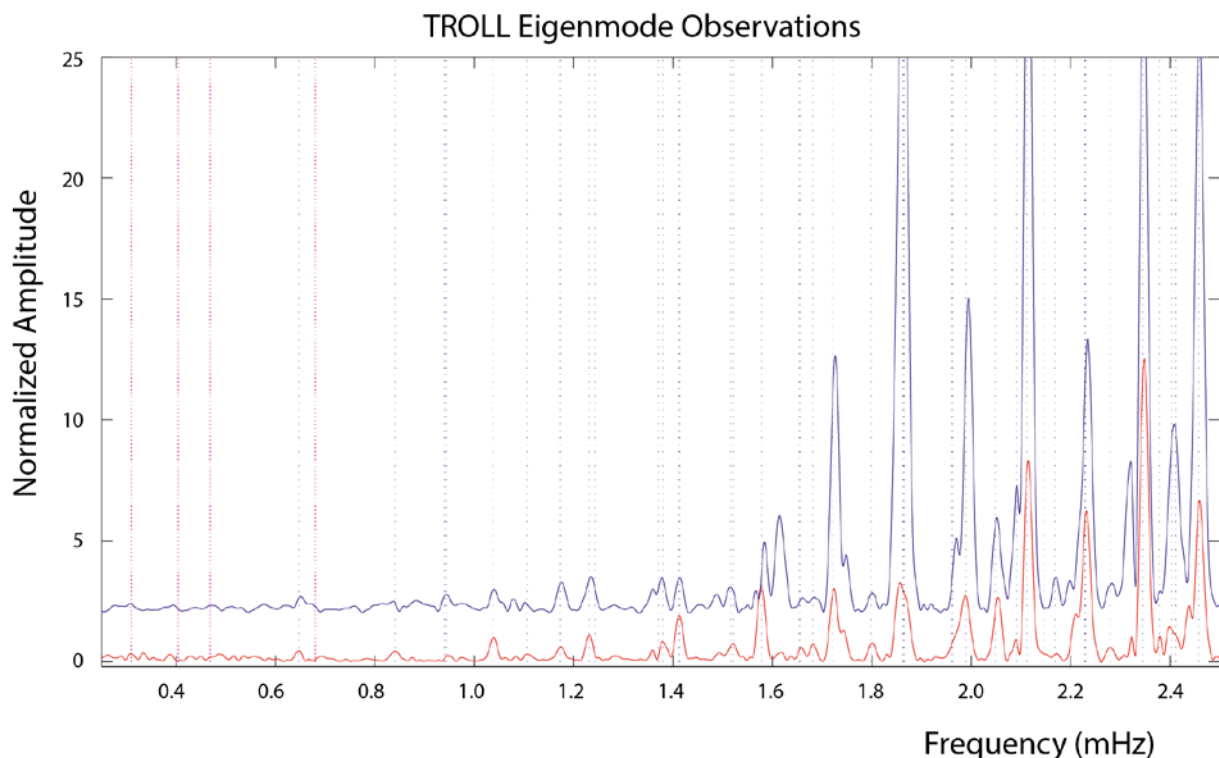

Fig. 6.4.11 Vertical component long-period spectra of 30 hour long TROLL data observed after the 11 April 2012 MS 8.5 Sumatra earthquake (blue) and the 6 February 2013 MS 7.4 Santa Cruz Islands earthquake (red). For more details see text.

To calculate the shown spectra, 30 hour long time windows starting at the event source time were bandpass filtered between 100 and 4000 s. Then, the seismic traces were tapered with a Hanning window and the spectra calculated with an FFT. The two data examples show normalized spectra for the 11 April 2012 MS 8.5 Sumatra earthquake (blue) and the 6 February 2013 MS 7.4 Santa Cruz Islands earthquake (red). Note that the blue spectrum has been offset vertically to improve its readability. Observable spheroidal normal mode frequencies (*e.g.*, Dziewonski and Anderson, 1981 or Deuss *et al.*, 2013) are indicated with dotted lines, with blue dotted lines indicating observed and magenta dotted lines non observed normal modes.

6.4.5 Conclusions

From the analysis of a 6 month dataset, we have shown that TROLL has an overall event detection capability which is $0.1 - 0.2$ magnitude units better than SNAA for teleseismic events. Using the method of Kværna and Ringdal (2013) to estimate the overall detection capability of IMS stations, we show in Fig. 6.4.12 the offset of the best-fitting (m_{b1}) teleseismic detection capability curve for IMS auxiliary stations. These estimates are based on IDC REB data from the 11-year time period 1 January 2001 to 31 December 2011. As SNAA shows to be among the very best performing three-component stations of the IMS, TROLL is thus considered to be even better for detection of teleseismic events. The $1 - 2$ Hz noise levels at SNAA and TROLL are comparable, but there is a tendency of higher noise levels at TROLL for higher frequencies, caused by *e.g.*, periodically occurring small icequakes in the nearby glaciers. This may influence the detection capability for regional and local events where high frequencies are dominant. Although located directly on bedrock with relatively little protection against environmental disturbances, the protection of the new station TROLL is good enough that the station can be used for studies of very long-period signals (normal modes of the Earth).
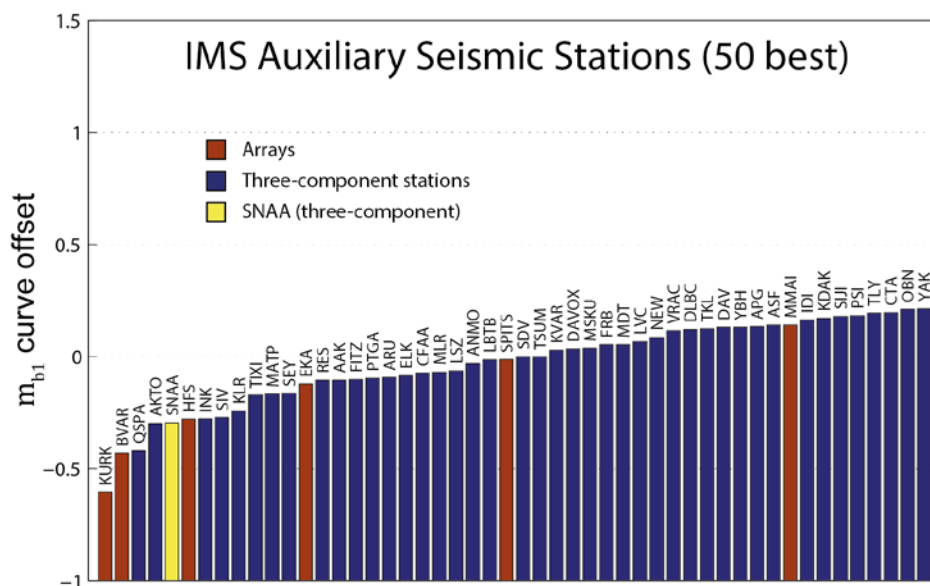

Fig. 6.4.12 Offset of the best-fitting m_{b1} detection capability curve for the 50 best IMS auxiliary stations for events in the teleseismic distance range $20 - 90°$. Array stations are shown red and three-component stations are shown blue. SNAA is highlighted yellow.

The installation of additional thermal insulation at the TROLL station in February 2013 led to a significant reduction of the long period noise levels of the vertical component data. For the horizontal component the improvements are less significant, and we plan to have the TROLL site revisited during the austral summer season in January-February 2014 to check out if there are ways to further reduce the noise levels at horizontal components.

T. Kværna
J. Schweitzer
M. Pirli
M. Roth

References

Deuss, A., J. Ritsema and H. van Heijst (2013). A new catalogue of normal mode splitting function measurements up to 10 mHz. *Geoph. J. Int.*, **193**, 920-937.

Dziewonski, A.M. and D.L. Anderson (1981). Preliminary Reference Earth Model. *Phys. Earth Planet. Int.*, **25**, 1271-1302.

Kværna, T. and F. Ringdal (2013). Detection capability of the seismic network of the International Monitoring System for the Comprehensive Nuclear-Test-Ban Treaty. *Bull. Seism. Soc. Am.,* **103,** (2A), 759-772.

Peterson, J. (1993). Observations and modeling of seismic background noise. *USGS Open-File Report* 93-322, 95 pp.

Pirli, M. (2012). First Data and Analysis Results from the New, Permanent Seismic Station TROLL, Dronning Maud Land, Antarctica. *NORSAR Sci. Rep.*, **1-2012**, Kjeller, Norway, 47-55.

Schweitzer, J., M. Roth and M. Pirli (2012). The new three-component broadband station at Troll, Antarctica. *NORSAR Sci. Rep.*, **1-2012**, Kjeller, Norway, 39-46.

6.5   Seismological Research Related to Geophysical Processes in the European Arctic

6.5.1   Introduction

The characteristics of earthquake activity in the European Arctic are poorly known, mainly due to the scarcity of high-quality seismic stations in many parts of this region. However, a number of significant earthquakes have been recorded in the last decades, the most recent one occurring on 21 February 2008 in Storfjorden, Spitsbergen (Pirli *et al.*, 2010). This earthquake had magnitude 6.1, which makes it one of the largest instrumentally recorded earthquakes on Norwegian territory. Several thousands of aftershocks were recorded after this earthquake, the aftershock sequence slowly progressing towards its end more than five years later (Pirli *et al.*, 2013). Fortunately, the earthquake occurred offshore, and no injuries or considerable damage to infrastructure was reported, however, its nucleation on a previously unmapped fault underlines the necessity for improved mapping of seismic sources in the region.

Moreover, this earthquake is a reminder that the Svalbard Archipelago and surrounding regions are far more exposed to seismic hazard than the northern Eurasian mainland. Active earthquake zones are found on Heerland and on Nordaustlandet (e.g., Mitchell *et al*., 1990). In addition, there is significant earthquake activity along the Mid-Atlantic Ridge (Knipovich Ridge) about 100-200 km west of Spitsbergen and the Gakkel Ridge, north of the Barents Sea (e.g., Engen *et al*., 2003; Korger and Schlindwein, 2012). The Western Barents Sea south of Svalbard also exhibits frequent earthquake activity (see Fig. 6.5.1), as exemplified by observed events close to the island of Hopen, with magnitudes up to 5.4 (4 July 2003, see e.g., Stange and Schweitzer, 2004).

The eastern part of the Barents Sea is somewhat less exposed to earthquake activity, although an interesting recent event, with a magnitude of 4.6, which is uncharacteristic for the particular region, occurred on 11 October 2010 on the north part of Novaya Zemlya (Kværna and Gibbons, 2011). It should be noted that the monitoring of the eastern Barents Sea has until recently been less than satisfactory due to a shortage of high-quality seismic stations east of the Norwegian border. The situation is now changing, as is further discussed in this paper.
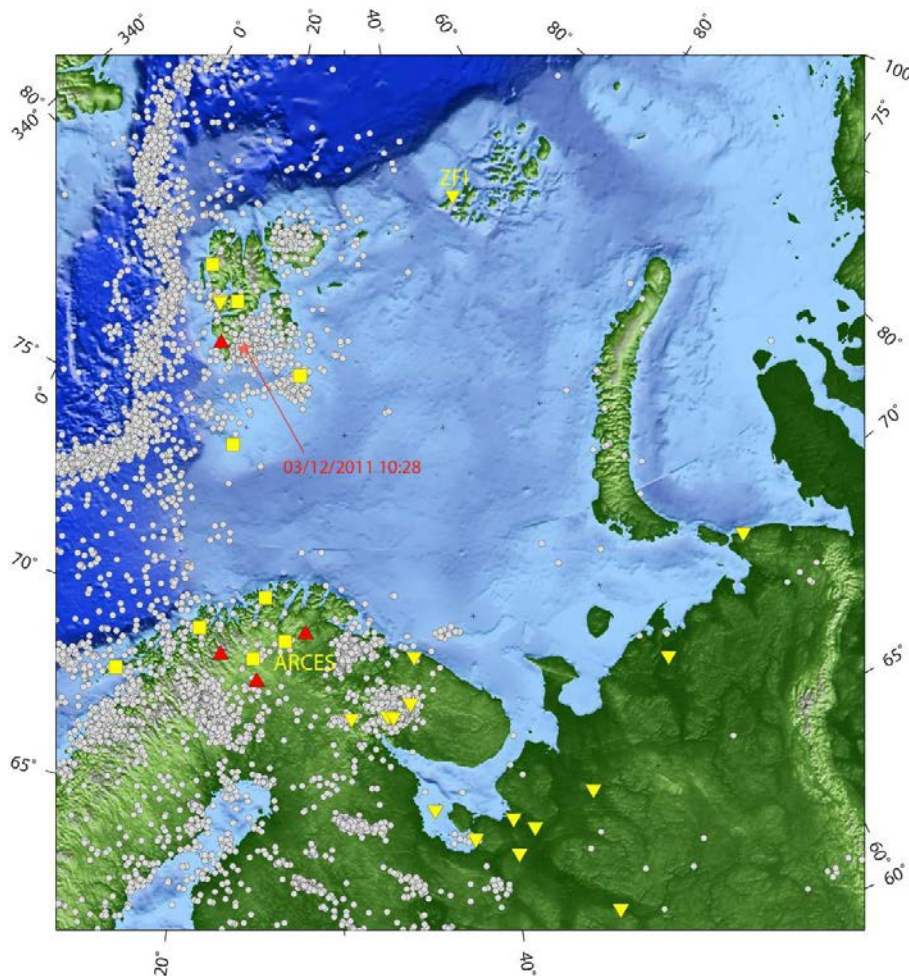
6.5.2   Monitoring the seismicity of the European Arctic

NORSAR has for more than 20 years cooperated with the Kola Branch of the Geophysical Survey of the Russian Academy of Sciences (KB GS RAS), situated in Apatity, in seismic and infrasonic monitoring of the western part of the Barents region. This cooperation began with the establishment of a modern seismic array in Apatity, and the most recent of the joint projects has been aiming at improving the seismological infrastructure in the Barentsburg settlement on Spitsbergen (Roth *et al*., 2011). This project was completed by the end of 2012, and the resulting improved infrastructure forms an important component of the seismic network described in this paper.

One of the benefits of the cooperation has been the establishment of several new contact points between Norwegian and Russian scientists. In particular, in 2012 a trilateral agreement for scientific cooperation was signed between NORSAR, the KB GS RAS and the Institute of Environmental Problems of the North of the Ural Branch of the Russian Academy of Sciences (IEPN UB RAS), stationed in Arkhangelsk, Russia. The IEPN UB RAS group operates several seismic stations along the

southern shoreline of the Barents Sea between the Kola Peninsula and Novaya Zemlya, and on Franz-Josef Land in the high Arctic (Morozov and Konechnaya, 2013). This network is still under development, and will complement the previously available seismic network.

Fig. 6.5.1 shows locations of seismic stations and arrays in and around the target area from which data are currently available. Russian (triangles) and Norwegian (squares) stations are shown in yellow. We have also access to data from other international stations (red triangles) in the region. The grey symbols show seismic events since 1980 with magnitudes of 2.5 or larger as listed in the event catalogue of the International Seismological Centre - ISC (ISC, 2010).

Fig. 6.5.1
Seismic stations (squares and triangles) currently available for monitoring the European Arctic and observed seismicity (circles) in the Barents Sea and the surrounding regions since 1980 (ISC, 2010). Russian stations (triangles) and Norwegian stations (squares) are shown in yellow, while some of the international stations are shown in red. The star notes the location of the earthquake shown in Fig. 6.5 2.

NORSAR is partner in the Norwegian National Seismic Network (NNSN) jointly operated with the Department of Earth Science of the University of Bergen. As NNSN partner NORSAR has free access to all NNSN station data. NORSAR has furthermore access to the data from the International Monitoring System (IMS) for the Comprehensive Nuclear-Test-Ban Treaty (CTBT), and the circum-arctic stations in this system are useful for locating the larger earthquakes in the European Arctic. However, by far the most important contributions for monitoring this region comes from the Norwegian and Russian stations mentioned earlier and shown in Fig. 6.5.1, since monitoring of earthquake activity at low magnitudes requires stations at local or near- regional distances.

6.5.3   Data processing

Currently, data from the station networks of the different institutions (Norwegian and Russian) in the Arctic and around the Barents Sea (see waveform example in Fig. 6.5.2) are separately analyzed at the different institutes. We have begun a process to jointly analyze the data from the combined networks of our three institutions, as further detailed below. In addition, we consider it important to carry out a study of a complete set of all observed data and a common relocation of all events in the region. Such a study should cover both recent historic data (e.g., the last two decades) and current observations, and would result in a more complete seismic bulletin with improved earthquake locations for the entire European Arctic. For a relocation of all events the latest 3D seismic velocity models of the Barents Sea developed at or jointly with NORSAR (Hauser *et al.*, 2011; Levshin *et al.*, 2007; Ritzmann *et al.*, 2007) could be used to achieve a more realistic picture of event distribution and their uncertainties. Alternatively, the RSTT model (Myers *et al.*, 2010) can be employed. To achieve this, NORSAR's existing seismic event location algorithm HYPOSAT (Schweitzer, 2001) could be extended to utilize 3D velocity models. Such a complete, high-quality and up-to-date seismic bulletin of relocated events for the Barents Sea and surrounding areas would constitute the basis for future seismic risk studies in the region and for crustal structure investigations.

To indicate the potential of the joint seismic network to improve the coverage of the European Arctic, we present in Figs.6.5. 3, 6.5.4 and 6.5.5 a comparison based on the first six months of 2013 between the Reviewed Event Bulletin of the CTBT International Data Centre (Fig. 6.5 3), the NORSAR reviewed regional seismic bulletin using data from Fennoscandia, Spitsbergen and the Kola Peninsula (Fig. 6.5 4), and the bulletin produced by IEPN UB RAS using data from their own network (Morozov and Konechnaya, 2013) in combination with the data used to produce the NORSAR bulletin (Fig. 6.6 5).
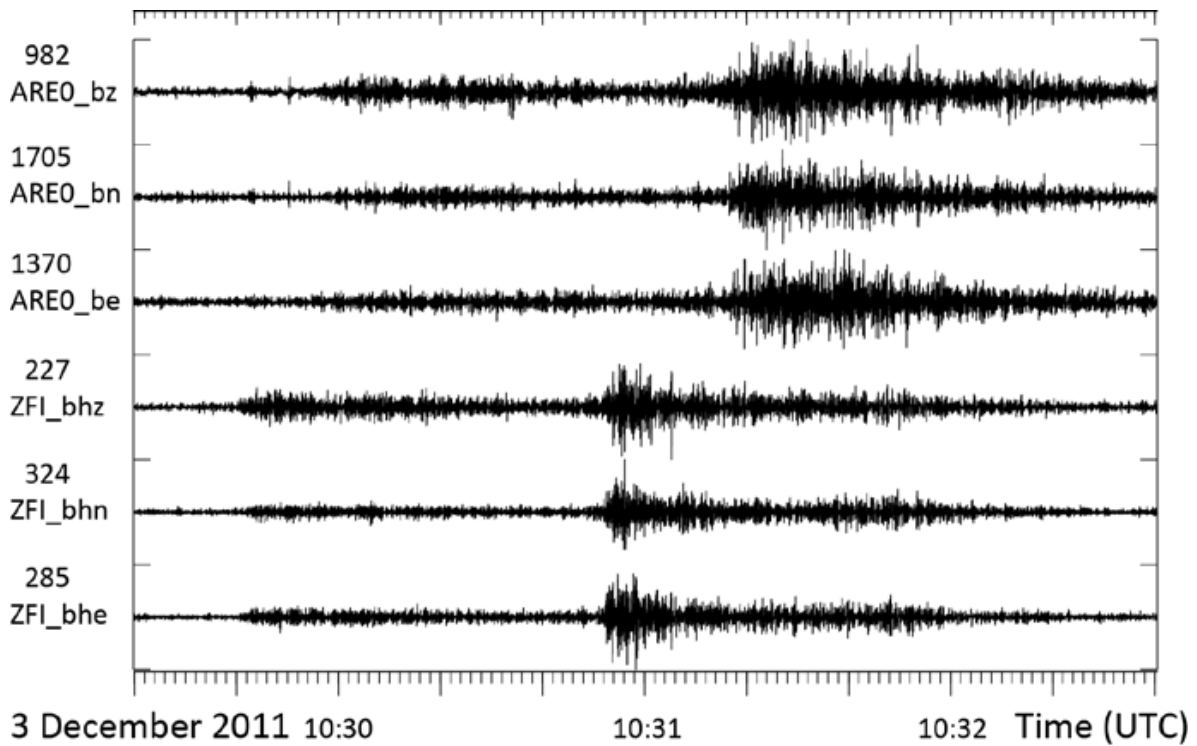
Fig. 6.5.2   Seismograms of a low magnitude (M = 2.9) aftershock from the 2008 – 2012 Storfjorden sequence as recorded at one site of the Norwegian seismic array ARCES (ARE0) in Finnmark and at the Russian seismic 3-component station on Franz-Josef Land (ZFI) in the high Arctic. Both stations are located at comparable distances from the activity in Storfjorden. Note the high data quality of the records at ZFI, which is comparable to that of ARCES – one of the highest quality stations in the CTBT International Monitoring System. The location of the event and the two stations are shown in Fig. 6.5.1.
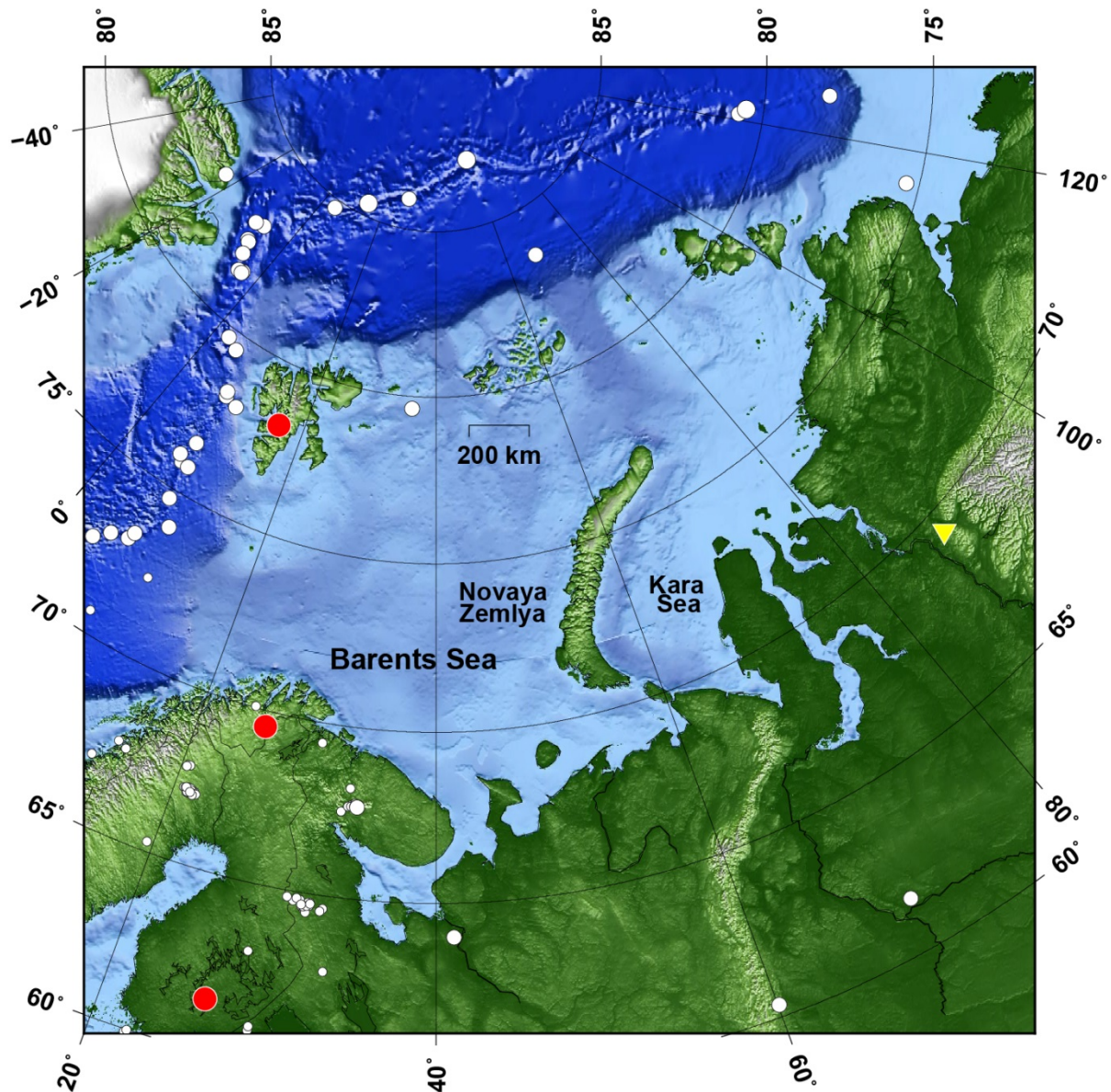
Fig. 6.5 3   Seismic events (white dots) listed in the Reviewed Event Bulletin (REB) of the CTBT International Data Centre (IDC). The size of the event symbols is scaled with magnitude and spans in this figure the magnitude range between 3 and 5. The figure covers data from the first 6 months of 2013. The red dots denote the IMS seismic arrays in the region, and the yellow triangle denotes an IMS 3-component seismic station (Norilsk). Note that the array on Spitsbergen is an IMS auxiliary station, while the other facilities are IMS primary stations. Also note that the IMS network covers the entire globe, although the stations shown here provide the main contributions to recording of seismicity in the European Arctic.
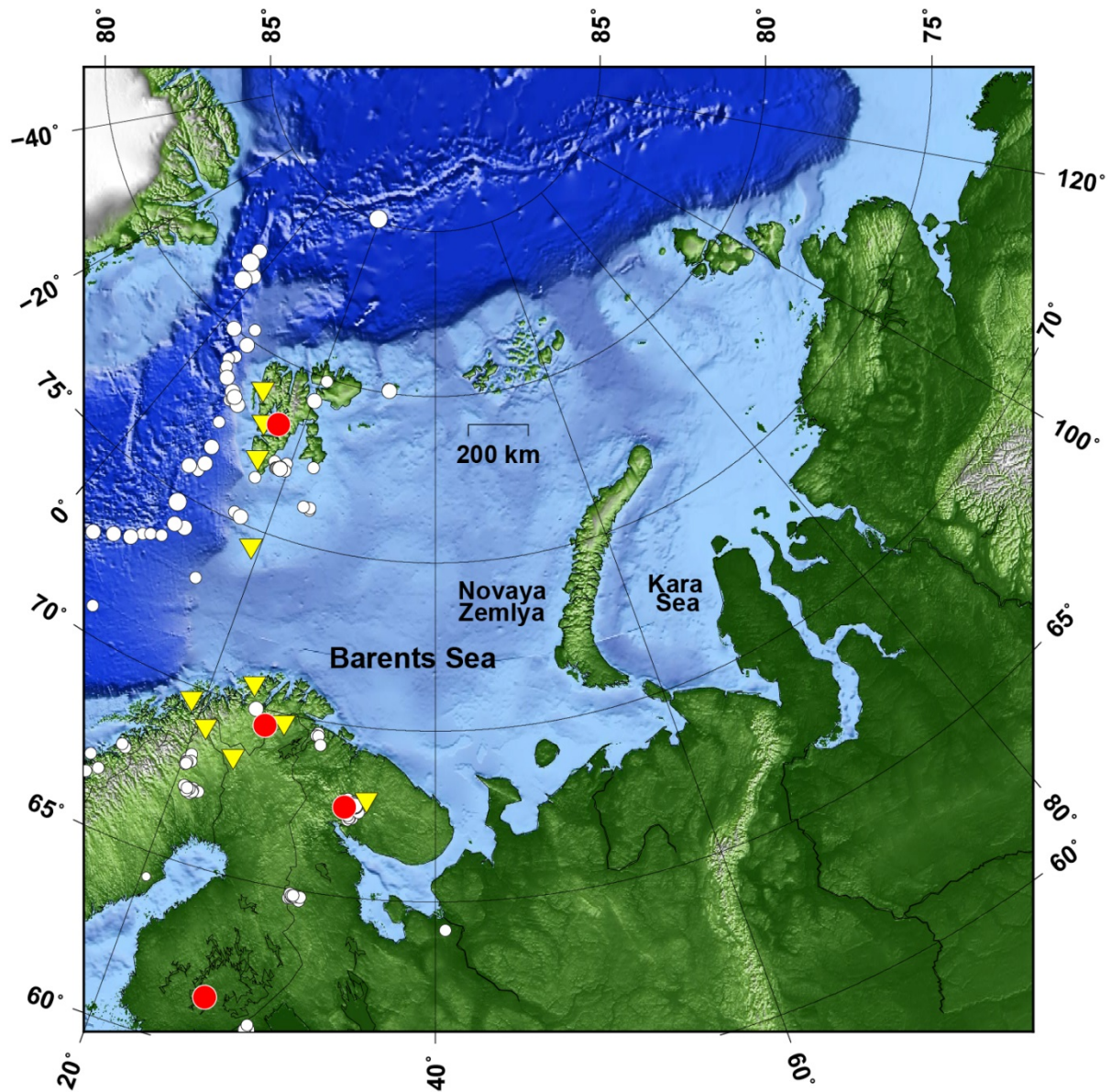
Fig. 6.5.4   Seismic events (white dots) listed in the reviewed regional seismic bulletin issued by NORSAR. This bulletin makes use of stations in Fennoscandia, Spitsbergen and the Kola Peninsula. The figure covers data from the first 6 months of 2013. The red dots denote seismic arrays and the yellow triangles denote 3-component seismic stations. Some additional stations in Fennoscandia which provide minor contributions to this bulletin are not shown on the map.
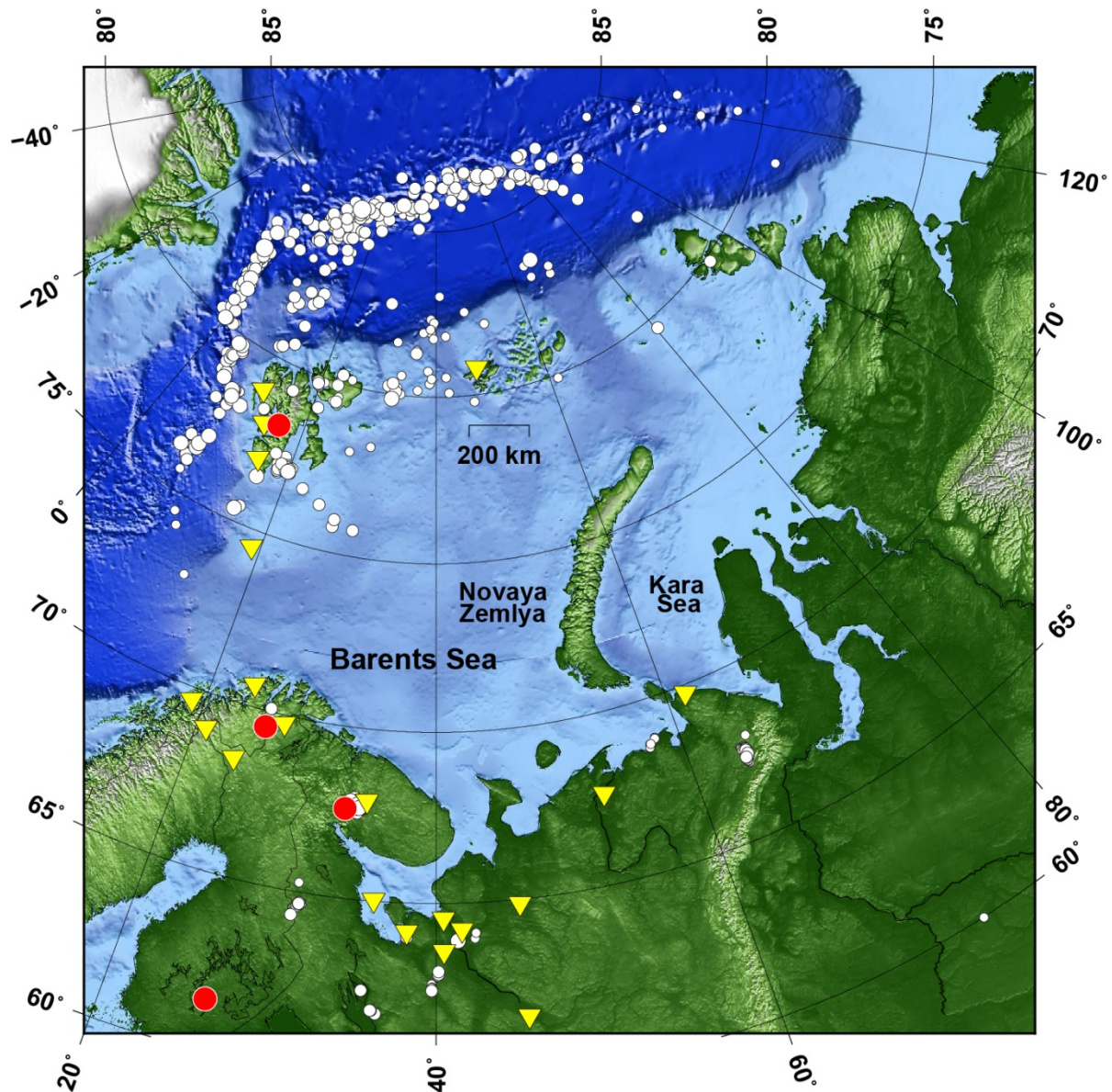
*Fig. 6.5 5   Seismic events (white dots) listed in the bulletin produced by the Arkhangelsk data center.
This bulletin is based on data from the stations used to produce the NORSAR regional
bulletin (Fig. 6.5 4) as well as the Arkhangelsk seismic network. The figure covers data
from the first 6 months of 2013. The red dots denote seismic arrays and the yellow
triangles denote 3-component seismic stations. Note the remarkable increase in recorded
seismicity compared to Figs. 6.5.3 and 6.5.4, especially along the Gakkel Ridge north of
Spitsbergen and Franz-Josef Land.*

It is important to be aware that the criteria for event definition are different in the three cases. The
REB has the strongest requirement for including a seismic event in the bulletin (3 primary IMS
stations), whereas the NORSAR bulletin requires at least two arrays with P-wave detections and
additionally at least one detected S-wave, further restricting the dataset by the application of a
magnitude threshold of 2. The Arkhangelsk event list includes also events detected by only one
station (requiring in such cases both a P and an S phase).

When comparing the three maps in Figs. 6.5.3-6.5.5, we note that the REB and the NORSAR bulletin are quite similar, which is not so surprising given that the three most sensitive seismic arrays in Fennoscandia (ARCES, SPITS and FINES) are part of the International Monitoring System (IMS) network. The REB has a few more events than the NORSAR bulletin in the far north, whereas the NORSAR bulletin has more events in Svalbard and on the mainland. It can also be noted (although not illustrated here) that the more complete Late Event Bulletin (LEB) issued by the IDC, which has a more relaxed event definition threshold than the REB, still has only a few additional events compared to the REB.

We note that the addition of the Arkhangelsk network leads to a considerable increase in the number of located seismic events. This is particularly pronounced along the Gakkel Ridge to the north of the Svalbard and Franz-Josef Land archipelagos. A closer investigation shows that these additional events in the High Arctic are included due to the contribution from the station ZFI on Franz-Josef Land. These events are either located by ZFI in combination with the Spitsbergen stations SPITS or KBS, or in some cases located using P and S phases from ZFI alone. We also note that the vast majority of the events along the Gakkel Ridge have been located slightly to the south of the ridge. We interpret this as an effect of the lack of recording stations closer to and north of the Gakkel Ridge, and the use of a one-dimensional velocity model which is not fully representative for travel-times along observed propagation paths.

Fig. 6.5.6 shows an example of three-component recordings of a low-magnitude Gakkel Ridge earthquake (ML=2.6) from the Spitsbergen array center site and from the station ZFI on Franz-Josef Land. ZFI is closer to the earthquake epicenter and has a higher signal-to-noise ratio (SNR) than the SPITS central site. However, the SPITS array beam (not shown) achieves a similar SNR to the ZFI station for the P-phase. It appears that these two stations in combination would be capable of detecting and locating earthquakes in this area even down to about a full magnitude unit below that of the event shown in Fig. 6.5.6.
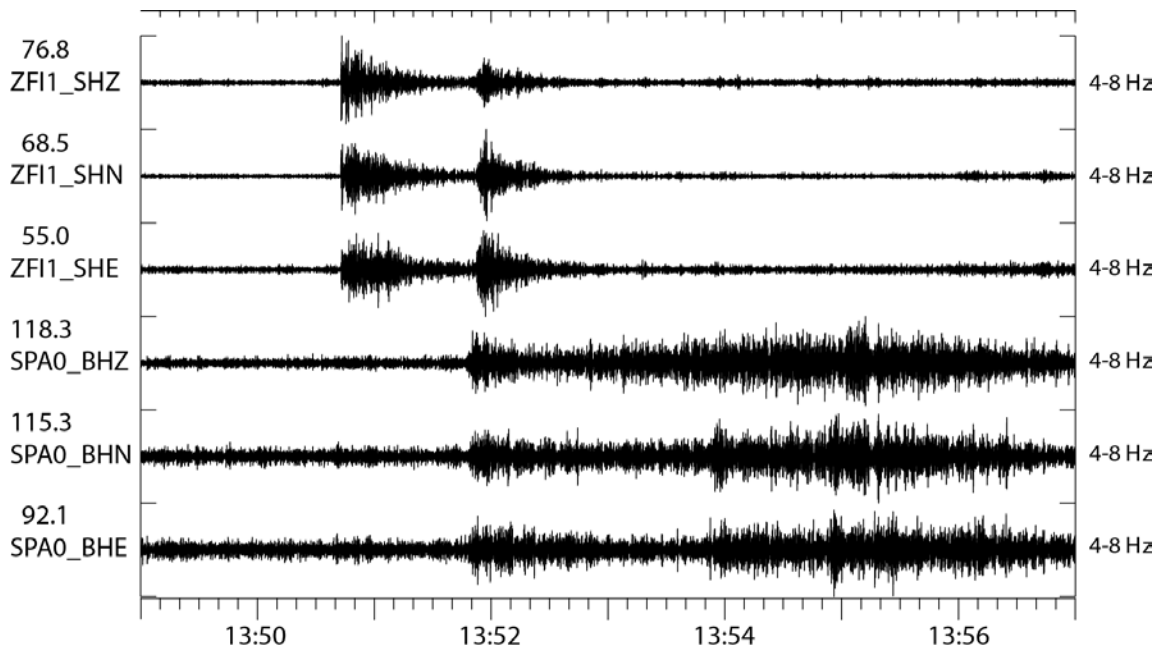
Fig. 6.5.6   *Seismograms of an earthquake on the Gakkel Ridge recorded at the Russian seismic 3-component station on Franz-Josef Land (ZFI) and the central site (SPA0) of the Spitsbergen array (SPITS). The ZFI station is located somewhat closer to the event than SPITS. Note the high signal-to-noise ratios at both stations.*

In contrast to ZFI, the other stations in the Arkhangelsk network mainly contribute to record events at local distances from those stations. Thus, the six-month bulletin contains several hundred mining related events near Vorkuta, all of them recorded by the Amderma station, as well as a number of mining related events south of Arkhangelsk. Only very few such events are detected by stations contributing to the NORSAR bulletin.

Another potential contribution of the Arkhangelsk network is the overall improvement in event detection capability in the Barents Sea region. The fact that only very few events in the Eastern Barents Sea are included in the Arkhangelsk bulletin (none during the six month period studied here), is important by itself, since this network can be expected to have a superior detection capability for this region compared to either the Fennoscandian network or the International Monitoring System. This would be important for e.g. assessing the 'background seismicity' of the region, since even in the absence of recorded seismic events a high detection capability would provide a strong constraint on the seismic background level in the region. We have at this stage not attempted to quantify the detection capability of the joint networks, but as more data is accumulated, this will be an interesting topic for future studies. In any case, the addition of the Arkhangelsk network to the previously existing networks has the potential of providing a considerable improvement in the monitoring of seismicity in the European Arctic region, both in terms of detecting and locating additional seismic events and with regard to establishing a baseline for the seismic background level.

6.5.4   Developing a joint seismic bulletin

With the perspective of this increased potential in mind, the primary objective of the continued cooperation among the three parties is to produce a very high quality reviewed seismic bulletin for the Barents Sea and surrounding areas. This will be an important contribution to all future seismic risk studies in the region, and will also provide a baseline for future studies of microseismicity during oil and gas extraction. It will require the full use of the networks operated by the Norwegian and Russian partners, in combination with other available data. Additional seismic stations, which are planned to be installed in the region, may in the future contribute to a further improvement of the monitoring capability.

From a technical point of view, the emphasis of the cooperation will be on maintaining high quality operation and joint processing of the data from the existing station networks. For some of the stations in the networks, data transmission is already in place, but for most of the newer stations (Morozov and Konechnaya, 2013) this is not the case. In those cases, we will maintain the on-site recording of seismic signals, with the aim to join all data in a common database with free access for all partners.

6.5.5   Conclusions and future perspectives

The cooperation among NORSAR, the Kola Branch and the Arkhangelsk Branch of the RAS involves joint seismological research related to geophysical processes in the European Arctic, using the combined seismic networks of the parties, as well as other available seismic stations in the region. Such research will contribute to a vastly improved mapping of the seismicity in the European Arctic and to achieving a more accurate baseline for background seismicity in the region. This is important for establishing the level of earthquake risk in this environmentally sensitive region, in particular when considering possible future exploration activities for oil and gas, while it is also crucial for the possibility to monitor microseismicity in connection with future hydrocarbon exploitation.

The application of microseismic recording methods for studying production and injection responses of reservoirs both for production optimization and for safety reasons is increasing in the hydrocarbon exploration industry. For the successful interpretation and utilization of microseismic recordings, the knowledge of the background seismicity (i.e., the spatiotemporal distribution of naturally occurring seismic events) is crucial. The low magnitude seismic activity in the European Arctic is poorly known, but can be significantly improved by establishing the appropriate cooperative seismic recording infrastructures as discussed in this paper.

Galina Antonovskaya   **IEPN UB RAS**
Yana Konechnaya   **IEPN UB RAS**
Elena O. Kremenetskaya   **KB GS RAS**
Vladimir Asming   **KB GS RAS**
Tormod Kværna   **NORSAR**
Johannes Schweitzer   **NORSAR**
Myrto Pirli   **NORSAR**
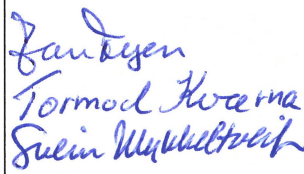**Frode Ringdal**   **NORSAR**

References

Engen, Ø., O. Eldholm and H. Bungum (2003). The Arctic plate boundary. *J. Geophys. Res.*, **108**(B2), doi:10.1029/2002JB001809.

Hauser, J., K.M. Dyer, M.E. Pasyanos, H. Bungum, J.I. Faleide, S.A. Clarck and J. Schweitzer (2011). A probabilistic seismic model for the European Arctic. *J. Geophys. Res.*, **116**, B01303, doi: 10.1029/2010JB007889.

International Seismological Centre (2010). On-line Bulletin, http:// www.isc.ac.uk, *Internatl. Seis. Cent.*, Thatcham, United Kingdom.

Korger, E.I.M. and V. Schlindwein (2012). Performance of localization algorithms for teleseismic mid-ocean ridge earthquakes: the 1999 Gakkel Ridge earthquake swarm and its geological interpretation. *Geophys. J. Int.*, **188**(2), 613-625.

Kværna, T. and S.J. Gibbons (2011). The Novaya Zemlya event on 11 October 2010. *NORSAR Sci. Rep.*, 2-2011, 36-43.

Levshin, A., J. Schweitzer, C. Weidle, N. Shapiro and M. Ritzwoller (2007). Surface wave tomography of the Barents Sea and surrounding regions. *Geophys. J. Int.*, **170**, 441-459.

Mitchell, B.J., H. Bungum, W.W. Chan and P.B. Mitchell (1990). Seismicity and present-day tectonics of the Svalbard region.*Geophys. J. Int.*, **102**, 139-149.

Morozov, A.N. and Y.V. Konechnaya (2013). Monitoring of the Arctic region: contribution of the Arkhangelsk seismic network. *J. Seismol.*, **17**, 819-827.

Myers, S.C., M.L. Begnaud, S. Ballard, M.E. Pasyanos, W.S. Phillips, A.L. Ramirez, M.S. Antolik, K.D. Hutchenson, J.J. Dwyer, C.A. Rowe and G.S. Wagner (2010). A crust and upper-mantle model of Eurasia and North Africa for Pn travel- time calculation. *Bull. Seism. Soc. Am.*, **100**(2), 640-656, doi: 10.1785/0120090198.

Pirli, M., J. Schweitzer, L. Ottemöller, M. Raeesi, R. Mjelde, K. Atakan, A. Guterch, S. J. Gibbons, B. Paulsen, W. Dębski, P. Wiejacz and T. Kværna (2010). Preliminary analysis of the 21 February 2008 Svalbard (Norway) seismic sequence. *Seism. Res. Lett.*, **81**(1), 63-75, doi: 10.1785/gssrl.81.1.63.

Pirli, M., J. Schweitzer and B. Paulsen (2013). The Storfjorden, Svalbard, 2008-2012 aftershock sequence: Seismotectonics in a polar environment. *Tectonophysics*, **601**, 192-205.

Ritzmann, O., N. Maercklin, J.I. Faleide, H. Bungum, W.D. Mooney and S.T. Detweiler (2007). A 3D geophysical model for the crust in the greater Barents Sea region: Database compilation, model construction and basement characterization. *Geophys. J. Int.*, **170**, 417-435.

Roth, M., M. Pirli, J. Schweitzer and E. Kremenetskaya (2011). Installation of the seismic broadband station in Barentsburg, Svalbard. *NORSAR Sci. Rep.* 1-2011, 53-60.

Schweitzer, J. (2001). HYPOSAT – an enhanced routine to locate seismic events. *Pure Appl. Geophys.*, **158**, 277-289.

Stange, S. and J. Schweitzer (2004). Source depths at regional distances: An example from the western Barents Sea/Svalbard region. *NORSAR Sci. Rep.*, 1-2004, 45-50.

Report Documentation Page

NORSAR

Report Number: 13-018	Draft: ☐ Final: ☐	Confidential: ☐ Unlimited: ☒	External: ☐ Internal: ☒	NORSAR Project No.
Title:	NORSAR Scientific Report No. 1-2013 Semiannual Technical Summary 1 January – 30 June 2013			
Client:	The work reported in this Semiannual Technical Summary is supported by various clients and relates to nuclear test ban verification activities at NORSAR			
Project Manager:				
Authors / Prepared by:	Tormod Kværna (Ed.)			
Submitted to:				
Contract Reference:				
Archive reference:	NORSAR folders/projects/Semiannual/JUN13			

Approved by:	Name:	Signature:	Date:
NDC Manager: Program Manager: Program Coordinator:	Jan Fyen Tormod Kværna Svein Mykkeltveit		4 December 2013